JORGE FERNANDO MÁRQUEZ-PEÑARANDA

The effect of biodeterioration on the mechanical properties of cement mortar

BOGOTÁ 2017

THE EFFECT OF BIODETERIORATION ON THE MECHANICAL PROPERTIES OF CEMENT MORTAR

A dissertation
by
JORGE FERNANDO MÁRQUEZ-PEÑARANDA

Submitted to School of Engineering, of
UNIVERSIDAD DE LOS ANDES
in partial fulfillment of the requirements for the degree of
DOCTOR OF PHILOSOPHY

Approved by:

Chair of Committee,	Mauricio Sánchez-Silva
Committee Members,	Johana Husserl
	Emilio Bartidas-Arteaga
	Franck Schoefs
	Andrés Fernando Guzmán-Guerrero
Vice Chancellor of Research,	Silvia Restrepo Restrepo

MARCH 2017
MAJOR SUBJECT: CIVIL ENGINEERING

Universidad de los Andes
School of Engineering
Carrera 1E. 19A-40 Edicio Mario Laserna

ISBN: xxx-xxxx-xx-x
Printed in Colombia
Bogotá 2017
Phone:
Fax:
Email:
http:

A Ana,

Angélica María y

María Fernanda

Acknowledgements

I want to thank to my principal advisor Dr. Mauricio Sánchez-Silva for his valuable and wise guide.

To Dr. Johana Husserl, my eternal gratitude for leading me rightly through new concepts.

My deferential recognition to Emilio Bastidas-Arteaga for his permanent professional and personal support.

To Franck Schoefs my appreciation for his ideas of aperture.

Also I want to thank to the fellow doctoral students from the Universidad de los Andes and Universitè de Nantes, their fresh and opportune help.

To the Universidad de los Andes and Universitè de Nantes my special gratitude for gathering all the possibilities for my professional and personal development through new experiences.

Many thanks to engineer Joachim Marais at the Institut Universitaire de Technologie (IUT de Nantes/Carquefou) of the Universitè de Nantes for his valuable helpful in the study of the topographic changes of the samples.

I want to thank to Michael O'Byrne, PhD Candidate of the Department of Civil, Structural and Environmental Engineering (Trinity College Dublin) for his collaboration in the determination of volume of samples using video technics.

I am highly grateful to Universidad Francisco de Paula Santander for its financial and academic support.

To my wife and daughters, the best of my feelings for their unconditional love and company.

PUBLICATIONS

The following publications are based on this research:

Papers in refereed journals

- Márquez-Peñaranda J, Sánchez-Silva M, Husserl J, Bastidas-Arteaga E. Effects of biodeterioration on the mechanical properties of concrete. Materials and Structures. Published on line:29 December 2015. DOI 10.1617/s11527-015-0774-4
- Márquez-Peñaranda J, Sánchez-Silva M, Husserl J, Bastidas-Arteaga E. Influence of biodeterioration in structural design of reinforced concrete sewers. In process.

Papers in conferences

- Márquez-P J, Sánchez-Silva M, Husserl J. Review of reinforced concrete biodeterioration mechanics. In: VIII International Conference on Fracture Mechanics of Concrete and Concrete Structures FraMCoS-8. Spain 2013. p. 2088-2096.
- Márquez-P J, Sánchez-Silva M, Husserl J. Biodeterioration of Portland Cement Mortar Produced by Sulfur Oxidizing Bacteria. In: Pipelines 2014: From Underground to the Forefront of Innovation and Sustainability. USA 2014. p. 1568-1577

SUMMARY

Reinforced concrete (RC) is the hybrid material most used in construction worldwide and its importance in modern engineering is paramount. Thus, to evaluate its lifecycle performance, it is important to understand the RC behavior under adverse environmental conditions. In particular, this work addresses the problem of concrete deterioration over time as a result of microbial attack. In this document, there is a description of novel experimental work directed to determine the effect of microbial attack on both physical and mechanical concrete properties. Also a proposal to take the biodeterioration effects into account in real structural design situations is presented.

The experimental work was conducted on a set of 13 mm x 13 mm x 10 mm mortar Portland type I cement that were inoculated with *Hallothiobacillus neapolitanus* NCIMB 8454 (H.n.) and *Acidithiobacillus thiooxidans* NCIMB 9112 (A.t.) using aseptic and non aseptic condition. Samples were exposed in two different experiments to peaks of 131 and 222 ppmv H_2S, $0.3\pm0.1\%CO_2$, for 300 and 153 days respectively. The analysis of porosity and strength changes in cement mortar from biodeterioration is a novel contribution of this study. Changes in porosity using mercury intrusion porosimetry, compressive strength and dry weight were measured. Total porosity loses up to 32% and 13% were observed after exposition of inoculated samples and non-inoculated samples, respectively. Major changes were observed in pore-sizes between 10 nm and 5000 nm, slightly smaller changes in pore sizes larger than 5000 nm and no changes in pores smaller than 10 nm. Inoculated samples showed a pronounced strength and weight loss after five months of exposition to bacteria compared to non-inoculated samples.

Previous findings and others reported in the literature were used to propose some considerations as to how to include biodeterioration into concrete design practice. To do so, probability of failure curves were fit from a model based on results obtained from a Matlab® code designed to run the structural analysis and simulate the Montecarlo's method simustaneously.

RESUMEN

El concreto reforzado (RC) es el material híbrido más usado a nivel mundial en la construcción. Su importancia en la ingeniería moderna es innegable. Por ello, entender su comportamiento bajo condiciones ambientales adversas es clave para comprender su desempeño durante su vida útil. Este trabajo se enfoca en el problema del deterioro del concreto producido por ataque microbiano a través del tiempo (biodeterioro). En este documento se presenta una descripción de un trabajo experimental novedoso dirigido a determinar el efecto del ataque microbiano sobre las propiedades fsicas y mecnicas del concreto. También se presenta una propuesta para tomar en cuenta el efecto del biodeterioro en situaciones reales de diseño.

El trabajo experimental usó muestras de 13 mm x 13 mm x 10 mm fabricadas con mortero de cemento Portland tipo I que fueron inoculadas con bacterias *Hallothiobacillus neapolitanus* NCIMB 8454 (H.n.) y *Acidithiobacillus thiooxidans* NCIMB 9112 (A.t.) inoculadas en condiciones asépticas y no asépticas. Las muestras fueron expuestas a picos de 131 y 222 ppmv $H_2S, 0.3 \pm 0.1\% CO_2$ durante 300 y 153 días respectivamente Un aporte novedoso de este estudio es la determinación de los cambios de porosidad y resistencia producidos por el biodeterioro en el mortero de cemento. Cambios de porosidad usando técnicas de porosimetría por intrusion de mercurio, cambios en la resistencia a la compressión y cambios en el peso seco de las muestras fueron medidos para las muestras. Después de la exposición, valores de porosidad total hasta de 32% y 13% fueron registrados en muestras inoculadas y no inoculadas respectivamente. Los cambios más pronunciados se observaron en tamaños de poro comprendidos entre 10 nm y 5000 nm, menores cambios en poros ms grandes que 5000 nm y cambios despreciables en poros más pequeños que 10 nm. Después de cinco meses de exposición las muestras inoculadas mostraron una importante pérdida de resistencia y de peso.

Los hallazgos de este estudio en conjunto con los de otros estudios previos se usaron para proponer algunas consideraciones sobre cómo puede incluirse el biodeterioro en la práctica del diseño estructural del concreto reforzado. Para hacer esto, se ajustaron curvas de probabilidad de falla a partir de un modelo basado en los resultados obtenidos de un código Matlab® diseñado para ejecutar simultáneamente el análisis estructural y el método de Montecarlo.

Contents

Abbreviations

ASOM	Acidophilic Sulfur Oxidizing Microorganisms
A.t.	It refers to: a) *Acidithiobacillus thiooxidans* bacteria. b) Set of samples inoculated in aseptic conditions with *A. thiooxidans* grown in SM
At	Set of samples inoculated in non aseptic conditions with *A. thiooxidans* grown in SM
Ats	Set of samples inoculated in non aseptic conditions with *A. thiooxidans* grown in MM
Cons.	Set of samples inoculated in aseptic conditions with *H. neapolitanus* and *A. thiooxidans* grown separately in SM
C-S-H	Calcium silicate hydrate ($3CaO_2SiO_24H_2O$)
ctrl	Set of abiotic samples used as control when studying effects related to bacteria inoculated in aseptic or non aseptic conditions
ESVR	Exposed surface/volume ratio (mm^2/mm^3)
H.n.	It refers to: a) *Hallothiobacillus neapolitanus* bacteria. b) Set of samples inoculated in aseptic conditions with *H. neapolitanus* grown in SM
Hn	Set of samples inoculated in non aseptic conditions with *H. neapolitanus* grown in SM
Hns	Set of samples inoculated in non aseptic conditions with *H. neapolitanus* grown in MM
MICC	Microbial induced concrete corrosion
MM	Seawater (salty) modified liquid medium (DSMZ 68 or DSMZ 35) for H.n. or A.t. growth
NSOM	Neutrophilic Sulfur Oxidizing Microorganisms
nt	Set of samples inoculated in non aseptic conditions with *H. neapolitanus* and *A. thiooxidans* grown separately in SM
nts	Set of samples inoculated in non aseptic conditions with *H. neapolitanus* and *A. thiooxidans* grown separately in MM
OD	Optical density
OM	Ordinary mortar samples
pH	Potential of hydrogen
PM	Pyritic mortar samples
ppmv	Parts per million in volume

RC	Reinforced concrete
RH	Relative humidity
SM	Standard liquid medium (DSMZ 68 or DSMZ 35) for H.n. or A.t. growth
SOB	Sulfur oxidizing bacteria
SRB	Sulfur reducing bacteria
TMI	Total mercury intrusion (ml/g)

Notation

As	Initial rebar area (m^2)
As_r	Reduced rebar area due to corrosion (m^2)
A_s	Spread wheel load area at the outside top of the pipe (m^2)
A_w	Wheel contact area (m^2)
b	Cross section width (m) for structural analysis of the pipe
B	Trench width (m)
c	Extreme fiber to rebar center distance (cm)
C	Trench load coefficient
d	Internal lever arm of the pipe section (m)
do	Available inner lever arm (m) at time $\tau = 0$
d_b	Mean bar diameter (m)
$d(\tau)$	Available inner lever arm (m) at time τ
Dw	Submerged depth of water in the inner of the pipe (m)
D_o	Outer pipe diameter (m)
D_i	Inner pipe diameter (m)
$f'c$	Compressive strength of concrete (kN/m^2)
f_y	Steel yield strength (kN/m^2)
H	Infill height placed upon the top of the pipe (m)
IM	Impact factor
k	Ratio of active unit pressure to vertical unit pressure
L	Relative sample weight loss computed from data (%)
Lfx, Lfy, Lfz	Final sample length side size in each perpendicular direction (cm)
Lox, Loy, Loz	Initial sample length side size in each perpendicular direction (cm)
Mn	Nominal bending capacity ($kN - m$)
pf	Probability of failure
P	Total live load applied at the surface (kN)
r	Thickness loss versus sulfur availability rate ($mm - cm^2/mgS$)
$s(t)$	Compressive strength (MPa) measured in each exposed sample at time t
s_i	Initial strength (MPa) measured in the control sample at time $t = 0$.

$Sa(t)$	Sulfur availability expressed in mg of elemental sulfur per cm^2 of exposed surface of mortar existing at time t
$Sa(\tau)$	Sulfur availability (mgS/cm^2) at time τ
Sa_{lm}	=Limit (threshold) value of Sa from which biodeterioration effects are evident (mg/cm^2)
t	Real time measured during the experiment ($days$)
u	Coefficient of friction between fill material and sides of trench
Vo	Initial volume of a sample computed from data (cc)
$w(t)$	Dry weight (mg) measured at time t
w_i	Initial dry weight (mg) measured at time $t = 0$.
Wf	Measured final dry weight of a sample (g)
Wo	Measured initial dry weight of a sample (g)
WL	Wheel load average pressure intensity (kN/m^2)
WF	Hydrostatic pressure at depth z(m) (kN/m^2)
WP	Pipe weight of a unit length arc (kN/m^2)
WS	Backfill pressure at the top of the pipe (kN/m^2)
$\vec{X}_R$	System resistance (i.e. bending moment capacity)
$\vec{X}_S$	Effect of loads demanding the system (i.e. demanded bending moment)
α	Bedding angle related to the soil reaction under the pipe
$\Delta_\phi(t)$	Porosity variation
$\Delta s(t)$	Compressive strength variation (%)
$\Delta t(\tau)$	Thickness loss (mm) at time τ
$\Delta w(t)$	Weight variation (%)
$\Delta x,\ \Delta y,$ Δz (cm)	Thickness loss in each perpendicular direction x, y, z of a sample
$\phi(t)$	Porosity (%) measured in each sample at time t
$\phi(i)$	Initial porosity (%) measured in control sample at time $t = 0$
γ	Backfill unit weight (kN/m^3)
ρ	Reinforcement steel ratio
$\sigma_\phi(Sa(\rho))$	Standard deviation of porosity variation estimated using the model at time τ (%)
$\sigma_s(Sa(\rho))$	Standard deviation of strength variation estimated using the model at time τ (%)
$\sigma_w(Sa(\rho))$	Standard deviation of weight variation estimated using the model at time τ (%)
τ	Time used in fitted equations into the model ($days$)

List of Figures

List of Tables

Chapter 1

INTRODUCTION

1.1 Description of the problem

Reinforced concrete (RC) is the hybrid material most used in construction worldwide and its importance in modern engineering is paramount. Reinforced concrete is a non-homogeneous material made of cement, aggregates (sand and gravel) and water, into which steel bars are embedded. Cement (Portland type) is mainly composed of dicalcium silicate ($2CaOSi_2$) (C_2S), tricalcium silicate ($3CaOSi_2$) (C_3S), tricalcium aluminate ($3CaOAl_2O_2$) (C_3A), tetracalcium aluminoferrite ($4CaOAl_2O_3Fe_2O_3$) (C_4AF), calcium sulfate or gypsum ($CaSO_42H_2O$), free lime and other compounds in small amounts. After hydration of the cement, calcium silicate hydrate C-S-H ($3CaO2SiO_24H_2O$) and Portlandite ($Ca(OH)_2$) are the most abundant and important products [7]. The presence of Portlandite in hardened cement paste can facilitate concrete deterioration as described in the following paragraphs.

RC constructions are subjected to different anthropic and natural hazards that cause the material to deteriorate. Concrete deterioration in RC structures can come in different forms. Sudden events (e.g. earthquakes, cyclones) or sustained demands caused by operation or environmental factors can lead to loss of structures' capacity. Large economic losses are usually associated with maintenance and recovery of deteriorated structures arising from physically, chemically and biologically adverse conditions.

As a result, RC structures' lifetimes can be severally reduced, bringing discomfort, unexpected costs, health problems, environmental detriment and low levels of service to a society.

The biological deterioration (biodeterioration) caused by microorganisms is a mechanism that has not been sufficiently studied yet. Nevertheless, the so-called microbial induced concrete corrosion (MICC) has become an important engineering issue in the last years. Understanding biodeterioration requires the consideration of both physical and chemical mechanisms by which microorganisms attack the material. In concrete structures, biodeterioration increases porosity and contributes to crack growth in the concrete matrix [8]. Proliferation of cracks and porosity augmentation in concrete that covers steel bars increases the rebars' exposure to the environment (e.g., chlorides, bacterial activity). In particular, changes in alkalinity from biological activity contribute to the depassivation of the reinforced steel surface, accelerating steel corrosion [9]. As a result, biodeterioration becomes a facilitator of failures in in RC structures (Figure 1.1).

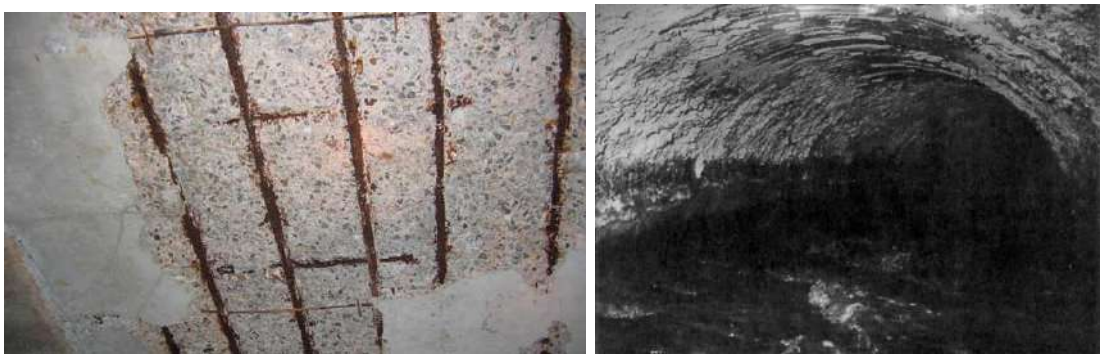

Figure 1.1: Examples of concrete biodeterioration (from http://www.engr.psu.edu) a) Exposed corroded reinforcement bars. b) Deteriorated concrete in sewer

1.2 Background of biodeterioration

Biodeterioration is defined as a reduction in material quality produced by vital activities of microorganisms [8]. For a better understanding of biodeterioration, it is helpful

to examine bioreceptivity, which is related to the intrinsic capability of a material to allow its colonization as well as the development living organisms [10] [11] [12] [13]. The bioreceptivity of concrete in indoor and outdoor environments can vary from inappreciable to very intense, influencing the biodeterioration start time [14].

Biodeterioration can be classified as: a) physical or mechanical; b) aesthetic; or c) chemical [8]. Physical or mechanical biodeterioration occurs when living organisms produce material breaking. In aesthetic biodeterioration organisms such as mold, mycelium and microalgae lead to surfaces fouling or soiling [15][16][17]. Finally chemical biodeterioration can come through assimilatory or dissimilatory paths. In assimilatory path organisms feed from material, while in dissimilatory path organisms excrete harmful products that damage it.

Between the previously described biodeterioration processes, chemical biodeterioration is usually the most aggressive. It is commonly produced from bacterial growth and requires humidity, cycles of humidification and drying, appropriate acidity and environmental nutrients to be viable. Bacteria, fungi, algae and lichens are the main organisms involved in concrete biodeterioration [8]. A comprehensive description of the processes and microorganisms related to concrete biodeterioration is presented in chapter 2.

1.3 Research objectives

The contribution of this study is the assessment of the physical (porosity and weight) and mechanical (i.e., compressive strength) consequences of biodegradation in mortar samples. The results would contribute to a better description of concrete biogenic corrosion processes, and consequently, to provide specific quantitative knowledge on concrete biodeterioration effects. This information is needed to improve the assessment of biodeterioration effects on concrete durability over time.

The specific objectives of this work are summarized as follows:

- To determine how biodeterioration produced by sulfur oxidizing bacteria affects

the physical properties (i.e., porosity and weight) of high surface/volume-ratio mortar samples.

- To determine how biodeterioration produced by sulfur oxidizing bacteria affects the mechanical properties (i.e., compressive strength) of high surface/volume-ratio mortar samples.
- To compare the effects produced by biogenic and chemical attack upon high surface/volume-ratio mortar samples.
- To evaluate the influence of sulfur availability on the biodeterioration produced by sulfur oxidizing bacteria upon high surface/volume-ratio mortar samples.
- To estimate the probability of failure of sewer pipes considering experimental results, and suggest the use of sacrificial layers in sewers pipes for guaranteeing given design service life values.

1.4 Thesis organization

This document is divided into six chapters. Chapter 1 presents the background and objectives of the thesis.

Chapter 2 describes the fundamentals of the concrete biodeterioration processes. Influence of biodeterioration in costs related to maintenance needs or reduction of service life of infrastructure systems is discussed. Also a description of the biodeterioration of sewers is presented. Finally, a summary of the more studied bacteria related to concrete biodeterioration and their effect upon the concrete health is presented.

Chapter 3 summarizes the applied experimental design. It explains the way in which the mortar samples were manufactured, inoculated and exposed to different environments. A description of the most important tests and the data to be collected is also presented. Data coming from qualitative description and variations in geometry, weight, porosity and strength of the samples are the most important outputs of the experimental work.

Chapter 4 presents the results and discussion of the preparations and general tests related to the experimental work. Descriptions of the bacterial growth and the sulfur availability achieved during the experiment are presented. Also results from chemical, topographic and volumetric tests such are summarized and interpreted.

Chapter 5 presents the results and discussion related to the physical and mechanical tests. Observed weight, porosity and compressive strength variations in mortar samples are described and analyzed. Besides, the strength to porosity relation is found and interpreted.

In chapter 6, a preliminary approximation to consider the effect of biodeterioration in practical applications is described. Firstly, the current practice in structural design of sewers is summarized. Secondly, the effects of the biodeterioration upon strength and inner forces redistribution are illustrated by an example. Thirdly, the probability of failure for different exposure and manufacturing conditions is computed. Finally, a proposal for including the effects of biodeterioration in the structural design of sewers is presented.

In chapter 7 the conclusions and recommendations of the thesis are presented. Also some ideas and suggestion for future work are given.

Chapter 2

FUNDAMENTALS OF BIODETERIORATION

2.1 Chapter overview

As explained in chapter 1, chemical biodeterioration produced by biongenic activity affects the concrete. It is necessary to understand how such processes occur. To achieve that, in this chapter a comprehensive description of the biodeterioration dynamics is presented. Then, in the following chapter the experimental development used in this study will be described. The objectives of this chapter are:

- To discuss critically the importance of the adverse effects of biodeterioration upon infrastructure systems, such as capacity and durability decrements, according to the existing literature and reports of previous studies.
- To describe how the chemical and biological processes affect the concrete sewers, underlining those related to the acidification of concrete surfaces.
- To describe bacteria that produce the most adverse effects related to biodeterioration of RC structures. This objective refers mainly sulfur oxidizing microorganisms

2.2 Importance of the biodeterioration effects upon infrastructure systems

Biodeterioration is usually overlooked because its kinematics is very slow and therefore, it remains undetected or neglected during the structural lifetime. Furthermore, although biodeterioration itself is rarely a direct cause of failure, it may play an important role in reinforced concrete degradation by accelerating other damaging processes such as chloride ingress (e.g., in marine environments or in structures subjected to deicing salt) and carbonation. These processes lead to corrosion propagation and loss of structural capacity [9][18].

The life-cycle analysis and modeling of infrastructure requires the understanding of concrete performance over time, which highly depends on the characterization of material degradation [19][20]. Although phenomena such as aging, fatigue and corrosion are known to be important agents for concrete degradation, it has been noted that in aggressive environments, the action of living organisms also affects critical infrastructure. These problems have been reported in, for example, oil pipelines [21], underground structures, sewage systems[22], and offshore structures [23][24]. Biodeterioration affects mainly concrete durability increasing maintenance costs [25][26], and reducing the capacity of structural members in the long term. Table 2.1 presents a summary of real costs associated to sewers failure.

Table 2.1: Cost arisen from sewers systems failure [6]

Asset description	Cost US$ billion/yr
Sewers replacement/Los Angeles, USA	468
Infrastructure repair and maintenance/United Kingdom	2,300
Sewers repair and maintenance/Belgium	6

2.3 Consequences of biodeterioration

2.3.1 Effects on concrete properties

Several studies have focused on the weight loss as an indicator of biodeterioration activity [19][27][28][29][30]. They report a wide range of weight loss observations (even for similar environmental conditions) ranging from negligible weight loss after 126 days of exposure [27] to total weight loss (100%) after 350 days [28]. The heterogeneity of the cementitious mortars and concrete, the variability of the environmental conditions, and the interactions and dynamics of the microorganisms involved in sulfur oxidation are only some of the aspects adding complexity to the description and quantification of the biodeterioration process [31].

Bielefeldt et al. measured a weight loss of 0.45% in samples cut from concrete pipes after 83 days of exposure to *Thiobacilli sp.* consortia and *A. cryptum* in a 300-600 ppmv H_2S atmosphere. Microbiological tests conducted by Monteny et al. showed that acidophilic microorganisms activity produced greater biodeterioration (weight loss up to 8%) than exclusive chemical effect (immersion and rotation in sulfuric acid) [32]. Parker and Prisk reported a weight loss of up to 12% after 90 days of exposure to sulfuric acid at pH=1.5 in plain concrete [33]. Starkey investigated the effect of *Thiobacilli sp.* by exposing concrete samples to H_2S, thiosulfate and methylmercaptan and found that bacterial growth only occurred in the first two. *T. thiooxidans* dominated the flora in the H_2S-rich environment while *H. neapolitanus* showed remarkable growth when thiosulfate was used as the main nutrient. *T. thiooxidans* produced the most severe deterioration with a weight loss of up to 5.8% after nine months of exposure [34].

Vollertsen et al. reported that even H_2S concentrations as low as 50-10 ppmv can produce deterioration in concrete sewers of up to several mm/year [35]. Aviam et al. used *H. neapolitanus* to degrade cement mortar samples and showed that a weight loss of up to 16% after 39 days of exposure is possible [36]. Okabe et al. measured weight losses of up to 37% in concrete coupons exposed to a succession of SOB for one year

[30]. Wells and Melchers reported that corrosion rates of old concrete were up to one order of magnitude greater (up to 7 mm/year) than those of new concrete [37]. They measured in situ H_2S concentrations of up to 680 ppmv , which could not necessarily be associated with the most severe corrosion compared to lower-H_2S-concentration environments. Beeldens et al., using microscope techniques, observed adverse effects of chemical and biogenic acid corrosion in concrete samples when exposed up to 250 ppmv H_2S [38].

In addition to weight loss, biodeterioration can also affect other physical and mechanical properties of concrete. During concrete biodeterioration, a layer of high porosity is produced by biogenic attack. This high porosity layer leads to greater permeability and diffusion within the inner matrix of the material [31][39]. On the other hand, compressive strength decreases for larger porosities in concrete and mortar specimens [40][41][42]. Consequently, the compressive strength of concrete components is affected by biodeterioration and must therefore be modeled as a time-variant property throughout the structural lifetime [6]. Although porosity and strength variations due to biodeterioration are paramount for structure condition assessment, to the authors' knowledge, nowadays there are no studies that include these parameters.

The relationship between compressive strength and porosity of concrete has not been sufficiently studied [42]. Some studies have investigated the effects of normal and acidic conditions on these two parameters, leading to models in which strength decreases while porosity increases [40][42]. For example, Kumar and Bhattacharjee exposed concrete specimens made of quartzite aggregates to atmospheric conditions and chemical acidic water reporting porosity values from 9.26% to 13.53% with no apparent preponderance of acidic conditions [42]. Solís-Carcaño and Moreno described porosity variations from 18.8% to 25.2% for water/cement ratios from 0.45 to 0.80 in a wide range of types of aggregates [43]. Ba et al. concluded that coarse pores have the most important influence on compressive strength [40]. Hincapié and Montoya found that dry concretes show major porosity that normal concretes but this condition does not affect the strength [44]. On the other hand, Bastidas et al. explained that,

once the steel corrosion process has been initiated in RC structures, low-density steel corrosion products fill the porous structure surrounding steel reinforcement and produce a volume increase that leads to cracking [9]. However, there is no concluding evidence from previous research related to the effect of biogenic attack on porosity and strength, making this an important issue to investigate. In summary, a good understanding of the porous structure of concrete is undeniable important.

2.3.2 Effects on chloride ingress

Another important aspect related to concrete biodeterioration is the effect of chloride ingress in offshore and inshore reinforced concrete structures like bridges [45]. Is is possible to find some sulfur oxidizing bacteria (SOB) belonging to the *Thiobacilli* species in the sea resulting in a possible path to biodeterioration by bacterial attack in chloride-rich environments [46][47]. Nevertheless, in most cases salty environments can inhibit *Thiobacilli* growth [48]. Biodeterioration weakens the RC matrix favoring cracking and porosity increase which facilitate chloride ingress. Chloride ingress through cracks or capillary structures within the concrete matrix leads to steel corrosion in RC structures. Moreover, steel reinforcement can also be corroded when exposed to sulfur-containing gases or microbial activity in the surrounding concrete [49].

Several models have attempted to describe and forecast chloride diffusion in saturated and non-saturated concrete [50][51][52][53]. There are also widely accepted tests to evaluate chloride diffusivity, like those stated in AASHTO T259 (ponding test) and ASTM C1202 (electrical conductance). This section is only intended to inform about the importance of the described topics and no work has been done related to this issue.

2.4 Biodeterioration in sewers

2.4.1 Chemical and biological deterioration in sewers

Hydrogen sulfide can be present in natural emissions, industrial waste, landfills, within sewers, and elsewhere. In concrete structures it can cause acidification directly from

chemical attack or indirectly from biological byproducts from microorganisms that use it as energy source. Nevertheless, sewer systems are known as one of the most probable and important biodeterioration targets. Permanent moisture, oxygen and water availability, formation of biofilms under anaerobic conditions, existence of partially oxidized sulfur compounds and H_2S, and warm temperatures can usually be found within sewers. In these systems, due to anoxic conditions commonly found in sewage, sulfate in wastewater is used by sulfur reducing bacteria (SRB) as an electron acceptor and sulfide is produced. At low pH, hydrogen sulfide gas volatilizes and rises to the tops of sewer pipes where aerobic microbial communities grow in biofilms [54][55]. Sulfur oxidizing bacteria (SOB) living in these biofilms use hydrogen sulfide or reduce sulfur compounds as electron donors and oxygen from air as an electron acceptor. The oxidation process generates sulfate or sulfuric acid [55][56]. The main consequence of sulfuric acid attack is the modification of the C-S-H structure of concrete that results from the reaction of sulfate ions with the cement hydration products. This process results in the formation of gypsum and ettringite, leading to the destruction of the hydration products that constitute the binder of concrete. The formation of ettringite may lead to increased tensile stress within the concrete matrix, resulting in cracking [31][57].

H_2S present in sewers is removed chemically by walls' sorption and biologically by bacterial metabolism in a process in which H_2S sorption to concrete surfaces is quite similar to H_2S biological uptake [58]. Cell adhesion and sulfuric acid attack are interfacial phenomena that depend on the surface area/surface roughness ratio [59][33]. The microbial succession is a surface phenomenon in which the Acidophilic Sulfur Oxidizing Microorganisms (ASOM) move into the corroding concrete while it becomes deeper but Neutrophilic Sulfur Oxidizing Microorganisms (NSOM) do not [60]. It has been observed that typical microorganisms in sewers are able to survive starvation up to for six months, recovering up to 80% of their initial growth rate when subjected to H_2S re-alimentation for a few days [61][62]

2.4.2 Sewer environment conditioning for biodeterioration

The ecology of the sulfur oxidizing microbial communities is highly dependent on the pH of the concrete matrix [63] [45]. After casting, the pH of concrete is higher than 12 (usually in the order of 13.5), which inhibits sulfur-oxidizing bacteria development. This alkalinity is produced mainly by formation of calcium hydroxide, $Ca(OH)_2$, during cement hydration. In sewer pipes, however, carbonation and exposure to hydrogen sulfide reduces concrete pH to a point at which neutrophilic microorganisms can grow. Among these, SOB grow and produce sulfuric acid (H_2SO_4), which also lowers the pH even further to a point at which acidophiles thrive. These new conditions trigger microbial growth with its correspondent metabolic byproducts. The so produced sulfuric acid reacts with calcium-hydroxide forming gypsum ($CaSO_4 2H_2O$). Gypsum reacts with tricalcium aluminate, leading to the formation of secondary ettringite (calcium trisulfoaluminate hydrate, $3CaOAl_2O_3 3CaSO_4 32H_2O$). Secondary ettringite causes swelling inside the concrete matrix, breaking its inner structure. [8][32][64][65].

When the typical pH of sewage environments has dropped to values lower than 6 or 7, H_2S becomes the dominant compound, which, in the presence of oxygen and sulfides, promotes the formation of partially oxidized sulfur like thiosulfate, elemental sulfur and polysulfate. These reactions, the turbulence of flow, the diameter of pipe and the depth of flow facilitate the augmentation of H_2S ingress into the condensed layer attached to the pipe walls. Then, because of the presence of CO_2, H_2S, oxygen, moisture and nutrients, *Thiobacilli sp.* can obtain energy, oxidizing sulfur to sulfuric acid (H_2SO_4) and growing in the new environment [8][34][64]. In general, it has been found that pH variations in concrete specimens subjected to biogenic attack are related to biodeterioration severity [19][27].

2.4.3 Bacteria species related to concrete biodeterioration

Biodeterioration from bacteria has been found to produce damage to aerial and buried RC structures. Sulfur-oxidizing bacteria and nitrifying bacteria can generate biogenic products that damage the concrete. *T. thioparus* (pH 4.5-10), *T. novellus* (pH 5-9.2),

H. neapolitanus (pH 4-9), *T. intermedius* (*Thiomonas intermedia*, pH 1.7-9), *Leptospirilium ferrooxidans* (pH 1.3-4.0), *T. ferrooxidans* (pH 1.5-3.3), *A. cryptum* (pH 0.1-5.2), *A. thiooxidans* (pH 0.5-4, formerly *T. thiooxidans*), *Thiothrix sp.*, *T. plumbophilus*, and *A. acidophilumn* are found in sewer environments [19][30][64][66][67]. *Acidithiobacillales* (which include *A. thiooxidans*) can represent only 4% of the total community living in sewers [65]. However, within this order, *Acidithiobacillus thiooxidans* (formerly *Thiobacillus thiooxidans*) has been found to be the most aggressive to concrete [30][64][66][67][68]. Other microorganisms such as the *fungus Fusarium* have been found to be harmful to concrete [22][69][70][71]. Nevertheless, Acidophilic Sulfur Oxidizing Microorganisms (ASOM) have been found to be more aggressive than Neutrophilic Sulfur Oxidizing Microorganisms (NSOM) and other bacteria an fungi.

In this study, one neutrophilic and one acidophilic bacterium have been selected for the experiment: *Hallothiobacillus neapolitanus* and *Acidithiobacillus thiooxidans*. The reason for this selection is that *H. neapolitanus* can be found on concrete at the beginning of the biocolonization when the pH is still high while *A. thiooxidans* thrives when pH is low. The optimum pH for the development of such bacteria varies about 6.7 and 3.0 for *H. neapolitanus* and *A. thiooxidans*, respectively [19].

Acidithiobacillus thiooxidans can be found in soils but are unable to survive after 24 hours of drying. However, it has been observed that these bacteria are able to develop after long periods of laboratory incubation [34].

In summary, *Acidithiobacillus thiooxidans* is an acidophilic and autotrophic bacterium capable of oxidizing sulfur compounds and obtaining its carbon from atmospheric CO_2. It is an aerobic obligately acidophilic Gram-negative bacterium that is motile by a polar flagellum and uses elemental sulfur, thiosulfate or tetrathionate. This bacterium, in the presence of oxygen, can convert hydrogen sulfide (H_2S) to sulfuric acid (H_2SO_4) [27]. A culture of *Thiobacillus thiooxidans* is not a homogenous community, but rather a set of organisms at different stages of development [72].

Hallothiobacillus neapolitanus, probably first isolated from sea water in Naples in 1902, is a halophile obligately chemolithoautotrophic Gram-negative bacterium that

obtains its energy from reduced inorganic sulfur compounds, among which thiosulfate is the best suited for optimal growth. This species was initially classified as *Thiobacillus X* and has been isolated from seawater and compost [73].

2.5 Summary and conclusions

The following conclusions respond to the objectives written at the beginning of this chapter.

- The biogenic and chemical deterioration can potentiate the physical damage due to the chemical reactions leading to the structural breaking of the concrete matrix. It has been observed that biogenic deterioration (biodeterioration) is usually faster and more catastrophic than pure chemical or physical deterioration.
- It has been found that *Acidithiobacillus thiooxidans* are the most harmful bacteria related to the concrete biodeteriortaion in sewers. Other microorganisms like the fungus Fussarium and the neutrophilic bacteria *Hallothiobacillus neapolitanus* have been found to be less aggressive but important to the sewer biodeterioration processes.
- Weight loss, porosity augmentation, and strength decrease are the most adverse changes resulting from concrete biodeterioration. Cracking and consequent permeability increase related to the described effects facilitate the chloride ingress and steel rebar corrosion shortening the structural durability.

Chapter 3

EXPERIMENTAL SETUP

Several reports related to the concrete biodeterioration based on weight loss measurements were cited in the previous chapter. No information related to the porosity and strength changes using the same samples is found in the literature. For this reason, in this study weight, porosity, and compressive strength variations produced by biodeterioration in mortar samples were measured. Such changes were measured using samples which have a high exposed surface in a non-aqueous environment.

3.1 Chapter Overview

This chapter presents the design of the experiment and its objectives are:

- To develop a methodology for measuring and interpreting the physical and mechanical changes produced by biodeterioration in mortar samples within a controlled environment.
- To design the experimental setup for manufacturing, conditioning, exposing, and measuring the mortar samples behavior when deteriorated by biogenic attack.
- To interrelate the physical, chemical and biological processes using the same samples and environmental conditions to facilitate a comprehensive interpretation of the results.

3.2 Basic principles of the experiment

As explained in chapter 2, most previous studies have focused their experiments on weight loss measurements. Samples used in those works have usually been cut and brushed to determine such measurements. In this study, not only weight losses were determined but strength and porosity were measured using scaled tests for the first one and mercury intrusion porosimetry technics for the second one. In addition, samples were not manipulated excesively. No brushes or cutting tools were used to modify the final condition of samples. Also, in this study samples have a high exposed surface to volume ratio (ESV). This feature and the low saturation degree of the surfaces (non-aqueous) probably impose to this experiment a more severe condition than previous studies.

Figure 3.1 presents a graphical summary of the experimental protocol. Four operational fringes have been defined for this study:

- First fringe (green) describes the biological processes in which the bacterial strains are resuscitated, cultured and precipitated. All these processes were made following the recommendations of the supplier of microorganisms. At the end of this fringe inoculum to be applied to samples was ready to use. This part of the protocol is explained in section 3.3.

- Second fringe (yellow) refers to the production of samples hospitable to the inoculum. Manufacturing, carbonation and sterilization of mortar samples are included in this part of the protocol. Also two common activities (samples inoculation and samples exposure) are considered in this fringe. Samples inoculation requires to apply the result of the first fringe upon the solid samples prepared as explained. Then, inoculated samples are exposed to the environment generated in the third fringe. In section 3.4. this part of the protocol is explained.

- Third fringe (violet) shows the procedures followed to manufacture containers and calibrate and produce the gaseous environment required at the inner of them. More details of this part of the protocol are described in section 3.5.

- Fourth fringe (white) contains the processes related to the mechanical and physical tests to be applied to the samples.

In this study three classes of samples were prepared:

- OM: Ordinary mortar samples whose characteristics are described in table 3.1 and section 3.4.1.
- PM: Pyritic mortar samples whose characteristics are described in table 3.1 and section 3.4.2.
- TM: Mortar samples added with Triclosan (TM) whose characteristics are described in table 3.1 and section 3.4.3.

Table 3.1: Description of mortar samples used in the experiment development

Class	Name	Raw material and additions	Qty
OM	Ordinary mortar samples	Portland cement, river sand, water	1.200
PM	Pyritic mortar samples	OM, Fe, S or FeS_2	1.500
TM	Mortar samples added with Triclosan	OM, Triclosan	500

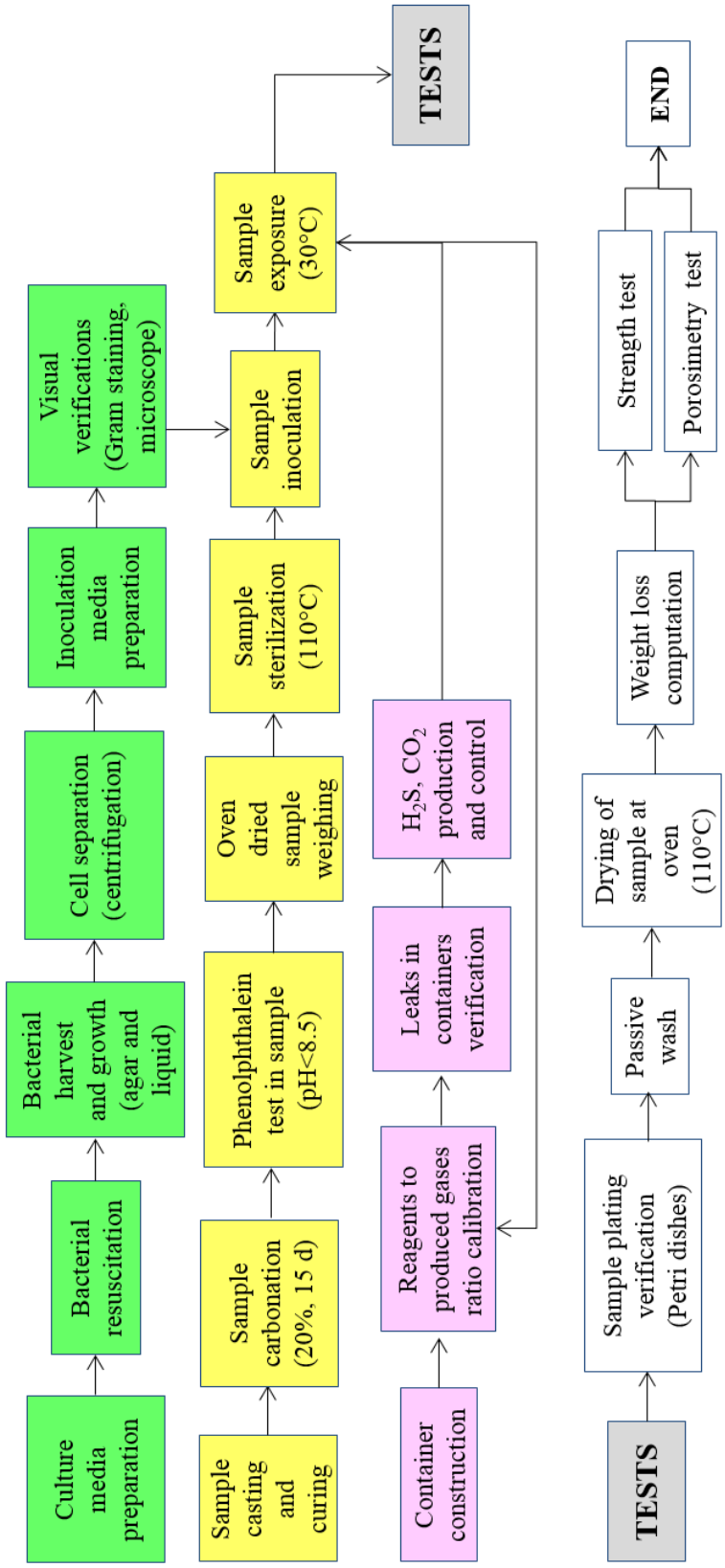

Figure 3.1: General experimental protocol

3.3 Culture growth and inoculation of mortar samples

Hallothiobacillus neapolitanus NCIMB 8454 and *Acidithiobacillus thiooxidans* NCIMB 9112 (ATCC8085) were purchased from American Type Culture Collection (ATCC) (Virginia, USA). Pure cultures were grown in DSMZ (Deutsche Sammlung von Mikroorganismen und Zellkulturen) 68 *Thiobacillus neapolitanus* agar/liquid medium or DSMZ 35 *Thiobacillus thiooxidans* agar/liquid medium, as recommended by supplier. Figure 3.2.

Figure 3.2: Culture grown in tubes and plates: *H. neapolitanus* (left) and *A. thiooxidans* (right)

In order to evaluate the effect of NSOM and ASOM on mortar biodeterioration, the prepared samples were subjected to different bacterial attack environments. NSOM

Hallothiobacillus neapolitanus (H.n.) and ASOM *Acidithiobacillus thiooxidans (A.t.)* growth in six standard and four salty media was implemented. DSMZ 68 *Thiobacillus neapolitanus* liquid medium and DSMZ 35 *Thiobacillus thiooxidans* liquid medium led to the best behavior of bacterial development in both standard (SM) and salty liquid (MM) (Table 3.2).

Figure 3.3: Orion 4Star pH meter and spectrophotometer Genesys 10UV (Thermo ®)

Prior to inoculating mortar samples, bacterial cells were grown in liquid media to an optical density (OD) 600 of 1.0. Figure 3.3. Cultures were centrifuged (4^{o}C, 13000 rpm, 15 min) to separate cells from growth medium and were triple washed with mineral medium containing no source of sulfur. Washed cells suspended in mineral medium (without sulfur) were used to inoculate mortar samples. Oven-dried mortar samples were soaked in cell suspensions of *A. thiooxidans*, *H. neapolitanus*, or a consortium of both.

Table 3.2: Description of medium used in cultures development (culture media)

Medium type	**Description**	**Related Samples**
SM	Standard liquid medium (DSMZ 68 or DSMZ 35)	Hn,At,nt
MM	Seawater modified liquid medium (DSMZ 68 or DSMZ 35)	Hns,Ats.nts

In order to have cultured bacteria available at any moment, the first incubated liquids were mantained, renovating them with fresh media approximately once a fort-

night. Furthermore, pH variation was measured throughout the experimentation time to verify that the bacteria were actually growing. pH variation was measured using an Orion 4Star pH meter (Thermo ®) (Figure 3.3).

Fresh inoculated media were applied to the samples three times on days 0, 15 and 30 to guarantee an initial bacterial dynamic activity.

Acidithiobacillus thiooxidans showed a similar growth rate in both SM and MM media, while *Hallothiobacillus neapolitanus* developed ten times faster in the salty medium than in the standard medium.

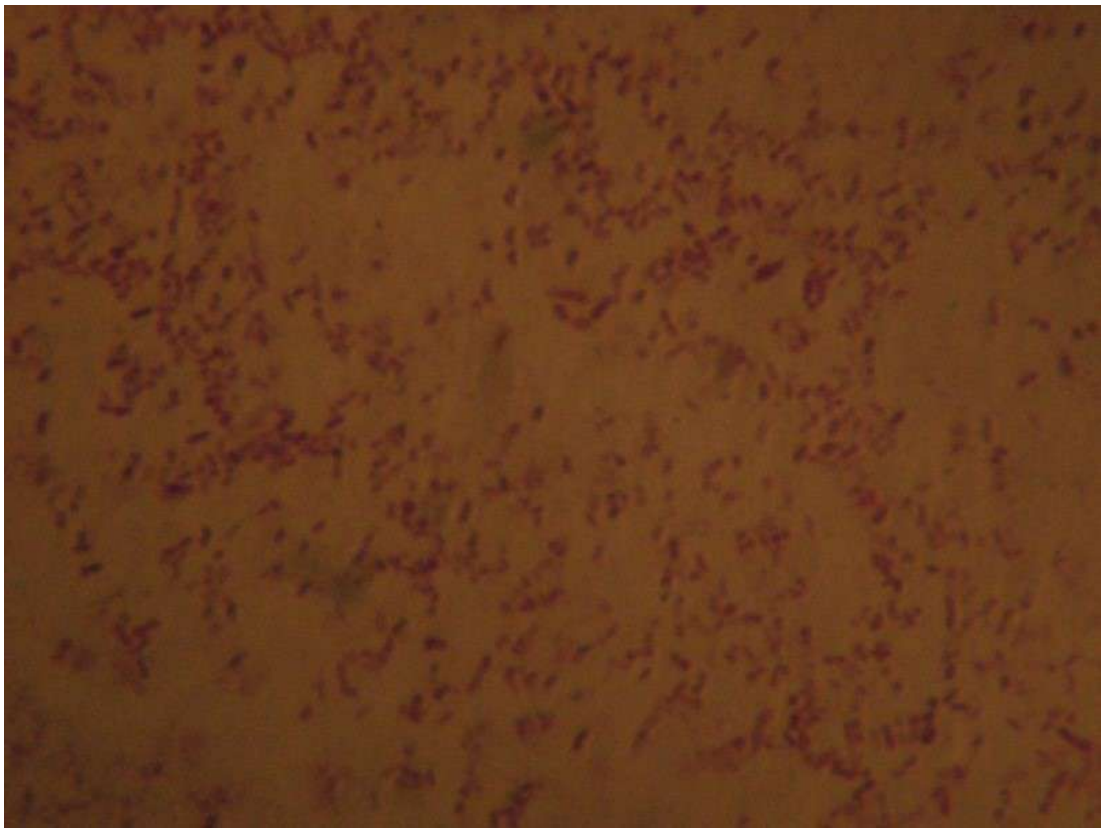

Figure 3.4: 100X photograph of *Hallothiobacillus neapolitanus* culture

In order to check the morphology of bacteria stuck on sample surfaces, microscope and SEM images were taken on day 15 of the experiment (Figure 3.4) and (Figure 3.5).

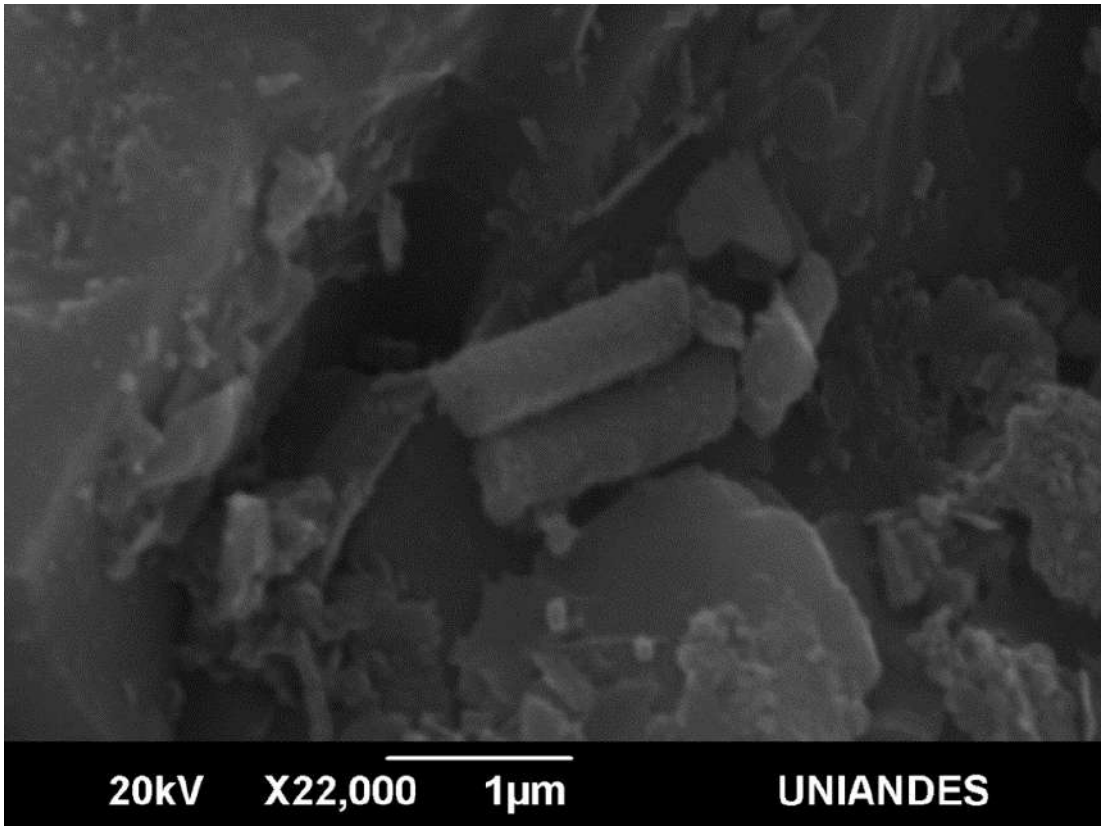

Figure 3.5: SEM image of initial inoculation with *A. thiooxidans*

3.3.1 Inoculation of OM samples in non aseptic conditions

Sterilized OM samples were submerged during 30 seconds into SM and MM media as described in Table 3.3. Then they were put into the apparatus described in section 3.6. In this case, no sterile conditions were guaranteed when manipulating the samples through the whole duration of the experiment. The term "non aseptic conditions" refers to the possible existence of many other microorganisms capable of surviving in the given experimental environment which could ingress to the containers while samples were extracted.

3.3.2 Inoculation of OM samples in aseptic conditions

Sterilized OM samples were submerged during 30 seconds into SM media as described in Table 3.4. Then they were put into the apparatus described in section 3.6. In this case, sterile conditions were guaranteed when manipulating these samples through the whole duration of the experiment to guarantee the purity of strains within the containers.

Table 3.3: Exposure conditions of OM samples inoculated in non aseptic conditions

Sample name	Superficial treatment (inoculation)	Environment
Hn	*H.neapolitanus* standard medium (SM)	$\leq$ 222 ppmv H_2S, $0.3 \pm 0.1\%$ CO_2
At	*A. thiooxidans* standard medium (SM)	$\leq$ 222 ppmv H_2S,$0.3 \pm 0.1\%$ CO_2
nt	Consortium (H.n+A.t.) standard medium (SM)	$\leq$ 222 ppmv H_2S, $0.3 \pm 0.1\%$ CO_2
ctrl	Abiotic control	Ordinary humid atmosphere
H_2S	Chemical control	$\leq 222 ppmv$ H_2S
Hns	*H.neapolitanus* seawater medium (MM)	$\leq$ 222 ppmv H_2S, $0.3 \pm 0.1\%$ CO_2
Ats	*A. thiooxidans* seawater medium (MM)	$\leq$ 222 ppmv H_2S, $0.3 \pm 0.1\%$ CO_2
nts	Consortium (H.n+A.t.) seawater medium (MM)	$\leq$ 222 ppmv H_2S, $0.3 \pm 0.1\%$ CO_2

Table 3.4: Exposure environments of OM samples inoculated in aseptic conditions

Sample Name	Superficial treatment (inoculation)	Feeding conditions
H.n.	*H. neapolitanus* standard medium	$\leq$ 131 ppmv H_2S, $0.3 \pm 0.1\%$ CO_2
A.t.	*A. thiooxidans*, standard medium	$\leq$ 131 ppmv H_2S, $0.3 \pm 0.1\%$ CO_2
Cons.	Consortium, standard medium	$\leq$ 131 ppmv H_2S, $0.3 \pm 0.1\%$ CO_2
H_2S	Chemical exposure (abiotic)	$\leq$ 131 ppmv H_2S, $0.3 \pm 0.1\%$ CO_2
Ctrl.	Control	Ordinary humid atmosphere

3.3.3 Inoculation of PM samples in non aseptic conditions

Sterilized PM samples were submerged during 30 seconds into SM and MM media as described in Table 3.5. Then they were put into the apparatus described in section 3.6. No sterile conditions were guaranteed when manipulating these samples through the whole duration of the experiment. The term "non aseptic conditions"refers to the possible existence of many other microorganisms capable of surviving in the given experimental environment which could ingress to the containers while samples were extracted.

Table 3.5: Contents of containers for biodeterioration test of pyritic mortar

Sample Name	Addition	Bacteria and environment
HnF1	Fe: 0.47%	*H.neapolitanus*, 30^oC, $50 \pm 10\%$ HR
HnS1	S: 0.53%	*H.neapolitanus*, 30^oC, $50 \pm 10\%$ HR
HnFS1	FeS_2: 1.00%	*H.neapolitanus*, 30^oC, $50 \pm 10\%$ HR
HnF5	Fe: 2.35%	*H.neapolitanus*, 30^oC, $50 \pm 10\%$ HR
HnS5	S: 2.65%	*H.neapolitanus*, 30^oC, $50 \pm 10\%$ HR
HnFS5	FeS_2: 5.00%	*H.neapolitanus*, 30^oC, $50 \pm 10\%$ HR
AtF1	Fe: 0.47%	*A. thiooxidans*, 30^oC, $50 \pm 10\%$ HR
AtS1	S: 0.53%	*A. thiooxidans*, 30^oC, $50 \pm 10\% HR$
AtFS1	FeS_2: 1.00%	*A. thiooxidans*, 30^oC, $50 \pm 10\%$ HR
AtF5	Fe: 2.35%	*A. thiooxidans*, 30^oC, $50 \pm 10\%$ HR
AtS5	S: 2.65%	*A. thiooxidans*, 30^oC,$50 \pm 10\%$ HR
AtFS5	FeS_2: 5.00%	*A. thiooxidans*, 30^oC, $50 \pm 10\%$ HR
F1	Fe: 0.47%	Non-inoculated, 30^oC, $50 \pm 10\%$ HR
S1	S: 0.53%	Non-inoculated, 30^oC, $50 \pm 10\%$ HR
FS1	FeS_2: 1.00%	Non-inoculated, 30^oC, $50 \pm 10\%$ HR
F5	Fe: 2.35%	Non-inoculated, 30^oC, $50 \pm 10\%$ HR
S5	S: 2.65%	Non-inoculated, 30^oC, $50 \pm 10\%$ HR
FS5	FeS_2: 5.00%	Non-inoculated, 30^oC, $50 \pm 10\%$ HR
Ctrl	0%	Non-inoculated, 30^oC, $50 \pm 10\%$ HR

3.3.4 Inoculation of TM samples in aseptic conditions

Sterilized TM samples were submerged during 30 seconds into SM media as described in Table 3.6. Then they were put into the apparatus described in section 3.6. Sterile conditions were guaranteed when manipulating these samples through the whole duration of the experiment to guarantee the purity of strains within the containers.

Table 3.6: Exposure environments of TM samples inoculated with Consortia (Cons.).

Sample Name	Aggregate replacement	Environment
T1	0.25% Triclosan	≤ 131 ppmv H_2S, $0.3 \pm 0.1\%$ CO_2
T2	0.50% Triclosan	≤ 131 ppmv H_2S, $0.3 \pm 0.1\%$ CO_2
T3	1.00% Triclosan	≤ 131 ppmv H_2S, $0.3 \pm 0.1\%$ CO_2
H_2S	Chemical exposure (abiotic)	≤ 131 ppmv H_2S, $0.3 \pm 0.1\%$ CO_2
Ctrl.	Control	Ordinary humid atmosphere

3.4 Sample casting and curing

The following three classes of samples were cast and exposed to different environments. Both classes were made using Type I Portland Cement (Cement).

- Ordinary mortar samples (OM). These samples were made using Cement, River Sand and Water. They were inoculated and exposed to two different H_2S-rich environments as explained later as shown in Table 3.3 and 3.4
- Pyritic mortar samples (PM). These samples were made using Cement, River Sand mixed with variable proportions of FeS_2, Fe, S, and water. They were inoculated and exposed partially submerged in water to ordinary environment as shown in table 3.5.
- Mortar samples added with Triclosan (TM). These samples were made using Cement, River Sand and Water. Little amounts of Triclosan were added. They were inoculated in aseptic conditions using a consortia of two strains and exposed to two one H_2S-rich environment as shown in table 3.6.

3.4.1 Ordinary mortar samples (OM)

Portland cement mortar 13mm×13mm×10 mm samples with water-to-cement ratios of 0.485 were cast into a plastic container without a mold release agent. Casting was made by compacting two successive layers with a plastic rammer after 30 seconds of vibration with a pneumatic motor table. ASTM C778-06 standard graded natural river sand and Portland cement type I were used. Commercial cement was used. No further chemical analysis was applied to the cement. Cement paste-sand mix was blended using a five-pound mixer (Hamilton Beach Commercial) with a cement-to-sand relationship of 1:2.75. Afterward, casting molds containing fresh samples were wrapped with stretch film and stored at 20^{o}C for 24 hours. During 30 days demolded samples were twice a day water sprayed and kept in an airtight container for curing (90% $\pm$ 5 relative humidity (RH) measured at headspace). Cured samples were oven dried at 110^{o}C for

Figure 3.6: Casting and curing of samples

24 hours and then subjected to an "ordinary atmospheric"period for another 60 days at 20 ± 2^oC and $60 \pm 10\%$ RH (Figure 3.6). This two-month initial phase attempted to simulate the typical waiting period before new sewer pipes are put into service. RH and temperature measurements were taken using a digital thermo-hygrometer Thermo®. During the curing and preparation period samples were not oven-dried. Oven-drying was carried out only prior to the weighing process and for sterilization.

A strength scaling process was carried out to extrapolate the results to 13mm×13mm ×10mm samples. In order to have a valid pattern to compare strength results obtained for samples, 50mm-side cubic samples were cast, cured and exposed under similar conditions to those of 13mm×13mm ×10mm samples (Figure 3.7). 50mm-side samples were made of ordinary Portland cement mortar using OM mix and following ASTM C109/C109M12. See section 3.8.3.

3.4.2 Pyritic mortar samples (PM)

This section describes the experimental conditions for high surface/volume-ratio pyritic mortar samples to bacterial attack in a moist environment at 30^oC and with continuous availability of atmospheric oxygen.

Samples of 13mm×13mm×10mm made of Portland cement and pyritic aggregates mortar with a water-to-cement ratio of 0.485 were cast into a plastic container without

Figure 3.7: Cubic 50mm×50mm×50mm samples made of ordinary mortar (OM mix)

a mold release agent. Casting was done by hand, compacting two successive layers with a plastic rammer after 30 seconds of vibration with a pneumatic motor table. ASTM C778-06 standard-graded natural river sand, pyrite, sulfur, iron, and Portland cement type I were used. Content of additions in percentage of weight of the aggregate are shown in Table 3.7. Pyrite and sulfur additions were sieved 50% below mesh size 16 and 50% below mesh size 50 (grain sizes smaller than 1.52 mm and 0.30 mm, respectively). Samples containing 0% additions were also cast to be exposed to ordinary atmospheric environment. Cement paste-aggregate mix was blended using a five-pound mixer (Hamilton Beach Commercial) with a cement-to-aggregate relationship of 1:2.75. Casting molds containing fresh samples were later wrapped with plastic and stored at 20^oC for 24 hours. Demolded samples were subjected to 90% RH curing for 30 days inside closed plastic boxes using sprayed water. Cured samples were oven dried at 110^oC for 24 hours and then subjected to a "normal atmospheric"period for two more days at 20 ± 2^oC and $60 \pm 10\%$ RH.

The inclusion of the PM samples in this study is an attempt to understand the biodeterioration effects upon concretes made using non-conventional aggregates. It is widely accepted that Pyrite (FeS_2) is the most abundant of the sulfide minerals on the Earth's surface [74]. Pyrite can exist in soils composed of shale, sandstone, granite and clay, which can be used as aggregates [75][76]. Nowadays, the building industry

Table 3.7: Mixes for pyritic-mortar casting

Name and description	Addition weight/Aggregate weight
P1: Pyrite (FeS_2, Alfa-Aesar ®)	1%
P2: Pyrite (FeS_2, Alfa-Aesar ®)	5%
I1: Iron (Fe, Sigma-Aldrich Iron puriss.<212um ®)	0.47%
I2: Iron (Fe, Sigma-Aldrich Iron puriss.<212um ®)	2.35%
S1: Elemental sulfur (S, Sigma-Aldrich Sulfur puriss.,99.5%/100.5% ®)	0.53%
S2: Elemental sulfur (S, Sigma-Aldrich Sulfur puriss.,99.5%/100.5% ®)	2.65%

demands high amounts of aggregates for concrete. Important cities in the world have been developed on lands where availability of high-quality materials is becoming scarce and pyritic sedimentary rocks are increasingly being used for concrete 77[78]. In addition, the development of green concretes is an attempt to use debris that could contain different types of minerals [79].

Pyrite is highly susceptible to natural weathering [80]. Oxygen availability, warm temperatures and moisture trigger a rapid chemical oxidation that can be developed in a few weeks or months. Pyrite is an effective reducing agent able to use dissolved oxygen in groundwater in a wide pH range, whereby oxidized deposits can be found even under the soil [75][76][81].

Typical pyrite contents in soils containing sulfides can vary from 0.1% to 20% [75][80][81][82]. When these soils are used as aggregates within concrete subjected to moisture, an oxygen-rich environment and medium temperatures (20-35%), oxidation of pyrite occurs inside of it. Oxidation of pyrite produces sulfuric acid (H_2SO_4) that reacts with Portlandite ($Ca(OH)_2$), causing important volumetric and mineralogical changes, which lead to cracking of the concrete matrix [78][81][83]. The volume changes produced this way can be equivalent to more than five times the initial volume of the pyritic matter and generate expansion pressures of 583 kPa or higher [76]. Sulfates and secondary ettringite are also formed in the described reaction, but their effect is much less than that mentioned above [82].

There is a lack of publications dealing with the chemical-microbiological oxidation processes of pyrite. Nevertheless, it has already reported that pyrite can also be degraded by biological processes [76]. *Thiobacilli* species, particularly *Acidithiobacillus ferroxidans*, *Acidithiobacillus thiooxidans* and *Thiobacillus thioparus* have been found to be able to oxidize pyrite, producing pH substrate variations from 5.0 to 1.5 and dissolving Fe and S species from FeS_2 [78][84]. Total bulk expansion of soil mixed with low pyrite content after 400 days of reaction has been linked to volume increase of 57% at 21^{o}C and 110% at 38^{o}C. Otherwise it has been reported that the presence of carbonates like calcite ($CaCO_3$) can inhibit the adaptation phase of bacteria [81][84]. In synthesis, biological deterioration of concrete made with pyritic aggregates will only be possible if the pH range coincides with that of the bacterial survival and if the quantity of carbonates is not too high. In any case, production of (H_2SO_4) coming from the initial stages of reaction can lead to acidification of substrate, giving the bacteria a propitious environment in which to grow.

3.4.3 Mortar samples added with Triclosan (TM)

Ordinary mortar mix prepared as described in section 3.4.1 was modified replacing 0.25, 0.50 and 1.00% of the sand weight with Triclosan (5-chloro-2-(2,4-dichlorophenoxy) phenol) powder. Such additions of antimicrobial compound were intended to determine its inhibitory effect when forming part of the bulk mix of mortar. Referred proportions of Triclosan are economical and smaller than those used in the single similar study found in the literature [85]. Conditions of exposure are indicated in Table 3.6 3.6.

3.5 Carbonation of samples

To lower the surface alkalinity of the mortar samples, they were submerged in distilled water enriched with commercial carbon dioxide (22$\pm$3%CO_2). In this paper this process is referred as "carbonation". For 14 days CO_2 gas was bubbled into the water of each airtight container, on daily basis for 60 s, until the CO_2 pressure in the headspace

reached 0.22atm. Surface pH of all samples was reduced from around 12 to less than 9 (verified with phenolphthalein test) [12][86] (Figure 3.8). Depth of carbonation was not measured. After carbonation nine groups composed of 76 samples each were oven dried at 110^{o}C for 24 hours. Then samples were kept at room temperature for ten minutes and then weighed. These data were recorded as initial dry weight (t=0). Once weighed all the samples were wrapped using foil and oven dried 110^{o}C for 24 hours for sterilization purposes.

Figure 3.8: Non-carbonated (left) and carbonated samples (right) before exposure. In this picture, non-carbonated have the half of the size of carbonated samples

3.6 H_2S generation and sulfur availability

The device used for the exposure of the samples in each test is shown in Figure 3.9. Typical apparatus was assembled using a 5cmX18cmX18cm hermetic plastic container in which 8-mm high liquid layer was placed at the bottom. A plastic bearing structure

and a plastic net over which samples were placed, separating them 25 mm from the water surface, was placed into the container. Distilled water, hydrochloric acid (HCl), sodium sulfide nonahydrate (Na_2S9H_2O) and sodium bicarbonate ($NaHCO_3$) were mixed in variable proportions to achieve hydrogen sulfide (H_2S) and carbon dioxide (CO_2) concentrations required in each case. A uniform mix of those reagents was achieved by means of slight movements of three small crystal balls after closing the container. A gas reading port was set on the lid for the gas concentrations control. Each container served to expose 76 samples.

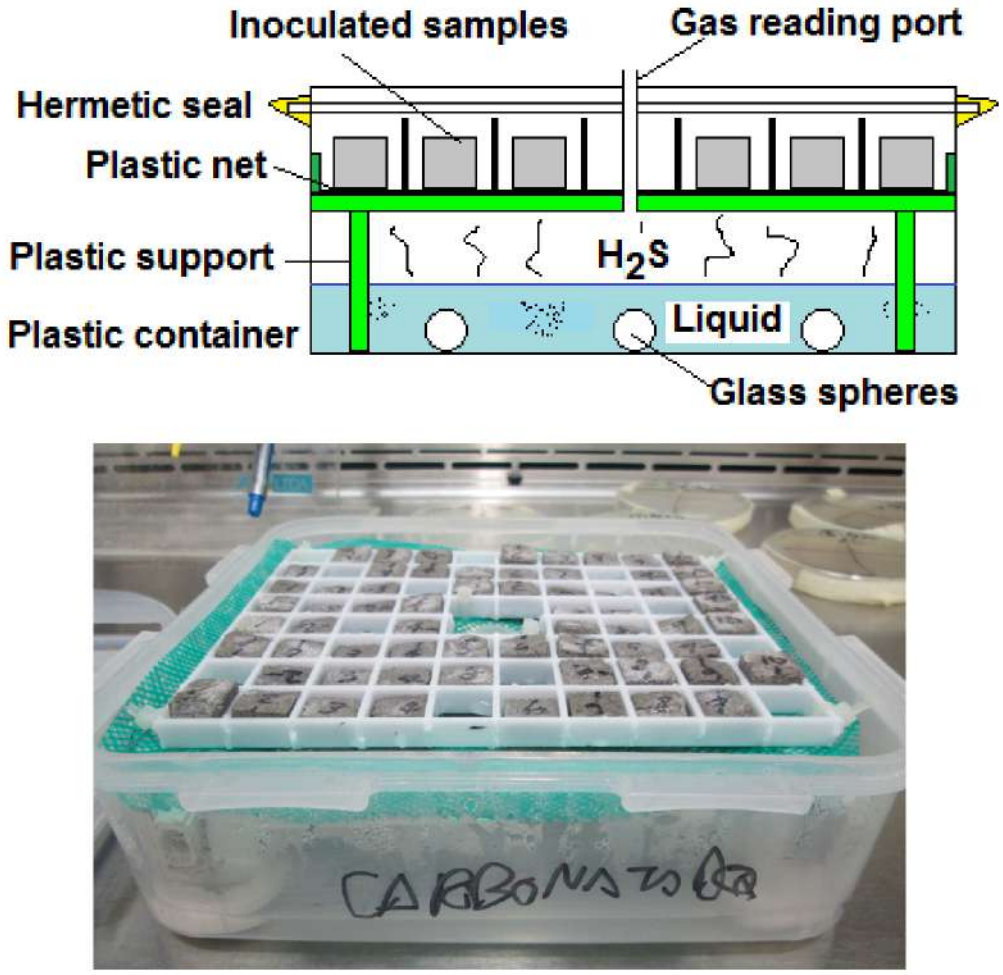

Figure 3.9: Apparatus for samples exposure

Leaching of gases from the container was verified by reading outside H_2S concentration within a sealed 30cm×40cm×60cm incubator after four hours of gas incubation. New containers showed outside concentrations below than 0.5 ppmv H_2S, while the oldest containers (after five months of exposure) showed almost 4 ppmv H_2S after accumulation of four hours. Portable Gas Analyzer BioGas CDM (LANDTEC ®) and Portable Gas Analyzer RKI GX2009 (RKI Instruments ®) were used to measure H_2S, CO_2 and O_2. Figure 3.10.

Figure 3.10: Portable Gas Analyzer BioGas CDM (LANDTEC ®) and RKI GX2009 (RKI Instruments ®)

A central element of the study is the variation of H_2S concentration over time. Addition of hydrogen sulfide and carbon dioxide resulted in the production of the gases in the environment that rapidly decreased over time. For H_2S concentrations up to 131 ppmv, an equivalent average continuous rate of 12±4 ppmv/h (mean ± one standard deviation) was computed. In this case, H_2S was available to microorganisms for only about 8 hours after addition of the reagents to the liquid underneath the mortar samples (Figure 3.11). For H_2S concentrations up to 222 ppmv, the average continuous rate was 25±6 ppmv/h (mean ± one standard deviation) consuming the totality of hydrogen sulfide applied in about 15 hours (Figure 3.12).

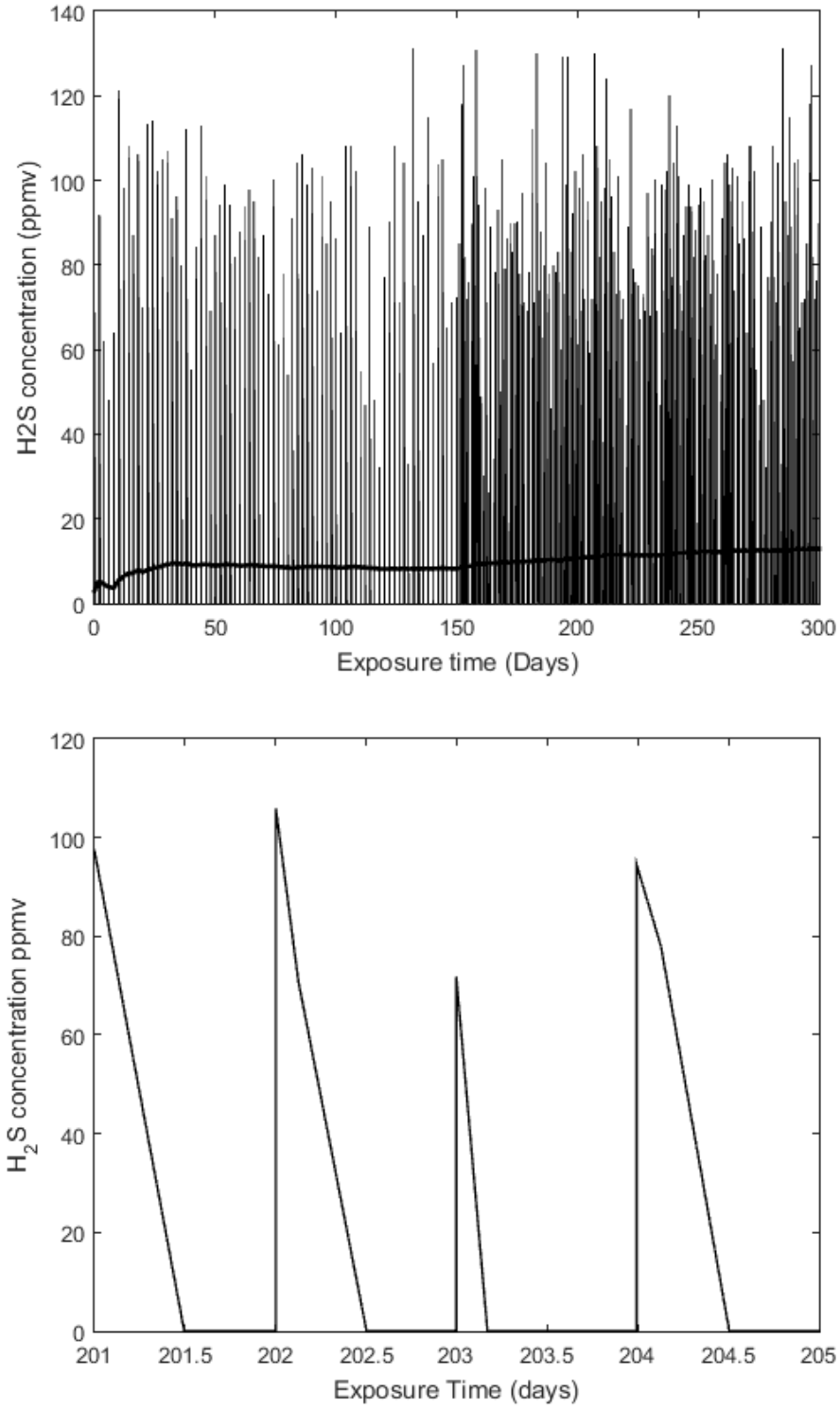

Figure 3.11: Hydrogen sulfide concentration observed in one container for H_2S peaks up to 131 ppmv: a) total time window (heavy line shows the continuous equivalent concentration), b) example of applications during 5 consecutive days

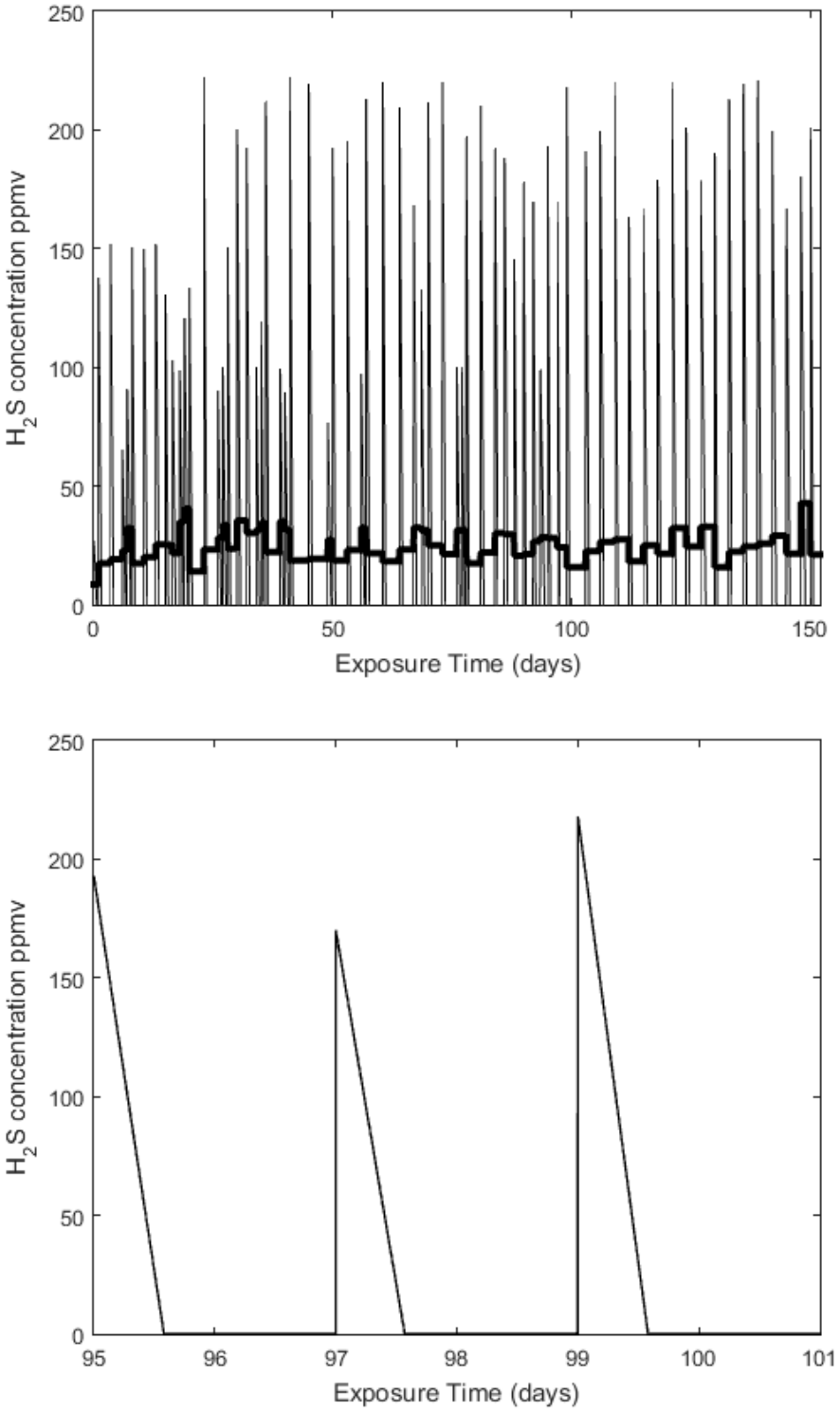

Figure 3.12: Hydrogen sulfide concentration observed in one container for H_2S peaks up to 222 ppmv: a) total time window (heavy line shows the continuous equivalent concentration), b) example of applications during 5 consecutive days

The rapid decrease of hydrogen sulfide concentration in the headspace suggests that there is a high sorption capacity of the concrete samples. It is likely that at low H_2S headspace concentrations, biogenic effects became more important than chemical sorption [62]. Figure 3.13 and Figure 3.14. show the sulfur availability $Sa(t)$ through the time for both H_2S concentrations. The sulfur availability is the accumulated amount of sulfur applied (mg) with respect to the exposed area (cm^2) of the samples at each age. Exposed-area-to-weight ratio of mortar samples was of 2.91±0.01 cm^2/g.

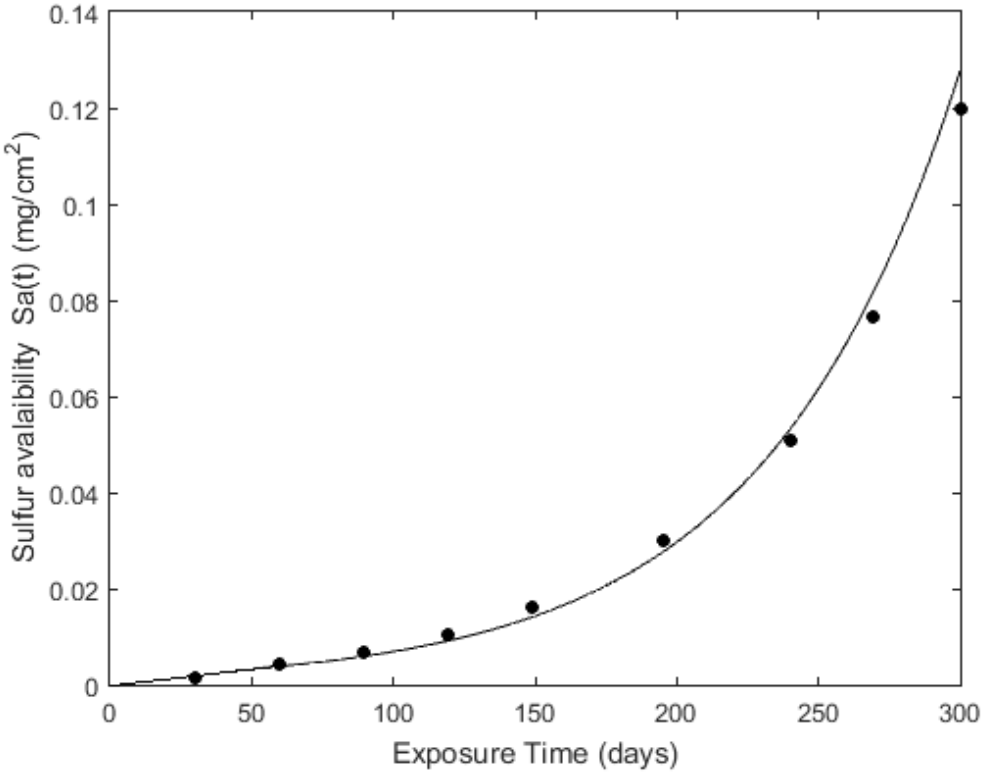

Figure 3.13: Applied sulfur to exposed samples (sulfur availability) for H_2S peaks up to 131 ppmv. Coeficient of variation varies between 0.5 and 1.8% making the error bars invisible.

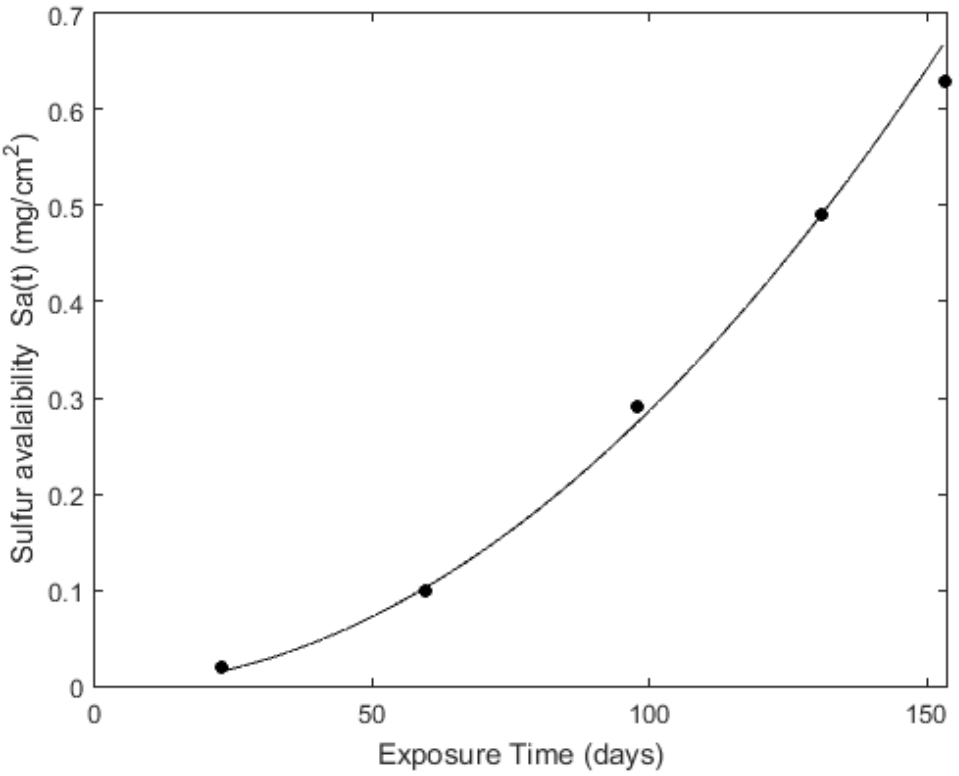

Figure 3.14: Applied sulfur to exposed samples (sulfur availability) for H_2S peaks up to 222 ppmv. Coeficient of variation varies between 0.7 and 2.6% making the error bars invisible.

Atmospheric oxygen uptake up between 5% and 10% was measured in all the containers. It is believed that this oxygen uptake variation is due to combined action of chemical and biogenic sulfides oxidation.

To compute the sulfur amount available for samples within each container, the ideal gas law was used as follows:

- Total volume inside a closed container, Vt=1620 cc
- Water volume inside a closed container, Vw=259 cc
- Plastic structure volume inside a closed container, Vb=650 cc
- Initial volume of samples inside a closed container, Vs=128 cc

- Available volume for generated gases (headspace), V=583 cc
- Temperature, T=303.15 °K (30°C)
- Pressure, P=75 kPa (0.75 atm)
- Weight of sulfur contained in 100 ppmv H_2S, Ws=0.073 mgS (reference value)

Using the H_2S concentration (ppmv) it was possible to compute the available sulfur weight within each container. To calculate the available sulfur in mgS/cm^2, the sulfur weight was divided by the total superficial area (cm^2) of the samples existing before extracting them for testing.

3.7 Exposure of samples to bacterial attack

3.7.1 Exposure of OM samples inoculated in non aseptic conditions

456 inoculated OM samples were subjected up to 222 ppmv H_2S, $0.3 \pm 0.1\% CO_2$ and 30^oC within six containers (biotic samples). Other 76 non-inoculated OM samples (control or Ctrl) were subjected only to humid atmospheric exposure within one container. Besides, 76 non-inoculated OM samples put into a container were subjected up to 222 ppmv H_2S (here named as H_2S or chemical control). H_2S supply was intended to simulate variable conditions in sewers, applying it in rates from 0-222 ppmv three times a week during 153 days.

Type-SM samples inoculated with *H. neapolitanus* (Hn), *A. thiooxidans* (At) and *H.neapolitanus+A.thiooxidans* consortium (nt) and type-MM samples inoculated with *H. neapolitanus* (Hns), *A. thiooxidans* (Ats) and *H.neapolitanus+A.thiooxidans* consortium (nts) were exposed as shown in Table 3.3.

3.7.2 Exposure of OM samples inoculated in aseptic conditions

Before inoculation and throughout the experiment (300 days), purity and presence of cultures was verified morphologically after growth in Luria Bertani (LB) agar. No

changes were observed in bacterial morphology of cultured plates from samples collected at different ages.

No bacterial growth was observed when some oven-dried mortar samples were "stamped"on LB agar. One group of 76 samples was inoculated with *H. neapolitanus* (H.n.), a second group was inoculated with *A. thiooxidans* (A.t.), and the third group was inoculated with a consortium (Cons.) composed by both bacteria. The fourth group was composed of abiotic samples exposed to the same environment of the biotic samples (i.e. H_2S+CO_2). The remaining group was used as control in which abiotic samples were exposed to a sterile environment at the same temperature (30 ± 1^oC) and relative humidity ($62\% \pm 5\%$) of the other four groups (Table 3.3). In all cases humid and warm environment inside the plastic boxes kept RH values within the mentioned ranges. For simplicity, the chemical exposure condition (fourth group) will be referred solely as "H_2S".

During the first 150 days of the experiment, sulfide was supplied to each container every 3 days to a H_2S initial concentration peak of about 131 ppmv. During the last 150 days, feeding was conducted on a daily basis, reaching the same concentration of hydrogen sulfide. This is a moderately low peak level H_2S concentration compared with reported in real sewers (2-650 ppmv) [87][37]. Containers were maintained with $0.3 \pm 0.1\%$ CO_2.

3.7.3 Exposure of PM samples inoculated in non aseptic conditions

Nineteen containers were used to expose pyritic samples as shown in Table 3.5. The whole experiment was developed in atmospheric conditions. Containers (76 samples each) were not handled into an aseptic environment. Inside the containers, the evaporation cycle guaranteed the availability of atmospheric oxygen and constant relative humidity. Apparent changes in the samples' surfaces were monitored twice a week during 153 days.

3.7.4 Exposure of TM samples inoculated in aseptic conditions

Five containers were used to expose samples containing little quantity of Triclosan to a H_2S-rich environment as shown in Table 3.6 Containers (76 samples each) were hermetically closed. During the first 150 days of the experiment, sulfide was supplied to each container every 3 days to a H_2S initial concentration peak of about 131 ppmv. During the last 150 days, feeding was conducted on a daily basis, reaching the same concentration of hydrogen sulfide. Containers were maintained with $0.3 \pm 0.1\% CO_2$.

3.8 Assessment of physical and mechanical consequences of biodeterioration

The effects of biodegradation were evaluated qualitatively and quantitatively as follows:

- Qualitative evaluation. Colors, texture and general appearance variations were checked and registered at each sampling time. Similar light fixture, workbench conditions and time of the day were used in each sampling procedure to guarantee minimal disturbance in the observation.

  Also,topographic changes of exposed surfaces were observed using an Alicona Infinite Focus optical device in the laboratory of Institut Universitaire de Technologie (IUT) de Nantes/Carquefou of the Universitè de Nantes (Figure 3.15). The apparatus was used to capture augmented images, measure the height variations and determine important parameters associated to the topographic description of samples surfaces. Results of these measurements are shown in section 4.2

Figure 3.15: Alicona Infinite Focus optical device ®

- Quantitative evaluation. Weight loss, porosity and compressive strength, of up to 257 and 404-day-old samples were measured over 153 and 300 days of exposure to bacterial attack in non aseptic and aseptic conditions respectively. Measurements of each one of these tests were made at 0, 23, 60, 98, 131 and 153 days of exposure for samples inoculated in non aseptic conditions. Also measurements were made after 0, 60, 120, 195, 240 and 300 days of exposure for samples inoculated in aseptic conditions. Additional measurements for weight loss and compressive strength were taken at days 30, 90, 150 and 270. To compute actual age of samples, 104 days must be added to the mentioned spans.

3.8.1 Weight loss

Samples were extracted from containers following a uniform-random selection sampling method. Once extracted, moist samples were weighed and later oven dried. The weighing process before and after the treatment was carried out after drying the samples at

110^{o}C for 24 h. Therefore, if some water were absorbed during the inoculation process, it would have been removed during oven-drying. The dry weight of the samples was measured using a precision scale (Ohaus Adventurer Pro Analítica AV264). To ensure correct weight measurements, prior to oven drying and weighing, extracted samples were subjected to a passive wash in which they were submerged in distilled water for one hour and shaken for 30 seconds every 20 minutes before being placed into the oven. Nine weight measurements were taken and averaged for each sample.

Weight variation was computed for each sample at the correspondent age as:

$$\Delta w(t) = \frac{w(t) - w_i}{w_i} \cdot 100 \tag{3.1}$$

where $\Delta w(t)$ is the weight variation (%), $w(t)$ is the dry weight (mg) measured at time t and w_i is the initial dry weight (mg) measured at time $t = 0$.

3.8.2 Porosity

Porosity measurements in triplicate were taken using mercury intrusion data from an AutoPore IV 9500 porosimeter (Micromertics Instrument Corporation ®) (Figure 3.16). Pores in solids can be classified according to their size as micropores, mesopores or macropores. In general it is accepted that adsorbed water can be found in micropores, condensed water in mesopores and bulk water in macropores [88]. In civil engineering applications, micropores are most commonly accepted to have widths between 0.5 and 10 nm, mesopores between 10 and 5000 nm, and macropores larger than 5000 nm [42]. This study used this standard (micropores being 0-10 nm, mesopores being 10-5000 nm and macropores being larger than 5000 nm).

Total porosity of any material can be computed as the sum of isolated pores volume existing inside the solid structures plus open (connected) pores volume existing amid those solid structures [89]. In this work only open porosity was measured and for simplicity it is called “porosity”. Total mercury intrusion (TMI) expressed in ml/g is used to compute the pores volume existing inside the entire sample.

Porosity variation (i.e.,) measured in percentage was computed for each sample at the correspondent age as:

$$\Delta\phi(t) = \phi(t) - \phi_i \tag{3.2}$$

where $\Delta\phi(t)$ is the porosity (%) measured in each sample at time t and ϕ_i is the initial porosity (%) measured in control sample at time $t = 0$.

Average porosity (in volume) and its distribution were determined from three measurements for each type of sample.

3.8.3 Compressive strength

Compressive strength was measured in triplicate using a 500 kg load cell hydraulic press (ELE International Digital Tritest®) (Figure 3.16). Records of load versus deformation at a deformation speed of 0.10 mm/min were obtained for samples at each stage of the experiment. A pre-load equivalent to $1.0-1.5$ MPa was applied five minutes prior to the start of the test to ensure uniform pressure on the upper and lower surfaces of each sample. Upper and lower surfaces were leveled prior to testing using rubber pieces. Slow load rate and rubber pieces avoided distortion from superficial deteriorated layers compressibility. Load machine was calibrated each two months using steel springs with known constant.

Compressive strength values were scaled so that results were comparable to the results of standard 5-cm-side-cube compressive load tests [90]. The effects of the small size of samples and the laboratory conditions were taken into account using a factor of 4.3 (COV=8%) to multiply the strength results from samples and obtain the equivalent strength in 50mm-side cubes. Such factor was computed dividing the initial strength of each 50mm-side cube over the initial strength of each sample. The mean value takes into account scaling effects related to contact surface area, grain size, roughness effect, and geometrical proportions of the sample. To have a more clear reference, in this work absolute scaled values and relative values of compressive strength are presented.

Figure 3.16: AutoPore IV 9500 porosimeter (Micromertics Instrument Corporation ®) and hydraulic press (ELE International Digital Tritest ®)

For simplicity, the compressive strength is referred solely as "strength"in the next sections. As stated in section 4 exposed samples were tested with no further physical adjustments. Therefore, reported results refer to samples containing indistinctly deteriorated and sound layers (deteriorated layers were not removed previous to strength test).

Strength variation was computed for each sample at the correspondent age by:

$$\Delta s(t) = \frac{st(t) - s_i}{s_i} \times 100 \tag{3.3}$$

where $\Delta s(t)$ is the strength variation (%), $s(t)$ is the strength (MPa) measured in each exposed sample at time t and s_i is the initial strength (MPa) measured in the control sample at time $t = 0$.

3.8.4 Volumetric measurements

Samples volume variation was computed following two procedures:

- Using the procedure recommended in the User Manual of the AutoPore IV 9500 porosimeter (Micromertics Instrument Corporation ®). Sample volume is computed using the weight and density of mercury (Hg). After purging the trapped air in pores, at low pressure (less than 15 psig), the variation in the weight of a penetrometer containing the sample and injected mercury is divided by the mercury density to calculate the sample volume.

- Using the protocol designed by Michael O'Byrne, PhD Candidate of the Department of Civil, Structural and Environmental Engineering (Trinity College Dublin). A record of the sample rotating to low speed is used to feed into VisualSFM, which is a free GUI application for 3D reconstruction using structure from motion (SFM), available at http://ccwu.me/vsfm/. The resultant point cloud is then converted to a watertight volume or reconstructed solid. The sample volume is computed using the reconstructed solid (Figure 3.17).

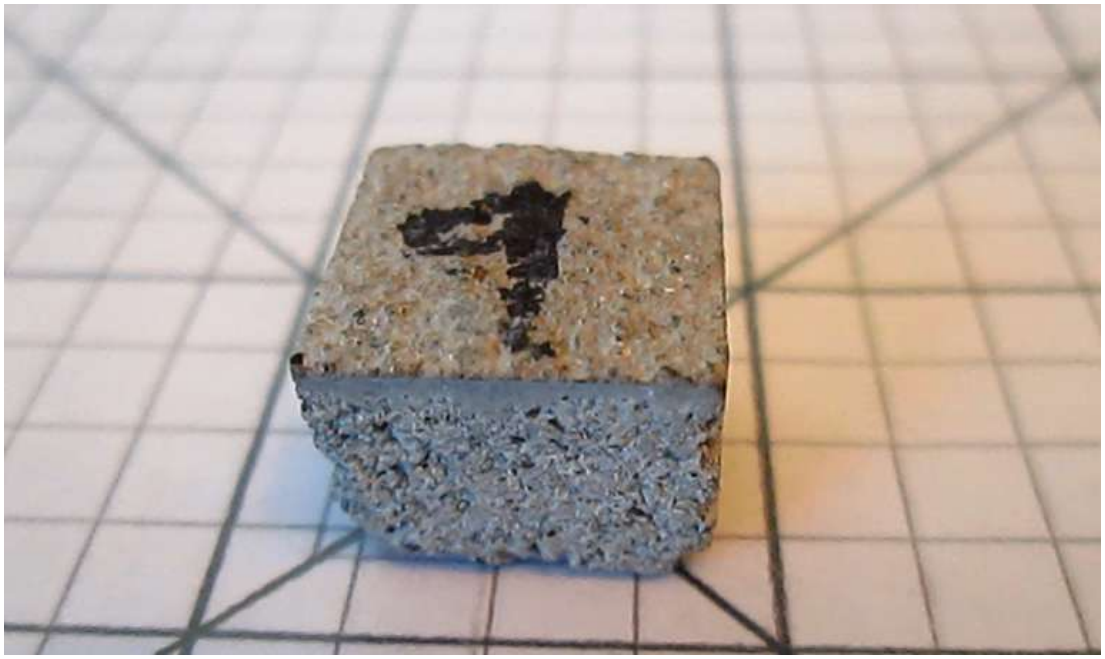

Figure 3.17: Typical scenario to take frames for volume determination from video technics

3.9 Determination of chemical compounds in biodeteriorated samples

An X-ray Powder Diffraction (XRD) analysis was performed upon 2 g of powder scraped from the surface of four exposed samples to determine the effects of biodeterioration upon the chemical compounds of the mortar. In section 4.3 the results of the XRD analysis are presented and discussed. An X-ray diffractometer RIGAKU Ultima III was used.

3.10 Summary and conclusions

This chapter explains how the experiment was conceived and conducted. The following are the most relevant aspects achieved in the present chapter:

- In this chapter the methodology for the experimental work was designed and

presented. Such methodology was described by means of a detailed protocol.

- The protocol of the experiment was designed to follow four fringes of activities: Biological, physical, chemical and common processes. The biological processes are related to the manipulation of microorganisms to be inoculated upon the mortar samples. The physical processes deal with the manufacturing and conditioning of mortar samples. The chemical processes consider the generation of gases required into the containers. Finally, the common processes link all the previous ones to produce the final results of the experiment.

- The protocol defined qualitative and quantitative evaluations which include weight, porosity and strength changes. Such evaluations are based on measurements taken from exposed samples made of ordinary mortar, pyritic mortar and Triclosan-added mortar inoculated with different cultures and exposed to different environments. The trends of the strength to porosity and strength to weight variations were proposed to interrelate those evaluations inwardly.

Chapter 4

SULFUR AVAILABILITY AND QUALITATIVE CHANGES

4.1 Chapter overview

In this chapter the results of the preparations and general tests from the experiment are presented and critically discussed. The objectives of this chapter are:

- To fit curves for the sulfur availability at each time of the experiment computed from actual H_2S concentrations measured in the experiment.
- To present a detailed description of the qualitative changes observed onto the exposed surfaces of the samples. This description is complemented using results of the XRD analysis applied to superficial layers of biodeteriorated samples.
- To present and comment the results obtained from the topographic and volumetric observations in the samples surfaces.

This study is based on an experiment in which the concrete alkalinity was dropped down using carbonation prior to inoculation and exposure of samples. For this reason, the experiment start time actually represents the stage of active biodeterioration once the concrete pH has been reduced and the concrete surface has been conditioned

for a long time. The length of the first stage (biodeterioration immunity) could be estimated by using carbonation models until a given pH level is reached (e.g. pH=7) [91][92]. Therefore, the fitting of curves of biodeterioration effects developed in this section are only applicable after the biodeterioration immunity stage has been overcome. Since the results were obtained from measurements taken during 153 days (or $Sa(t) \leq 0.63 mg/cm^2$), and 300 days of exposure (or $Sa(t) \leq 0.12 mg/cm^2$), the assessment of biodeterioration effects after this time (or sulfur availability) should be carried out with care.

In order to generalize the results to samples exposed to different environments, all biodeterioration effects (weight, porosity and strength changes), were expressed as a function of the sulfur added to the system; i.e., $Sa(t)$. Thus, based on the measurements, a regression analysis was carried out. The amount of sulfur put into the system at a given point in time can be computed as (Figure 3.13 and Figure 3.14):

$$Sa(t) = 0.0016e^{0.0146t} \tag{4.1}$$

$$Sa(t) = 3 \cdot 10^{-5} t^{1.9901} \tag{4.2}$$

where $Sa(t)$ is expressed in mg of elemental sulfur per cm^2 of exposed surface of mortar existing at time t (days); with $R^2 = 0.9879$ and 0.9994. Note that $Sa(t)$ took into account the reduction of exposed surface due to the progressive removal of samples from each container since the total surface available for reaction with sulfide decreased. On the other hand, the amount of H_2S in contact with samples surfaces could not be determined in an exact manner. Instead this study considered $Sa(t)$ as the total available amount of H_2S in contact with the samples surfaces. Results for control samples have also been referred to $Sa(t)$ only for comparison purposes (Figures 5.5, 5.6, 5.7, 5.8 and 5.9, Figures 5.29, 5.30, 5.31, 5.32 and 5.33, and Figures 5.40, 5.41, 5.42, 5.43 and 5.44). Three curve fittings were proven for $Sa(t)$: linear and second-degree polynomial and logarithmic equations. Solver tool by Microsoft Excel® was

used to identify the model parameters that minimize the mean square error in each case (analysis of residuals). In all cases the best fit was achieved by using logarithmic fittings (Table 5.3).

4.2 Qualitative changes in biodeteriorated samples

Dark green to black coloration was observed in samples inoculated in non aseptic conditions growth in SM before 30 days of exposure. They showed severe deterioration with cottage cheese consistency after 153 days, in contrast with those inoculated in non aseptic conditions growth in MM, which appeared to still be stiff, underlying the severity of biogenic deterioration in absence of salt in the inoculum (Figure 4.1). Similarly, samples exposed exclusively to H_2S did not show important deterioration indicating the preponderant effect of biogenic deterioration (Figure 4.2). Apparently ettringite crystals were visible in exposed samples after 48 days and covered a high portion of the surface after 62 days (Figure 4.3 and Figure 4.4). A white-brown-spotted layer was observed after day 84 in cracked samples evidencing the effects of H_2SO_4 reaction on the samples' surfaces (Figure 5.35).

Also qualitative observations related to color and texture changes were recorded at each sampling time for samples inoculated in aseptic conditions. Samples showed stains of different colors during the experiment: gray, green, bronze, and white shades appeared successively upon samples surfaces during the experiment. White crystals (which are supposed to be ettringite crystals that in turn could be dissolved when pH drops even more) [31] were visible after 90 days of exposure in biotic samples. Such crystals were observed only after 210 days over samples subjected to chemical exposure. It was not possible to quantify whether the changes affecting porosity and strength were uniformly distributed throughout the samples; however, the observations led to conclude that the effects were concentrated mostly on the surface degraded layer. Degradation depths were not measured nor deteriorated layers removed before testing. Therefore, reported changes must be interpreted as average changes over the whole

specimen volume (including deteriorated and not deteriorated zones).

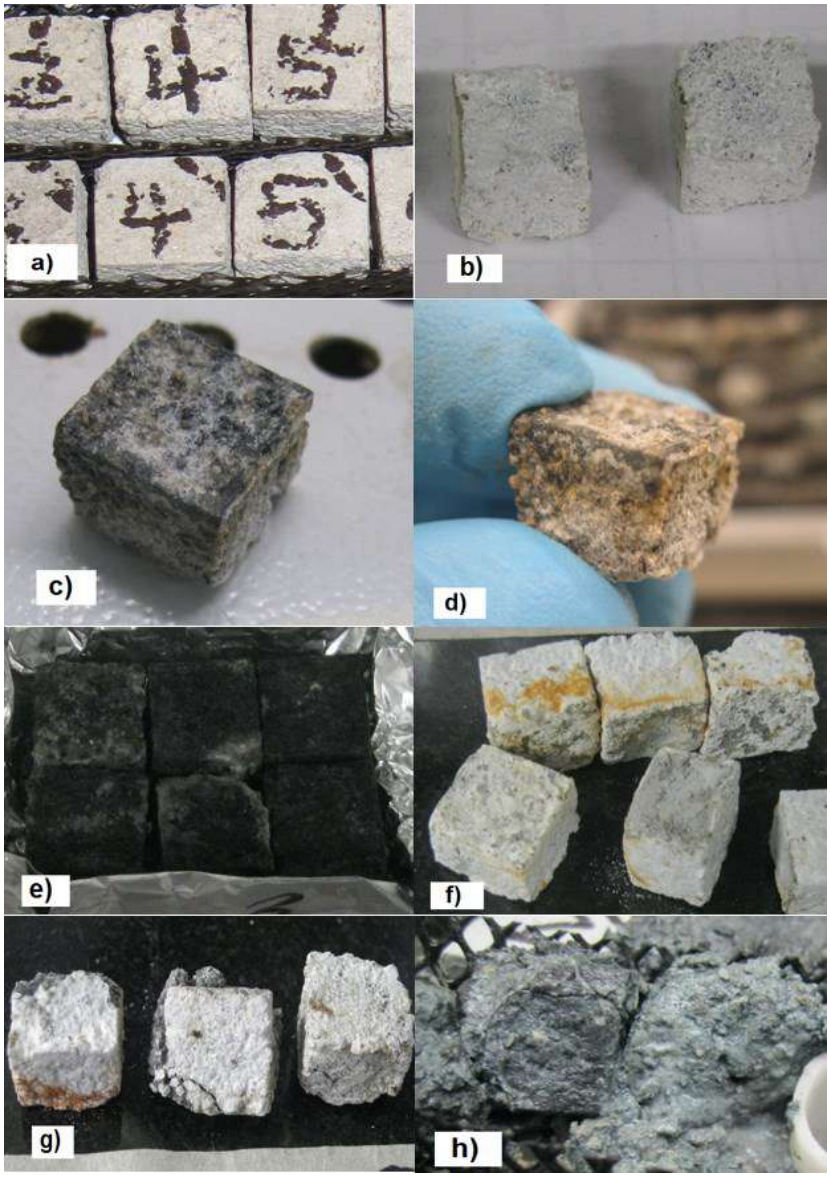

Figure 4.1: Stage of biotic samples inoculated in non aseptic conditions grown in SM after exposure: a) dried at 0 days, b) dried at 19 days, c) humid at 33 days, e) dried at 35 days, f) humid at 67 days, g) dried at 82 days, h) humid at 129 days

Figure 4.2: Stage of H_2S-only control samples after 153 days of exposure manipulated in non aseptic conditions

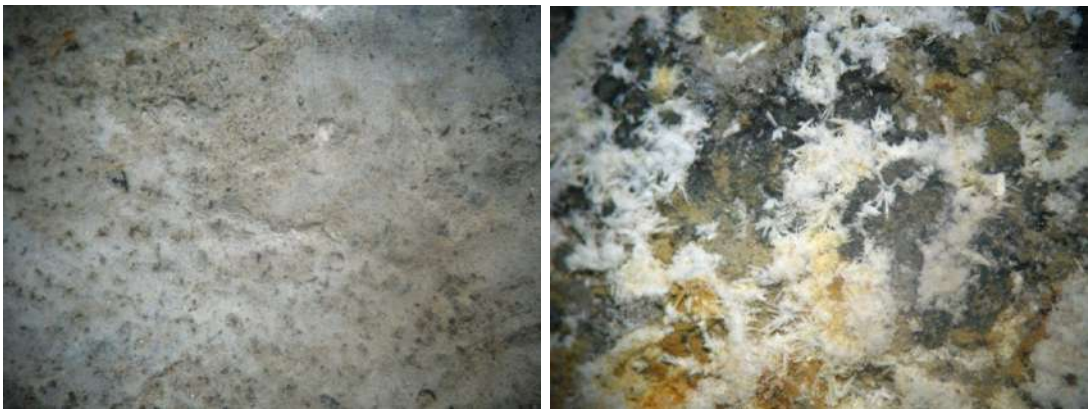

Figure 4.3: Surface of samples inoculated in non aseptic conditions in SM on days 0 and 48 of exposure (20X photograph)

Figure 4.4: Surface of samples inoculated in non aseptic conditions grown in SM after 62 days of exposure (20X photograph)

Figure 4.5 shows the evolution of the appearance samples inoculated in aseptic conditions during the experiment. Similarly to what was observed in the case of samples inoculated in non aseptic conditions, the most deteriorated samples were those inoculated with the consortium composed by H.n. and A.t. Also samples inoculated with A.t. showed major changes than those inoculated with H.n. Samples exposed exclusively to H_2S resulted less damaged than biotic samples confirming once more that biogenic effects are more adverse than chemical effects. Nevertheless, the larger H_2S availability and biotic richness in samples inoculated in non aseptic conditions produced a more severe deterioration in minor time than those inoculated in aseptic conditions (Figure 4.6)

Figure 4.5: Exposed samples inoculated in aseptic conditions: 1) H. n., 2) A.t., 3a) H.n.+A.t., 3b) H.n.+A.t.+Triclosan, 4) H_2S, 5) Control, 6) Non-carbonated

Figure 4.6: Comparison at the end of the experiment. Left: Samples inoculated in aseptic conditions (300 days); Right: Samples inoculated in non aseptic conditions (153 days)

Samples added with Triclosan showed no apparent changes up to approximately 180 days after the exposure start. Since that moment some little white traces were observed (Figure 4.5 and Figure 4.7).

Figure 4.7: Antimicrobial effect of Triclosan in samples inoculated in aseptic conditions after 150 days of exposure. Left: With no additions; Right: Added with Triclosan

4.3 Topographic variations in surfaces of biodeteriorated samples inoculated in aseptic conditions

Texture description can be achieved using the roughness measurement. Advanced devices and linked software are available to determine parameters associated to the roughness surfaces. In this study, attempts to use Atomic Force Microscopy were not successful due to the samples' high roughness. For this reason, an optical device was used: The Alicona Infinite Focus Optical Device ®. This apparatus constructs 3D images where a realistic vision of the surface topography is possible (Figure 4.8). Also it is possible to observe details such as the $CaSO_4$ crystals formation such as the white cumulus seen in Figure 4.9. A comprehensive analysis is made by the apparatus and a large amount of parameters is available in the form shown in Figure 4.10 and Figure 4.11.

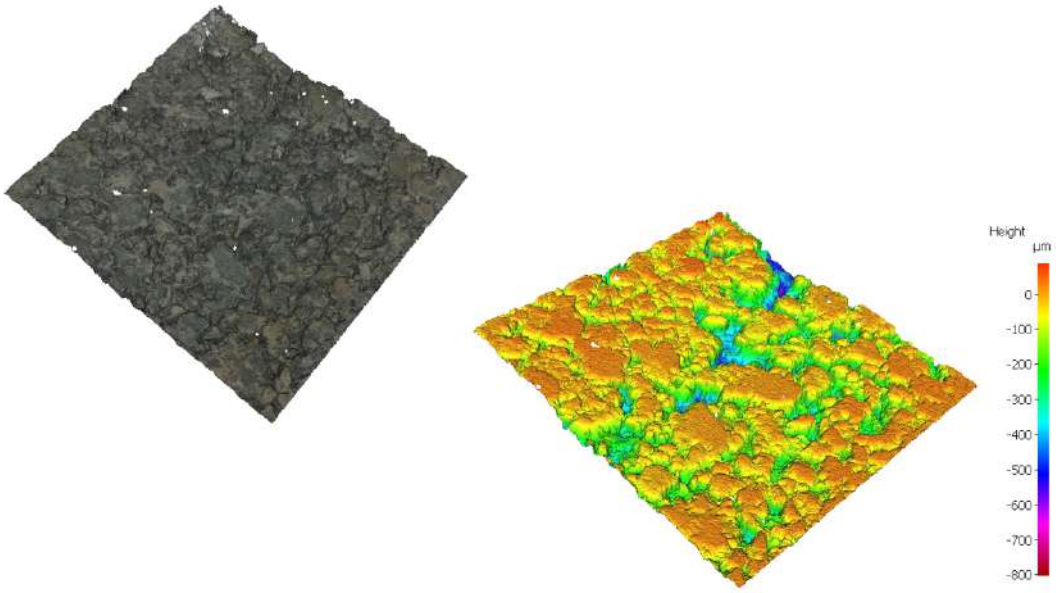

Figure 4.8: Tridimensional images obtained using the Alicona Infinite Focus ®

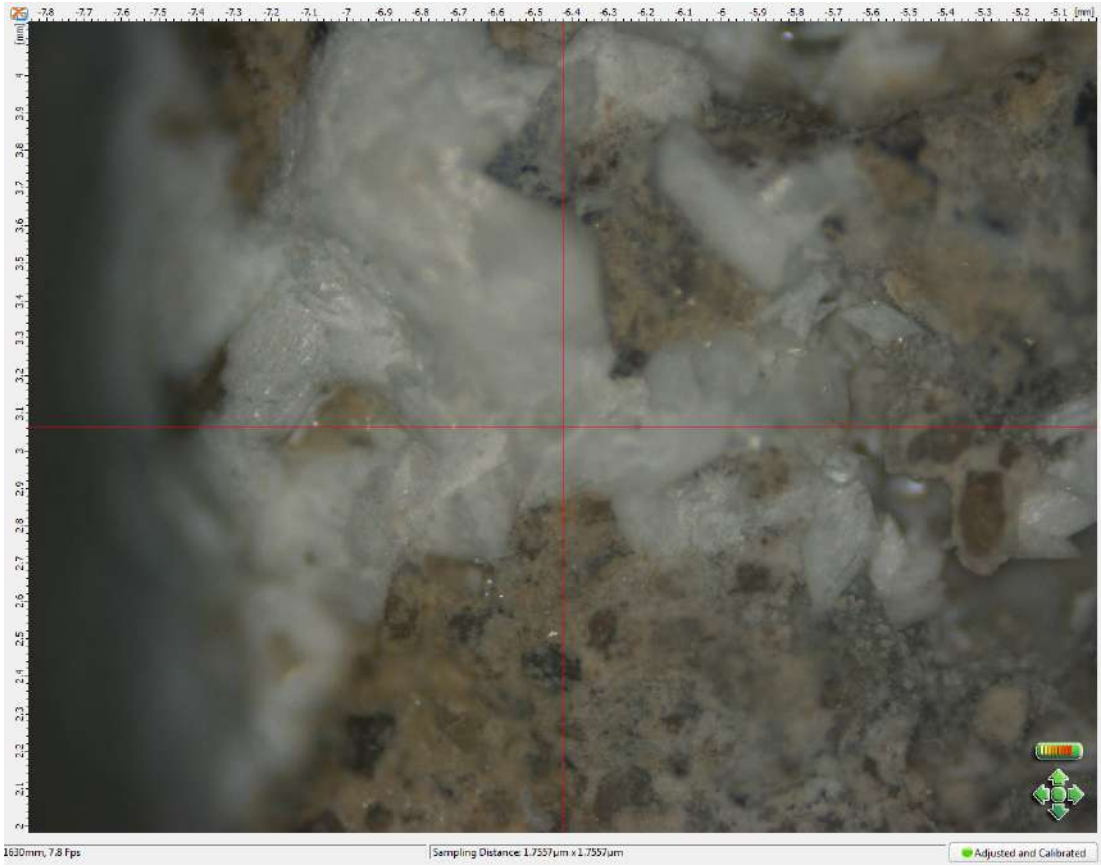

Figure 4.9: Scaled picture (X100) obtained using the Alicona Infinite Focus ®

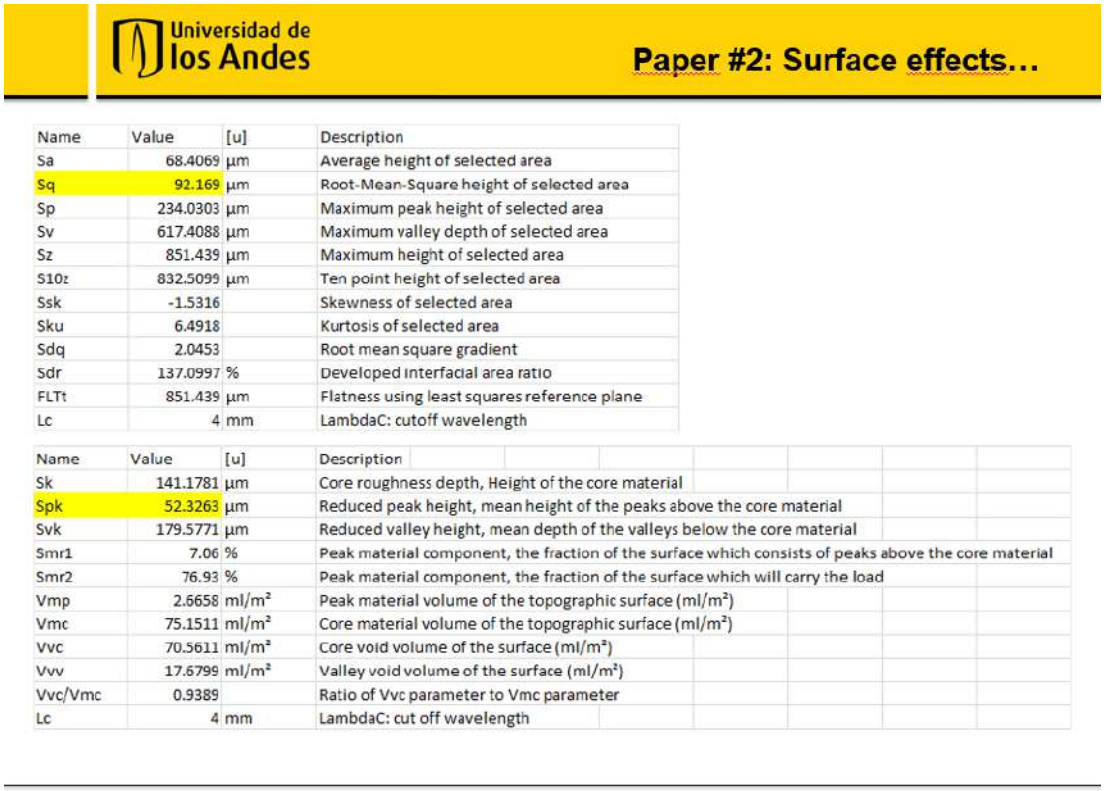

Name	Value	[u]	Description
Sa	68.4069	µm	Average height of selected area
Sq	92.169	µm	Root-Mean-Square height of selected area
Sp	234.0303	µm	Maximum peak height of selected area
Sv	617.4088	µm	Maximum valley depth of selected area
Sz	851.439	µm	Maximum height of selected area
S10z	832.5099	µm	Ten point height of selected area
Ssk	-1.5316		Skewness of selected area
Sku	6.4918		Kurtosis of selected area
Sdq	2.0453		Root mean square gradient
Sdr	137.0997	%	Developed interfacial area ratio
FLTt	851.439	µm	Flatness using least squares reference plane
Lc	4	mm	LambdaC: cutoff wavelength

Name	Value	[u]	Description
Sk	141.1781	µm	Core roughness depth, Height of the core material
Spk	52.3263	µm	Reduced peak height, mean height of the peaks above the core material
Svk	179.5771	µm	Reduced valley height, mean depth of the valleys below the core material
Smr1	7.06	%	Peak material component, the fraction of the surface which consists of peaks above the core material
Smr2	76.93	%	Peak material component, the fraction of the surface which will carry the load
Vmp	2.6658	ml/m²	Peak material volume of the topographic surface (ml/m²)
Vmc	75.1511	ml/m²	Core material volume of the topographic surface (ml/m²)
Vvc	70.5611	ml/m²	Core void volume of the surface (ml/m²)
Vvv	17.6799	ml/m²	Valley void volume of the surface (ml/m²)
Vvc/Vmc	0.9389		Ratio of Vvc parameter to Vmc parameter
Lc	4	mm	LambdaC: cut off wavelength

Figure 4.10: Typical parameters computed using the Alicona Infinite Focus ®

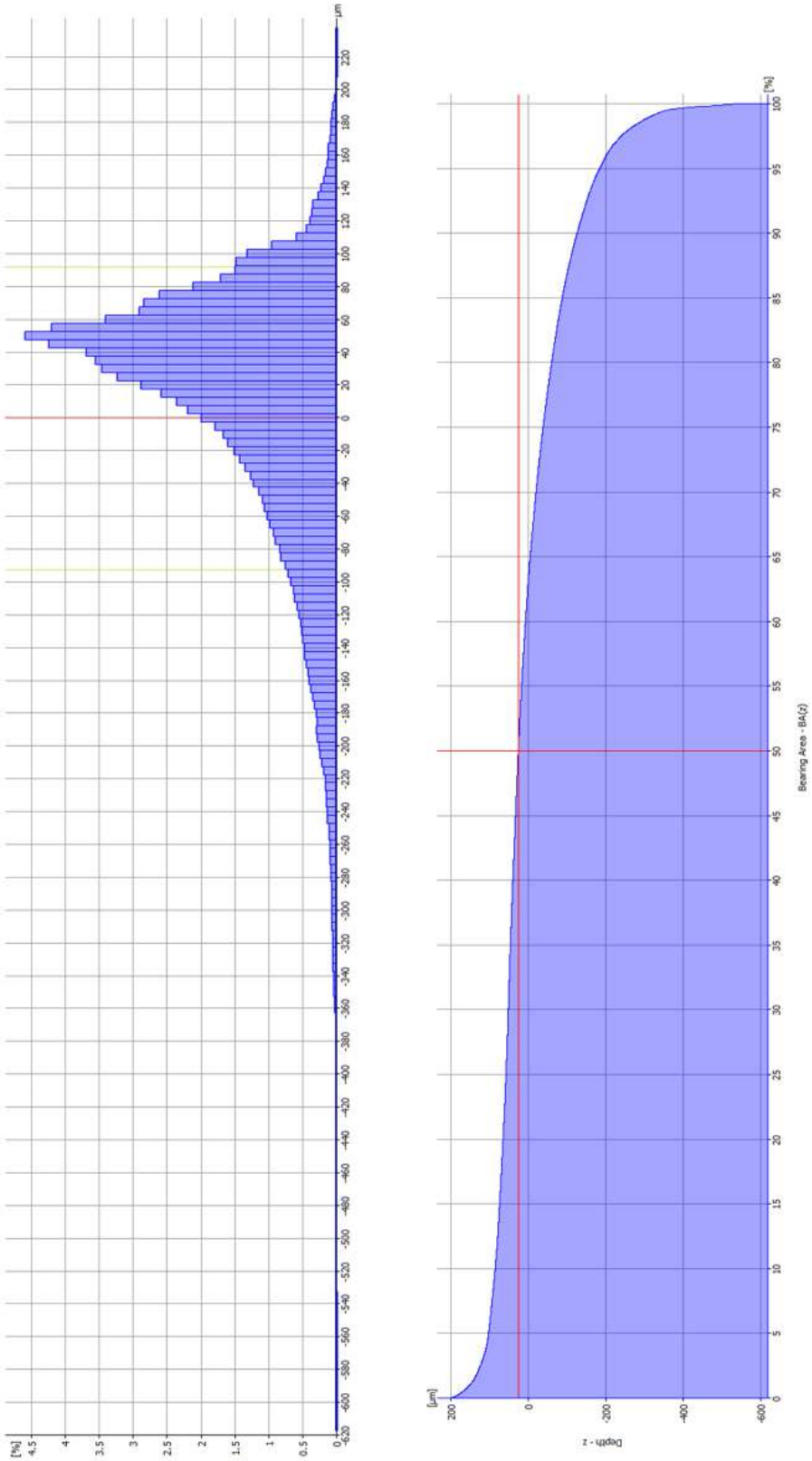

Figure 4.11: Typical curves generated by the Alicona Infinite Focus ®

The porosity per superficial area (ml/m^2) and the reduced peak height Spk (μm) are two important parameters related to the texture changes produced by biodeterioration. The first one is useful to understand how the superficial voids amount change during the exposure time. The second parameter is computed as the mean height of the peaks above the core material and helps to see how the irregularities behave.

Figure 4.12 was drawn using the average of three measurements at each age. After 300 days of exposure, a porosity gain of 130 and 190 ml/m^2 was observed in samples inoculated with H.n+A.t. and A.t. respectively. In contrast abiotic samples exposed to H_2S augmented 110 ml/m^2 confirming the larger gain in inoculated samples containing acidophilic bacteria. Samples inoculated with H.n. (neutrophilic bacteria) only augmented 60 ml/m^2 probably due to a clogging effect. Control samples reduced their superficial voids in 50 ml/m^2.

Figure 4.13 shows the mean height of the peaks above the core material. Initial mean height of samples was 70 μm. After 300 days of exposure control samples reduced such peaks to 51 μm. The largest reduction was observed in abiotic samples exposed to H_2S (34 μm). The smaller reduction was observed in samples inoculated with H.n.+A.t. (61 μm). Samples inoculated with A.t. and H.n. reduced their peaks to 40 and 48 μm. According to these results, the biogenic effects produced more variation than chemical effects.

From previous paragraphs it is concluded that samples inoculated with H.n.+A.t. showed the largest increase in superficial pososity and roughness. On the other hand, samples inoculated with A.t. and those of the chemical control reduced their roughness while gained superficial porosity. On the contrary, samples inoculated with H.n. and those of the control increased their roughness while their porosity was depressed.

As explained in section 2.4.1 biodeterioration is an interfacial phenomena that depends on the surface area/surface roughness ratio and it is desirable to study how the initial roughness can influence the biodeterioration effects. However, by the time that roughness was measured, non exposed samples had surely changed importantly their initial superficial texture. For this reason no valid conclusions can be made in this

matter.

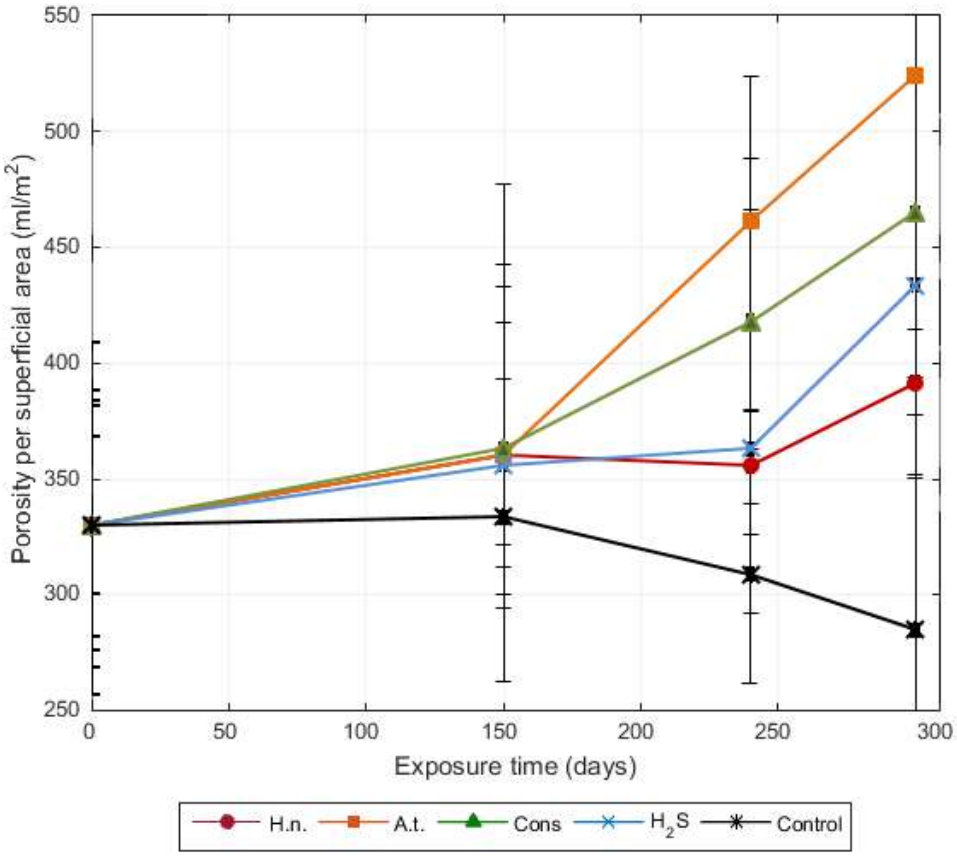

Figure 4.12: Superficial porosity evolution. COV: H.n. 3.5 to 4.2%, A.t. 11 to 15%, Cons. 7.5 to 9.1%, H_2S 8.6 to 12.1%, Control 8.1 to 9.8%

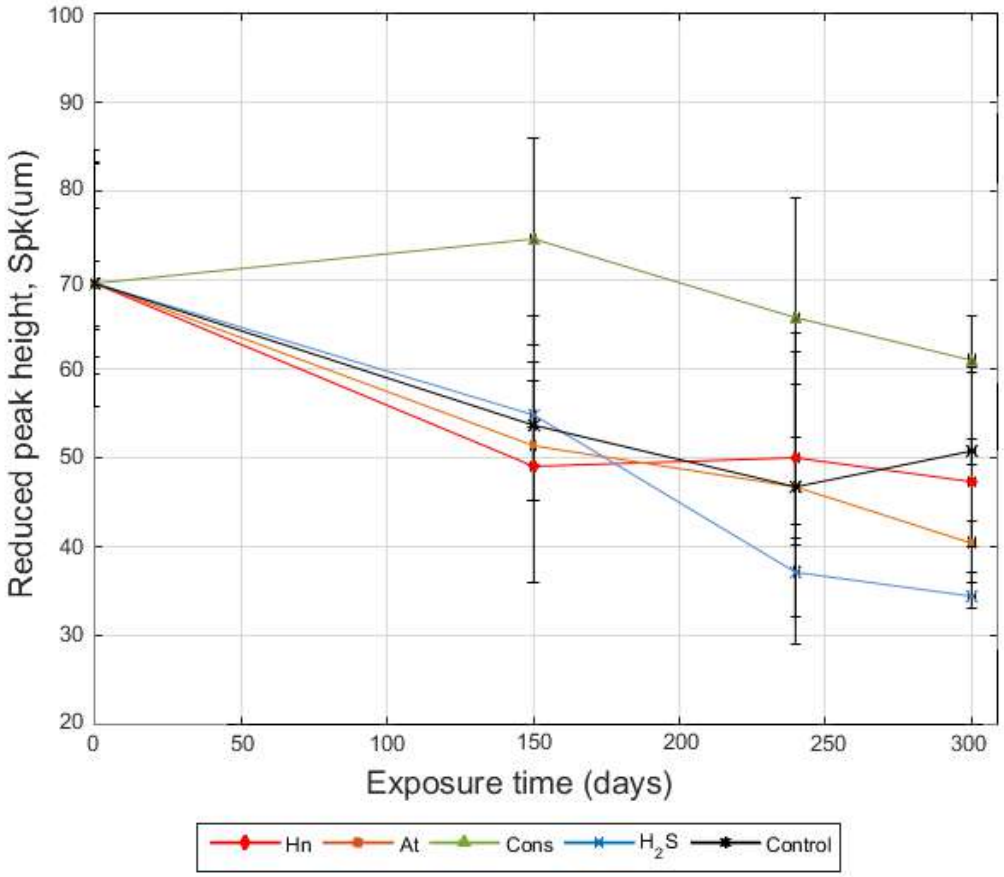

Figure 4.13: Superficial irregularity evolution. COV: H.n. 12.1 to 16.9%, A.t. 15.4 to 22.0%, Cons. 11.3 to 15.1%, H_2S 12.7 to 19.8%, Control 13.9 to 24.7%.

4.4 Chemical compounds in exposed ordinary mortar samples

2 g of powder were scraped from the surface of four exposed samples. Three specimens were selected from those inoculated in aseptic conditions with three different single inoculums while the last one was only exposed to H_2S. One sample was inoculated with H.n., other with A.t. and the third one with H.n.+A.t. Powder extracted from

each specimen was analyzed using XRD to determine the chemical compounds of the exposed mortar. Figure 4.14 presents a superimposition of the results. Quartz (SiO_2), Ferrous oxide or Wustite (FeO), Calcite ($CaCO_3$), Calcium Sulfate in Anhydrite form ($CaSO_4$), Iron Oxide Sulfate and Cupper Sulfide (Cu_2S) were identified in the analysis. The main peaks observed in Figure 4.14 correspond to Quartz and Calcite.

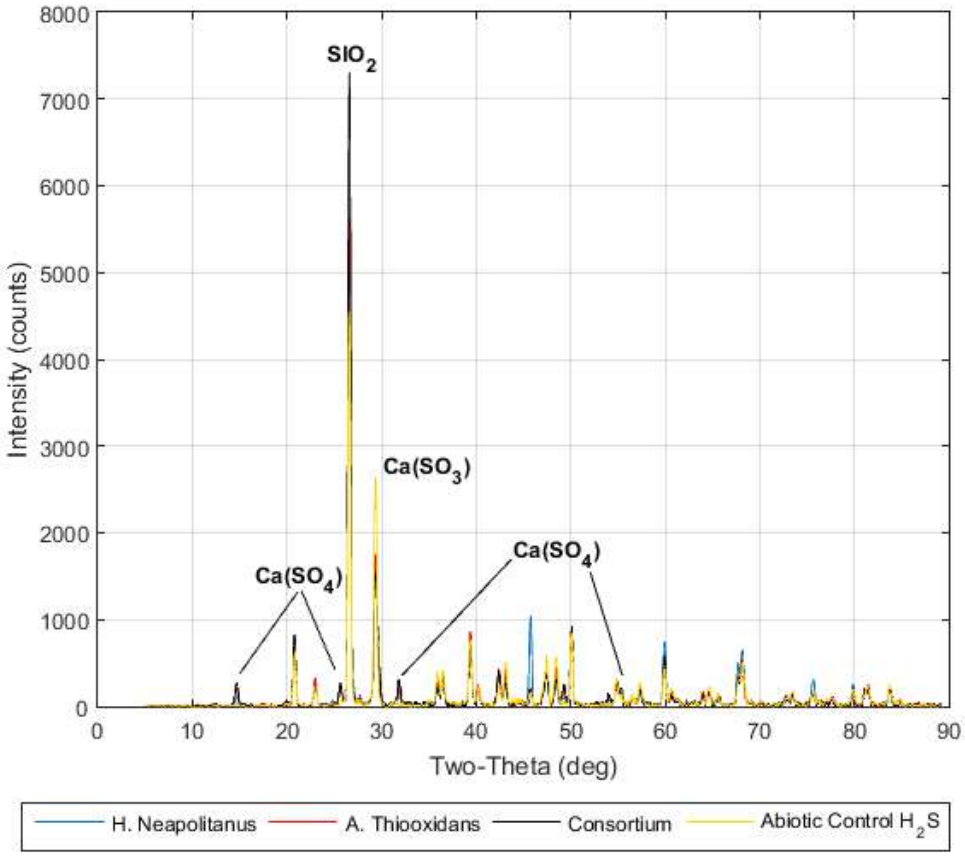

Figure 4.14: XRD analysis of biodeteriorated samples

No quantification of chemical compounds was made. For this reason, available information only can be used to get an approximate reasoning. To understand the approximate variations produced by biogenic attack, a ratio was computed dividing the

intensity (counts) of each inoculated sample by the intensity measured in samples exposed exclusively to H_2S. Figure 4.15, Figure 4.16 and Figure 4.17 show the H.n./H_2S, A.t./H_2S and (H.n.+A.t.)/H_2S ratios respectively. In these figures, four main visible peaks are linked to Calcium Sulfate Anhydrite and Calcium Sulfate Hydrate (Bassanite). Two-Theta values related to Calcium Sulfate compounds found in the samples are 14.76^o, 31.86^o and 54.07^o [93]. The amount of $CaSO_4$ in samples inoculated with H.n., A.t. and H.n.+A.t. resulted to be 94, 164 and 199 times that of the samples exposed exclusively to H_2S. It is evident the effect of biodeterioration in the production of $CaSO_4$. The largest augment of that compound was observed in samples inoculated with H.n.+A.t. and the shorter in those inoculated with H.n. This finding seems to confirm the enhancement effect of different $CaSO_4$ compounds such as of Gypsum, Bassanite and Anhydrite and the temporal influence of ettringite in the biodeterioration processes. The presence of any of those forms depends on the temperature at what reactions have taken place [94][95]. In this study the exposure was made at 30^oC at which the three mentioned forms are possible.

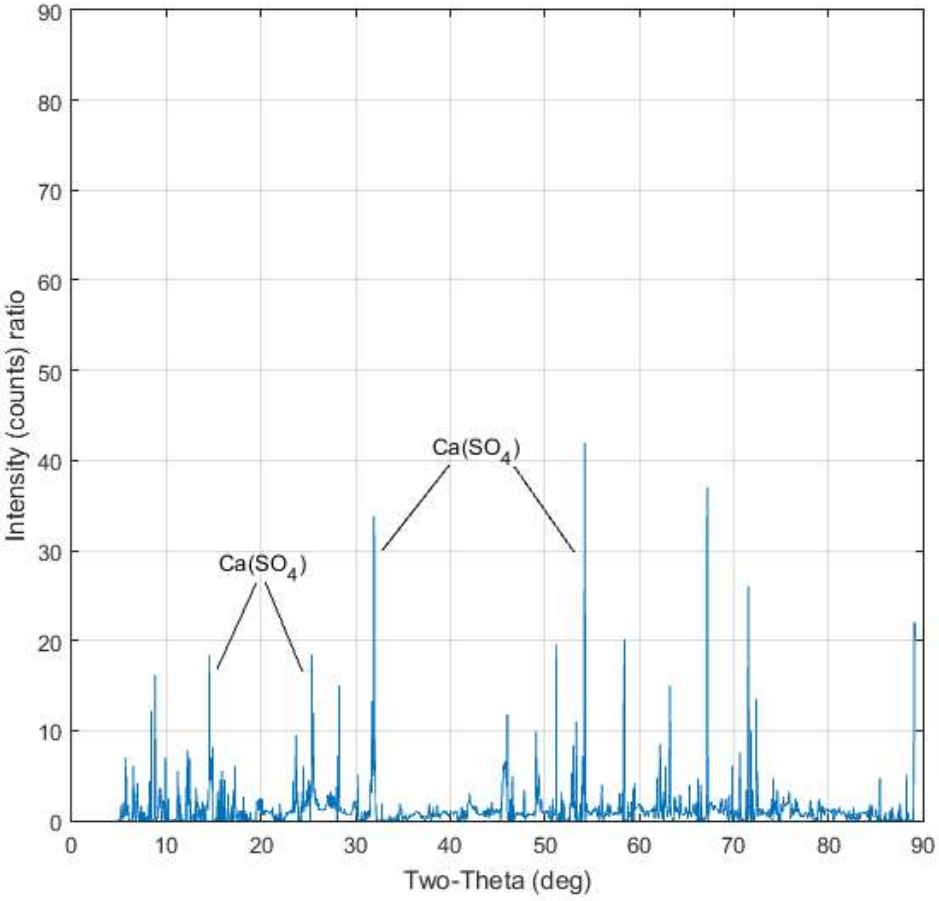

Figure 4.15: H.n. intensity to H_2S intensity ratio

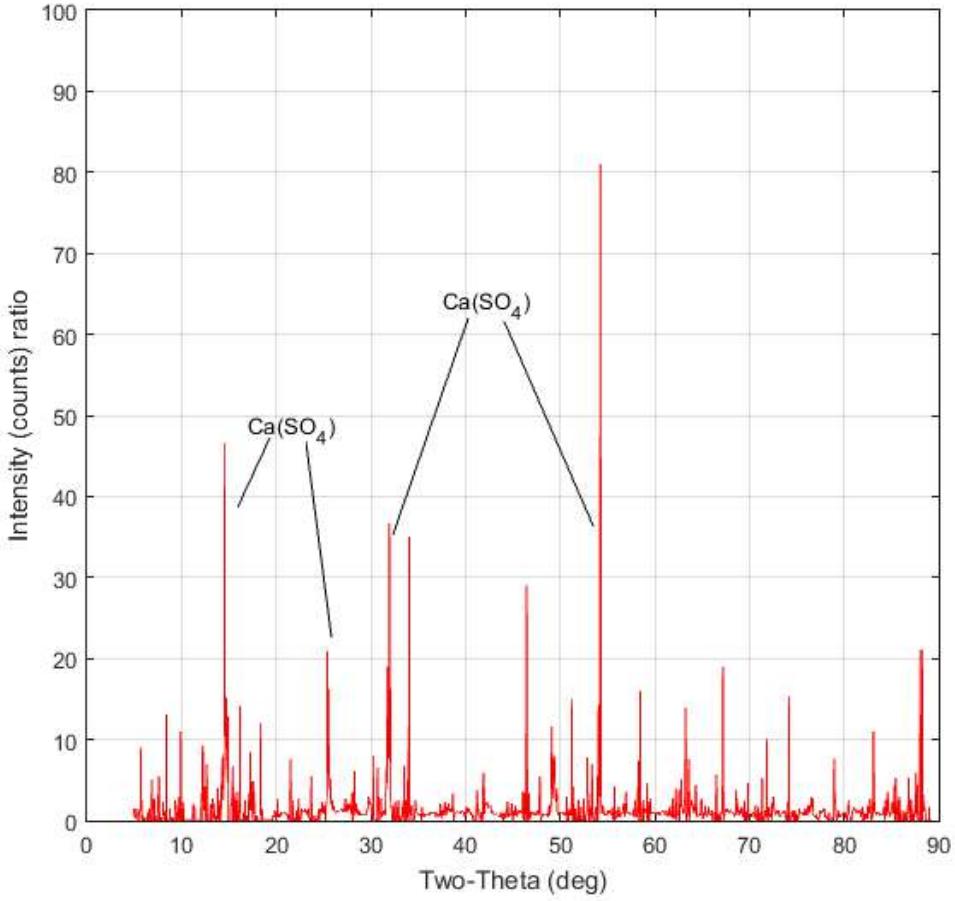

Figure 4.16: A.t. intensity to H_2S intensity ratio

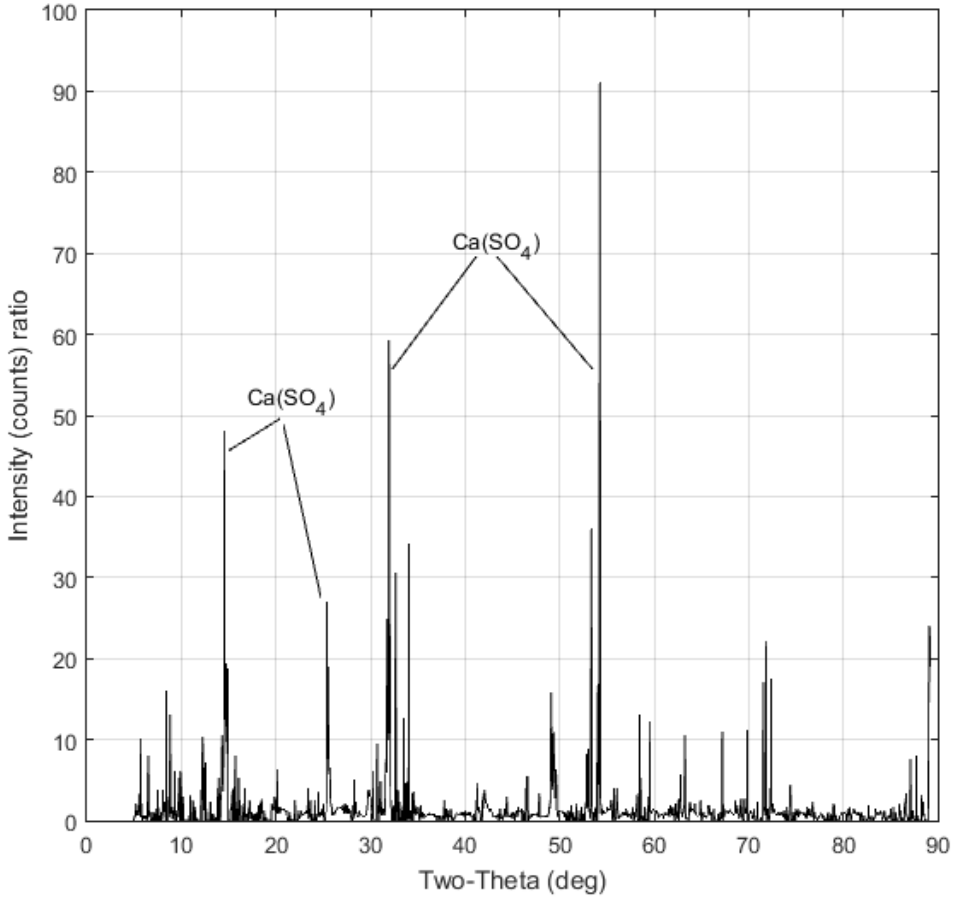

Figure 4.17: H.n.+A.t. intensity to H_2S intensity ratio

4.5 Volumetric variations in biodeteriorated samples

Figure 4.18 shows a typical reconstructed solid using video technics. According to the results of this procedure, all samples (even control) augmented their volume between 81 and 130 mm^3 corresponding to 3 and 6% of the initial volume. It was not possible to identify a clear volume trend through the duration of the experiment. On the other hand, a dissimilarity was found in the analysis of computed volumes from the MIP technic in which the variations were between 95 and 161 mm^3 corresponding to 4 and

8% of the initial volume. The volume increase in biodeteriorated samples could be explained as a result of clogging, sulfur precipitation and swelling from gypsum and ettringite crystals. However, in the case of the control samples, the volume increase could be asociated to errors of the measurement technics. This is an interesting issue to study in future works.

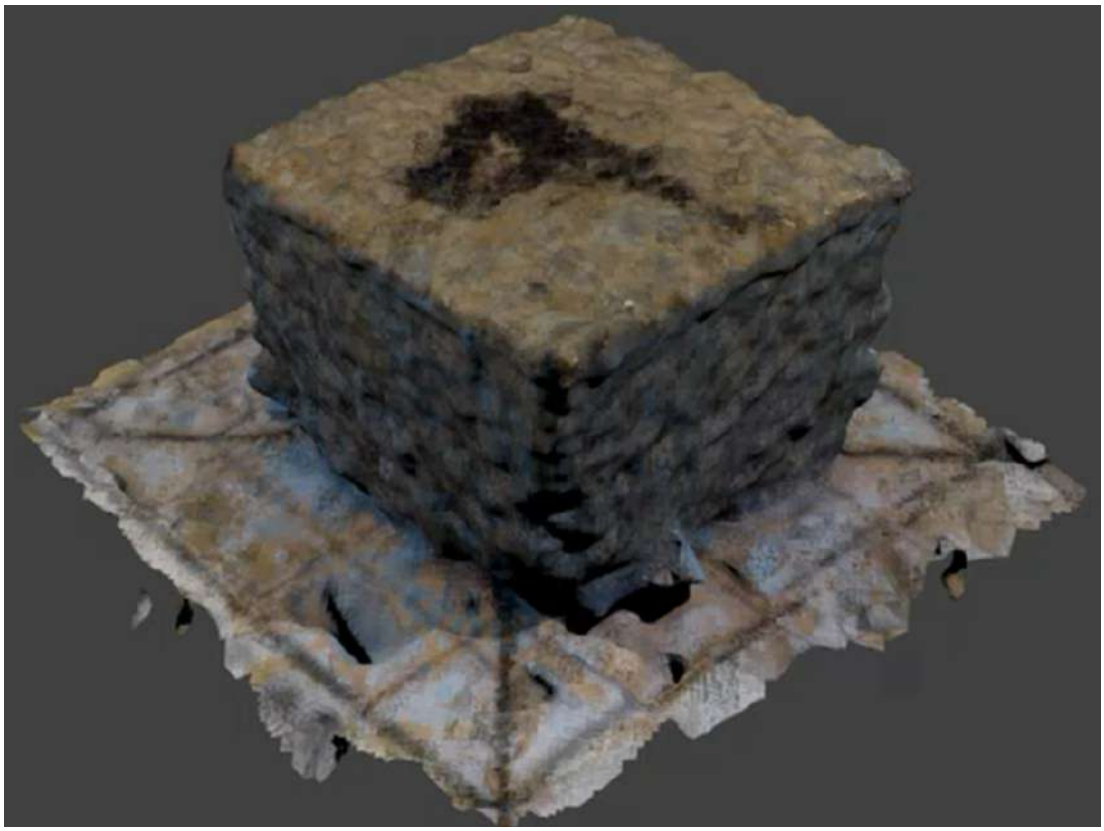

Figure 4.18: Reconstructed volume using video technics

4.6 Summary and conclusions

- Curves for the sulfur availability were fit from actual H_2S concentrations at each time of the experiment. Values of sulfur availability of 0.63 and 0.12 mg/cm^2 were obtained after 153 and 300 days of exposure for samples inoculated in non aseptic and aseptic conditions respectively.

- Samples inoculated in non aseptic conditions using standard medium showed a wide variety of colors from dark green to black. They resulted severely deteriorated with a cottage cheese consistency after 153 days. Conversely, samples growth in salty medium appeared stiff at the end of the experiment, underlying the severity of biogenic deterioration in absence of salt in the inoculum. Samples exposed exclusively to H_2S did not show important deterioration indicating the preponderant effect of biogenic deterioration. On the other hand, samples inoculated in aseptic conditions showed stains of different colors including gray, green, bronze, and white shades. White crystals were observed after two and seven months upon samples inoculated in non aseptic and aseptic conditions respectively.

- Superficial irregularities augmented in samples inoculated with acidophilic bacteria in comparison with those inoculated with neutrophilic bacteria. This difference can be explained because of a possible clogging effect coming from bacterial metabolism.

- Based on the observations and preliminary proofs, tests of samples inoculated with salty media, pyritic samples, and samples added with Triclosan were not completed. Therefore, only ordinary samples inoculated with standard media (non aseptic and aseptic conditionsf) were investigated comprehensively.

Chapter 5

BIODETERIORATION EFFECTS UPON PHYSICAL AND MECHANICAL PROPERTIES OF MORTAR

5.1 Chapter overview

The main parameters used to investigate the biodeterioration of mortar were defined in chapter 3. In addition, it was decided in chapter 4 that only tests related to ordinary mortar samples are of interest. In the present chapter, the results of the physical and mechanical tests are presented. Then, in chapter 6 an application considering biodeterioration on the structural design of sewer pipes will be shown. The objectives of this chapter are:

- To describe and discuss critically how the samples weight changed due to biodeterioration.
- To describe and discuss critically how the samples porosity changed due to biode-

terioration.

- To describe and discuss critically how the samples compressive strength changed due to biodeterioration.
- To propose fit curves for the strength-porosity relations obtained from biodeteriorated samples.
- To present a summary and conclusions related to the experimental findings.

5.2 Weight variations in biodeteriorated samples

Humidity of samples evaluated in terms of absorbed water followed an ascendant trend as can be seen in Figure 5.1. Samples inoculated in non aseptic conditions Hn, At and nt absorbed water in amounts up to 54%, 81% and 57% (COV=0.52, 0.24 and 0.48) of their own weight, meaning that a large quantity of water had to be trapped in the samples' capillary pores and cracks, augmenting their volume considerably. Indeed, it was observed that, in the final-stage, At and Hn apparently caused samples to double their initial volume. In contrast, the ctrl and H_2S samples and salty-inoculated samples sustained their humidity throughout the experiment. Interestingly there were not changes in weight of Ats samples, while in Hns and nts samples a slight change in weight was perceived.

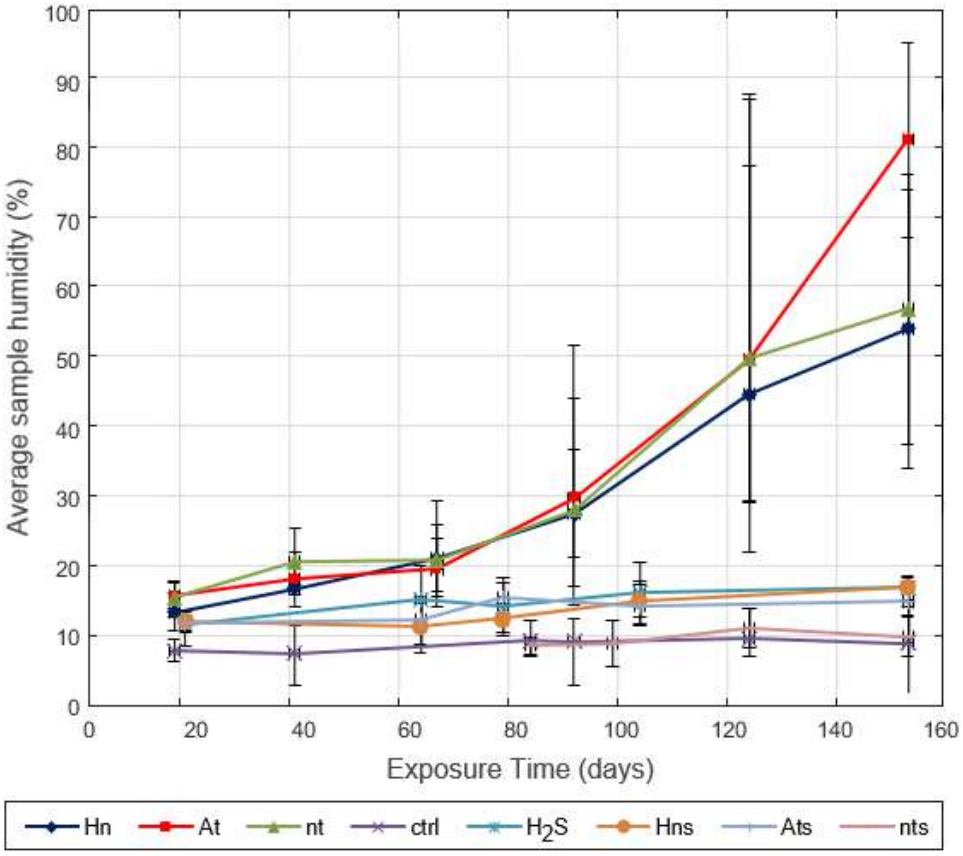

Figure 5.1: Humidity of exposed samples inoculated in non aseptic conditions. Error bars show minimum and maximum values.

Exposed surface/volume ratio (ESVR) of samples was approximately equal to 0.51 mm^2/mm^3, in contrast with the ESVRs used in previous research, which have varied between 0.12 *and* $0.41 mm^2/mm^3$ [30][57]. This characteristic and the high exposed surface could explain the greater weight loss found in this study compared with previous ones (Table 5.1).

After 153 days of exposure, weight losses of up to 23.22%, 32.44% and 20.27% (COV=0.50, 0.44 and 0.66) were measured in Hn, At and nt samples, respectively,

Table 5.1: Some exposed surface/volume ratios (ESRV) used in previous biodeterioration studies

Author	Sample size ($mm \times mm \times mm$)	ESRV (mm^2/mm^3)
This study	$13 \times 13 \times 10$	0.51
Nnadi and Madarriaga (2012)	$50 \times 50 \times 45$	0.12
Bielefeldt et al (2010)	$50 \times 20 \times 20$	0.24
Okabe et al (2007)	$40 \times 18 \times 8$	0.41

which strongly contrasted with those of the control (ctrl,1.05%) and H_2S-only control (3.79%)(Figure 5.2). It can be said that, within an ideal context, non-inoculated samples exposed to ordinary atmospheres did not have weight loss. A different trend was observed in samples inoculated with the salty medium. For example, while Hns and nts showed a slight weight loss up to 4.50% and 6.88%, respectively Ats showed a weight gain of 2.03% (Figure 5.3). Again it seems that biogenic deterioration from samples inoculated with *A. thiooxidans* in the seawater medium was negligible. Perhaps the halophile nature of *H. neapolitanus* made possible its weak growth and consequent affectation to concrete (weight loss up to 6.88%), while it seems that *A. thiooxidans* was not able to overcome the presence of salinity.

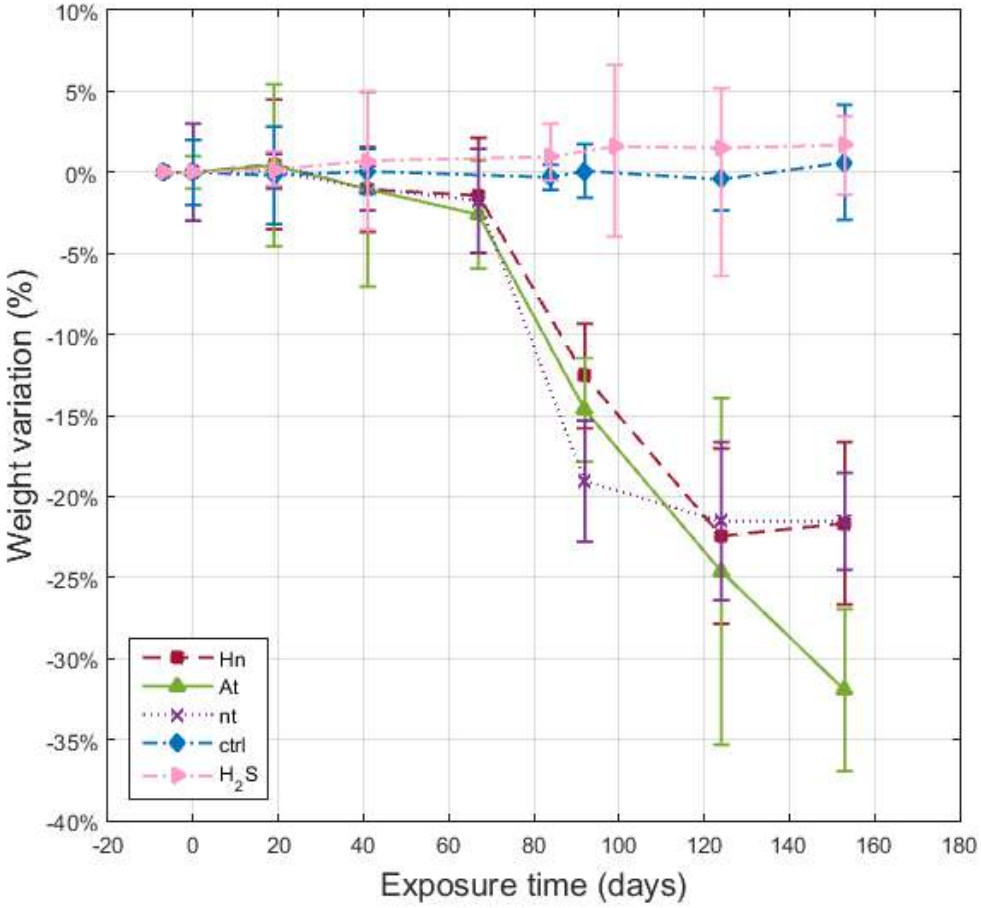

Figure 5.2: Weight loss of samples inoculated in non aseptic conditions using standard media

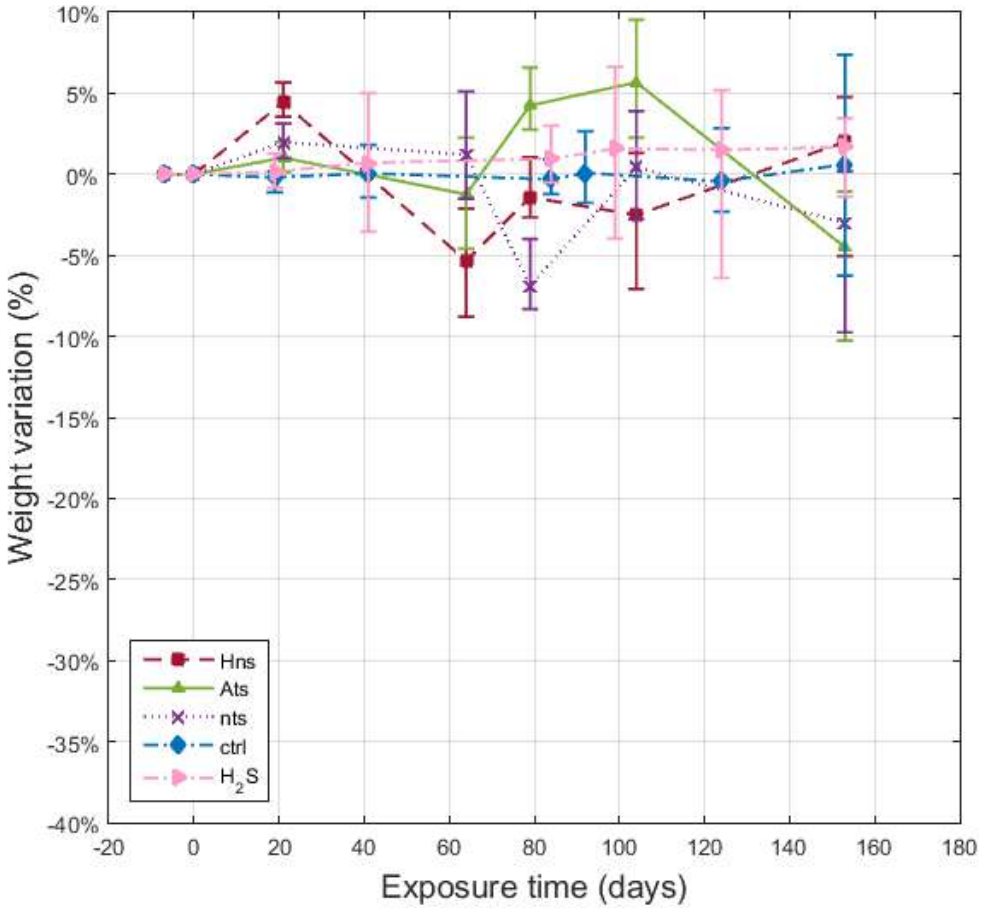

Figure 5.3: Weight loss of samples inoculated in non aseptic conditions using salty media

Table 5.2 shows the behavior of pyritic samples (PM) inoculated in non aseptic conditions and exposed to conditions described in section 3.3.3. Samples prepared with only Fe gained weight and augmented their volume due to the iron oxidation. Samples prepared with only S showed slight weight losses when inoculated with Hn and weight gains in other cases. Samples prepared with FeS_2 behaved similarly to control samples. These results cannot be considered as conclusive. This is an interesting issue to investigate in the future.

For OM samples inoculated in aseptic conditions, Figure 5.4 and Figures 5.5, 5.6,

Table 5.2: Average weight variations measured in pyritic samples during 153 days

	Bacterial exposure and sample properties. Values in %																	
Time (days)	H.n. Fe=0,47%	H.n. Fe=2,35%	A.t. Fe=0,47%	A.t. Fe=2,35%	Control Fe=0,47%	Control Fe=2,35%	H.n. S=0,53%	H.n. S=2,65%	A.t. S=0,53%	A.t. S=2,65%	Control S=0,53%	Control S=2,65%	H.n. FeS_2=1%	H.n. FeS_2=5%	A.t. FeS_2=1%	A.t. FeS_2=5%	Control FeS_2=1%	Control FeS_2=5%
0	0	0	0	0	0	0	0	0	0	0	0	0	0	0	0	0	0	0
23	2	1	0	1	1	2	-1	-1	1	1	1	0	0	-1	-1	-1	-1	-1
46	3	3	0	3	1	4	-1	-1	2	3	2	1	0	-2	-2	-1	-2	-1
60	2	2	0	3	1	3	-1	-1	2	2	1	1	0	-1	-1	-1	-2	-1
90	3	4	0	4	2	5	-1	-1	2	4	2	1	1	-2	-2	-1	-3	-1
120	3	5	0	5	2	6	-1	-1	3	5	2	2	1	-3	-2	-2	-4	-1
153	5	7	0	6	3	8	-1	-2	4	6	3	2	1	-4	-3	-2	-5	-2

5.7, 5.8 and 5.9. indicate that by the end of exposure (i.e., $Sa(t) \approx 0.12 mg/cm^2$), samples inoculated with the consortium showed a total weight loss of 6.8±1.4% (mean ± one standard deviation). Samples inoculated separately with *A. thiooxidans* and *H. neapolitanus* lost 4.6±1.4% and 2.4±0.5% of their initial weight, respectively. In contrast, weight gains of 1.0±0.8% and 0.5±0.6% were observed in abiotic samples exposed to H_2S and samples belonging to control, respectively. The abiotic samples exposed to hydrogen sulfide likely gained weight as a result of the accumulation of precipitated sulfur. The small weight variation in the control samples is within the expected error of the experimental measurement technique. Figures 5.4, 5.5, 5.6, 5.7, 5.8 and 5.9 include all measurements (from 6 to 9 measures) by exposure time. The greatest data variability was observed in samples inoculated with *Acidithiobacillus thiooxidans*.

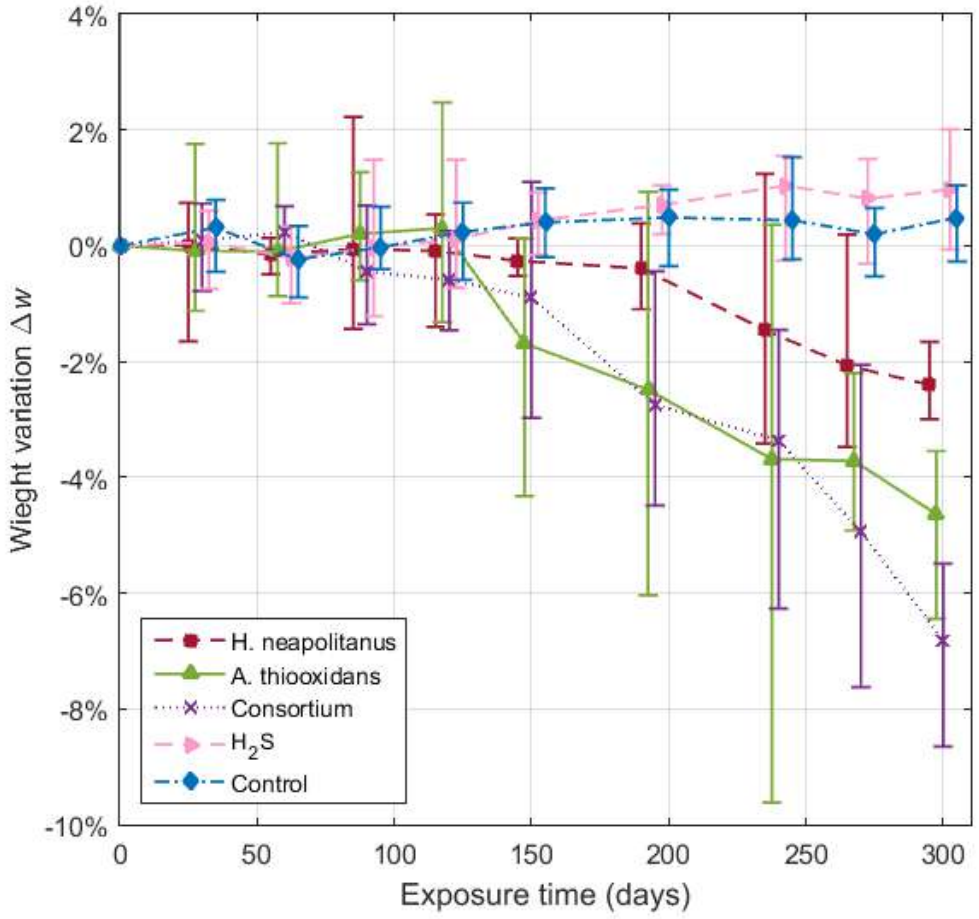

Figure 5.4: Average weight loss of samples inoculated in aseptic conditions

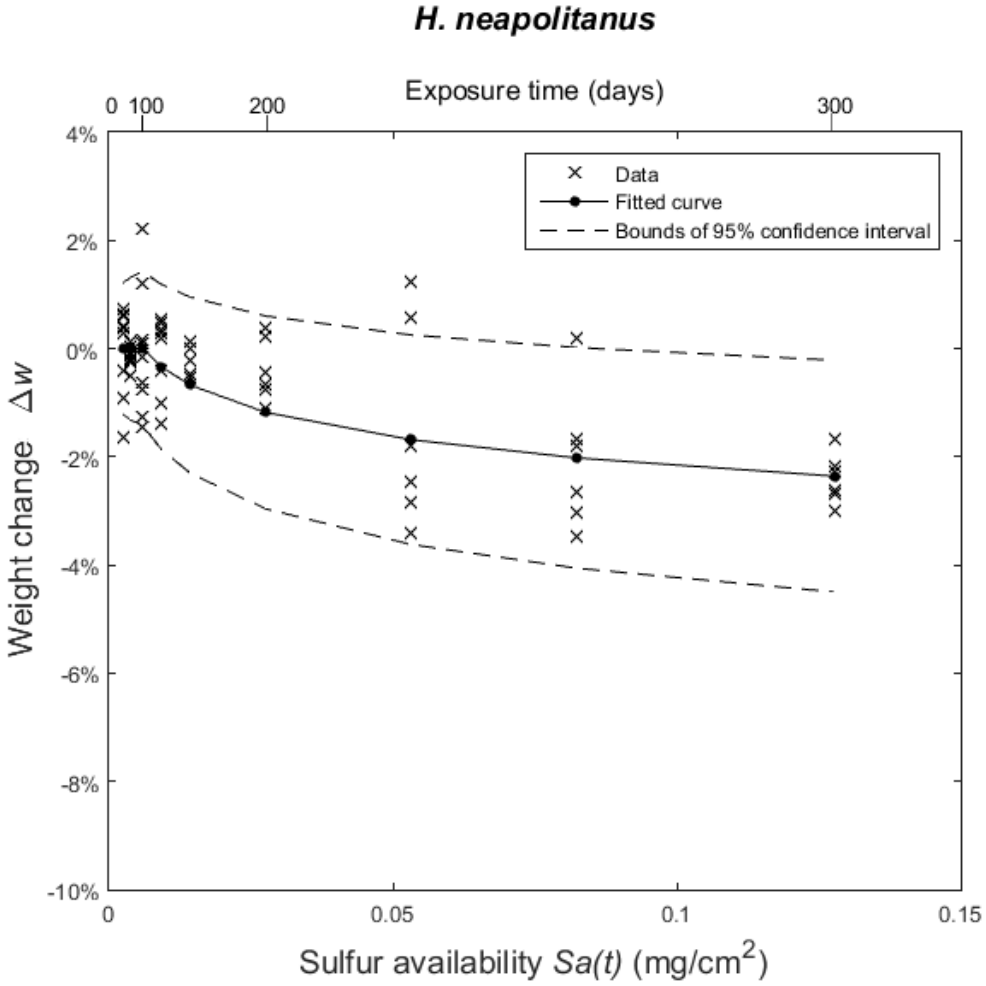

Figure 5.5: Comparison between proposed curves and measured data for weight changes in carbonated samples dried at 110^{o}C- *H.Neapolitanus*

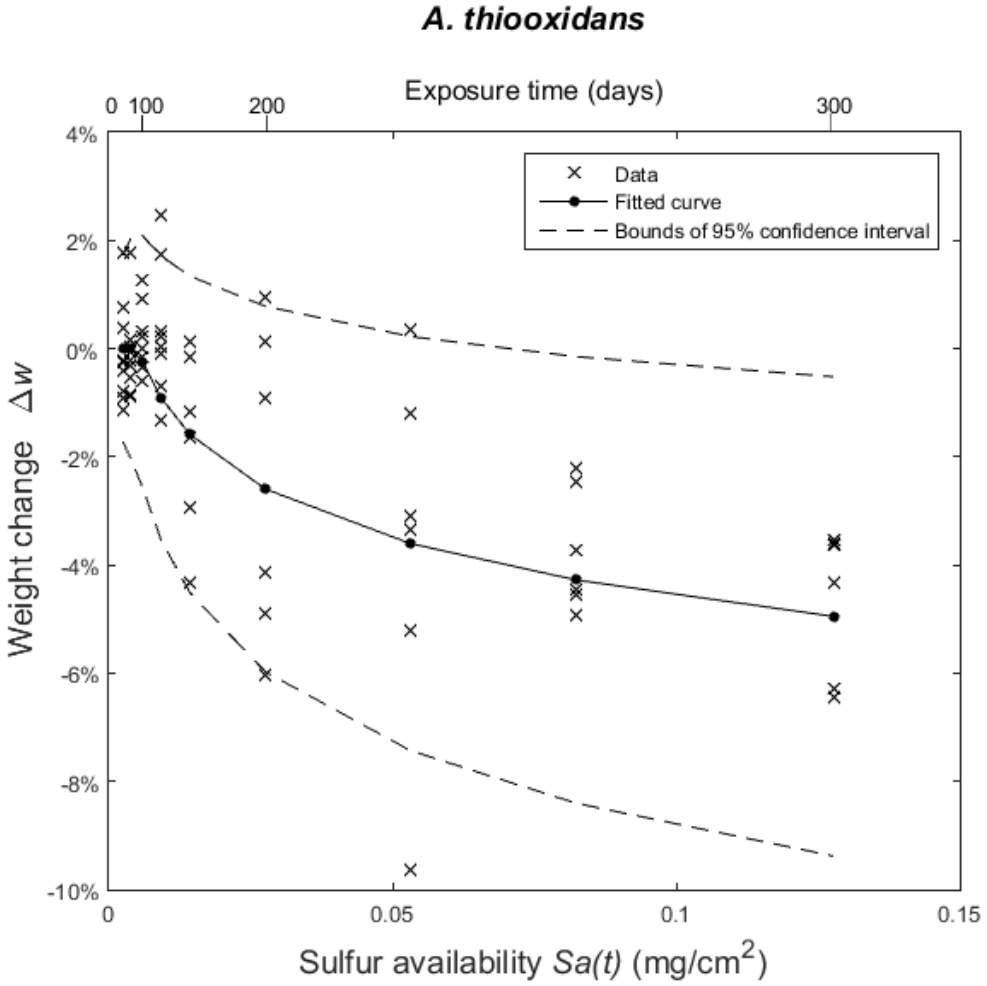

Figure 5.6: Comparison between proposed curves and measured data for weight changes in carbonated samples dried at 110^{o}C - *A.Thiooxidans*

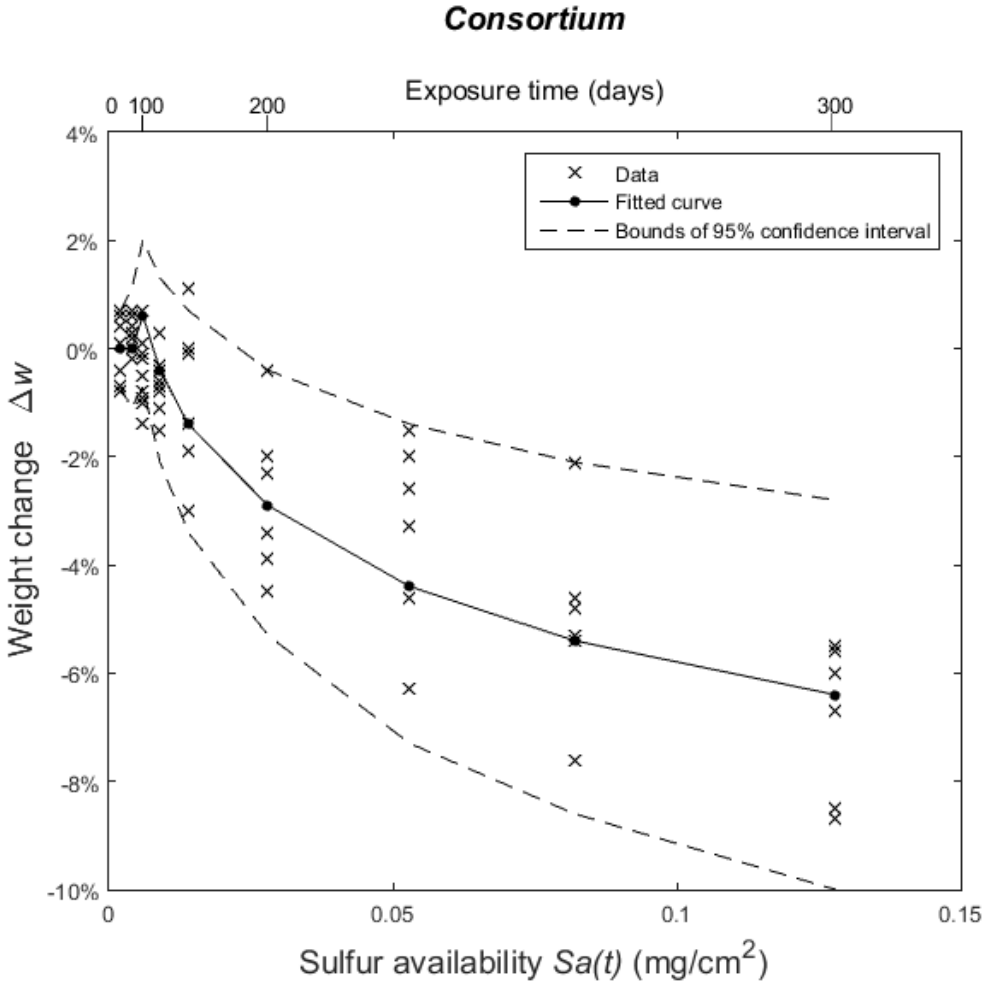

Figure 5.7: Comparison between proposed curves and measured data for weight changes in carbonated samples dried at 110^{o}C - Consortium

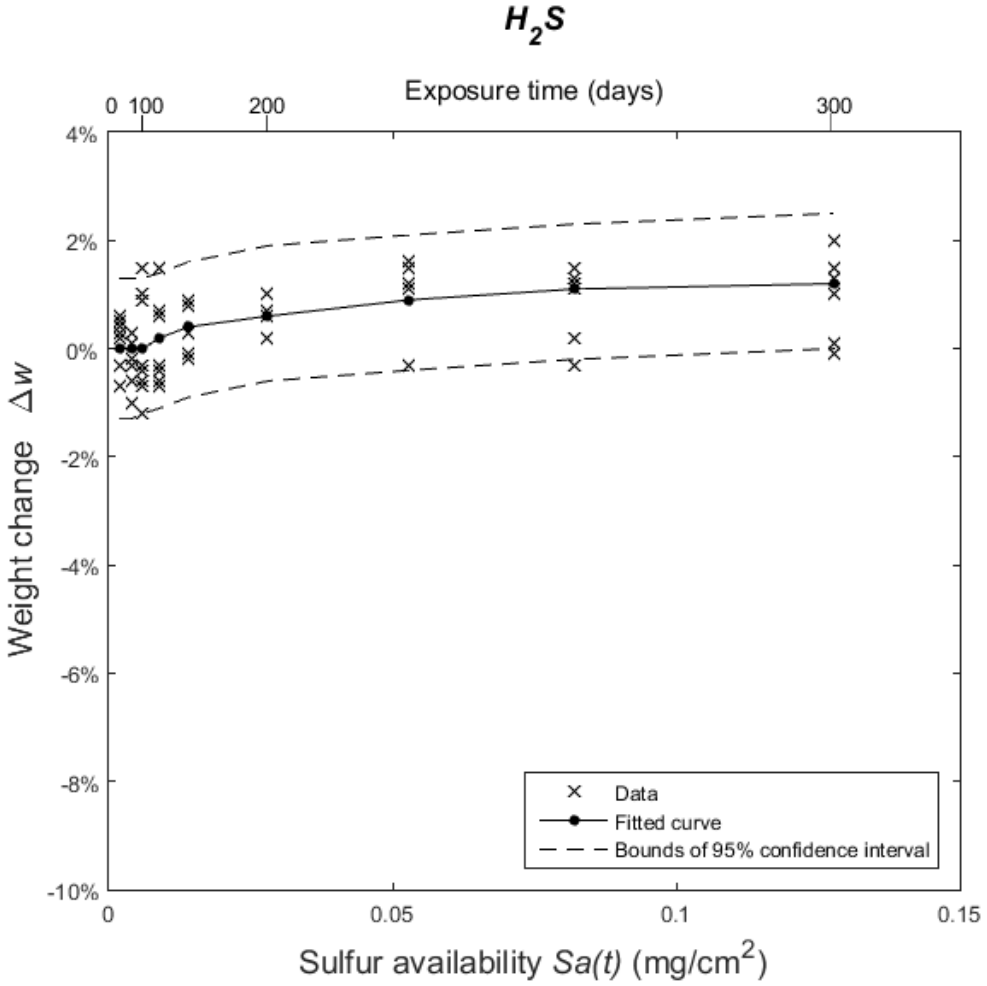

Figure 5.8: Comparison between proposed curves and measured data for weight changes in carbonated samples dried at 110^{o}C - H_2S

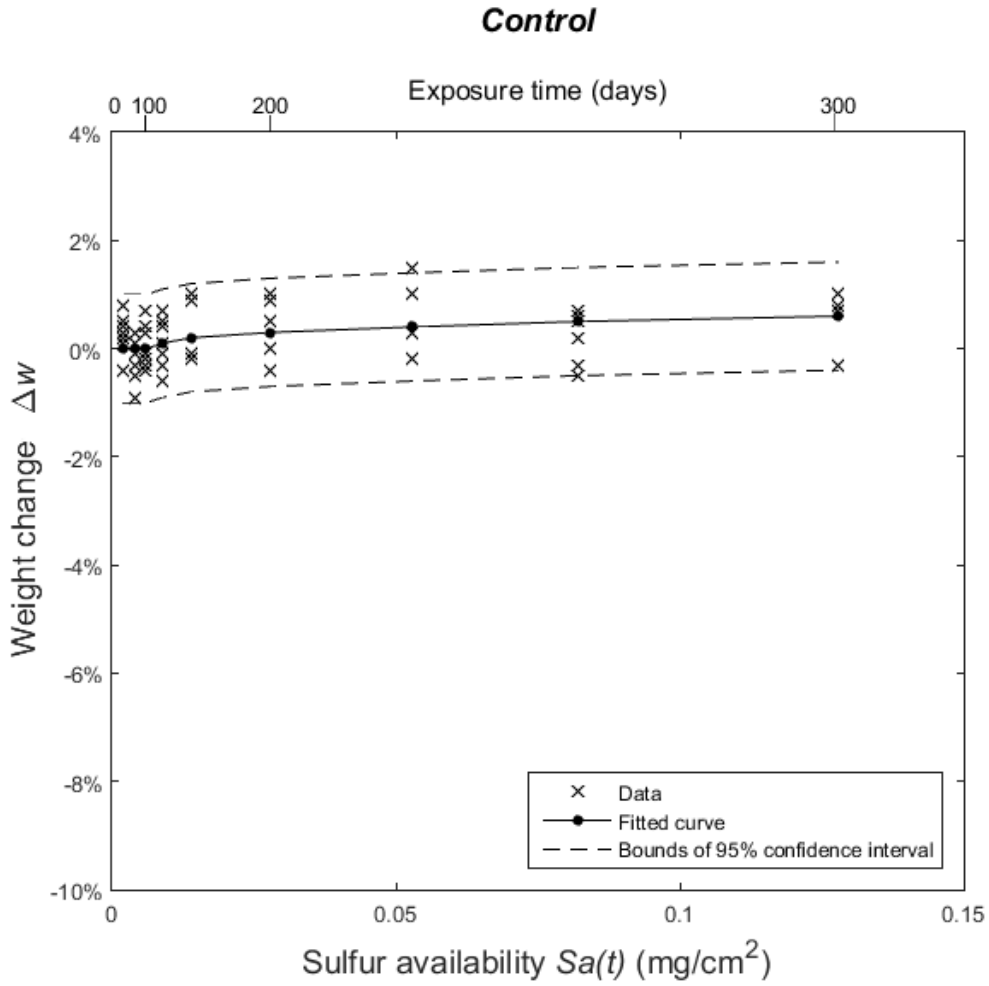

Figure 5.9: Comparison between proposed curves and measured data for weight changes in carbonated samples dried at 110^{o}C - Control

Table 5.3 provides the adjusted expressions for the standard deviation for all experimental conditions and Figures 5.5, 5.6, 5.7, 5.8 and 5.9 compares the fitted curves and measured data for weight change. Overall results indicate greater weight loss after feeding frequency was changed from once every three days to every day (day 150 or $Sa(t) \approx 0.016 mg/cm^2$) (Figure 5.10). Larger weight changes started after $Sa(t) \approx 0.011 mg/cm^2$ (120 days) in all biotic samples inoculated in aseptic conditions. Lower weight losses during the first three months of the experiment resulted

from the time required for superficial conditioning (pH drop, biofilm formation, roughness adaptation) and bacterial lag phase. After this span the acidophilic bacteria (alone and within the consortium) seemed to be capable of growing faster and acidifying the concrete surface leading to greater weight loss. The effect of the neutrophilic bacteria on the weight of the samples was less pronounced. The lower effects of *H. neapolitanus* than *A. thiooxidans* on the weight of the samples could be a result of differences in growth rates, selectivity of the reduced sulfur metabolites available, accumulation of toxic byproducts, and other metabolic differences.

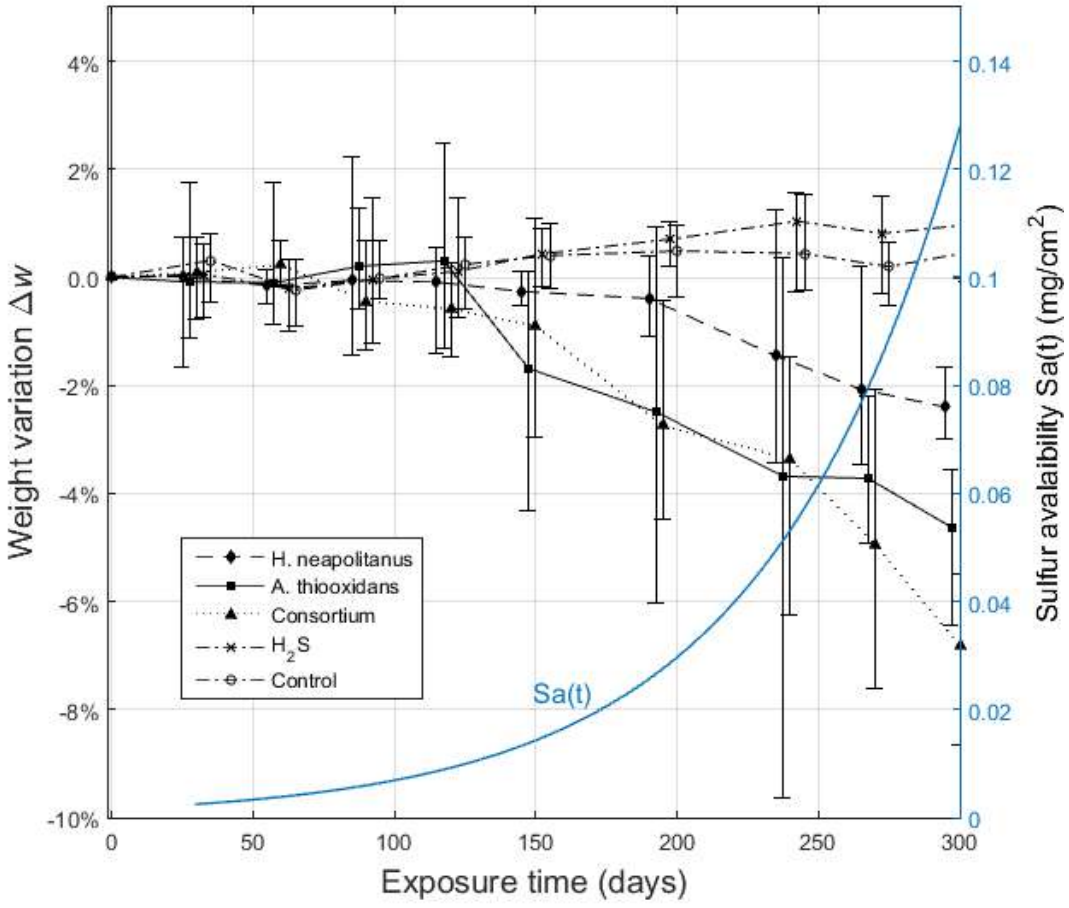

Figure 5.10: Relationship between weight changes and sulfur availability

Negligible weight variation (losses from 0.1 to 0.5%) is associated to $Sa(t) \leq Sa_{lim} = 0.006 mg/cm^2$. This value corresponds to the accumulated sulfur applied during the first 90 days of exposure (Figure 3.4). It is also noted that the mean weight change follows a logarithmic trend after this value. Table 5.3 summarizes the best fit equations for the weight variation once $Sa(t) \geq Sa_{lim}$. For practical purposes it can be assumed that there is no weight variation ($\Delta w = 0$) if $Sa(t) < Sa_{lim}$.

Table 5.3: Equations of curves fittings for properties variation when $Sa(t) \geq 0.006 mg/cm^2$

Condition	**Description**	**Property variation (%)**
Inoculated with *H.n.*	Weight change	$\Delta w(Sa(t)) = -0.77ln(Sa((t)) - 3.94$
	Porosity change	$\Delta \phi(Sa(t)) = 0.47ln(Sa(t)) + 3.06$
	Strength change	$\Delta s(Sa(t)) = -6.0ln(Sa(t)) - 40.00$
Inoculated with *A.t.*	Weight change	$\Delta w(Sa(t)) = -1.54ln(Sa((t)) - 8.11$
	Porosity change	$\Delta \phi(Sa(t)) = 1.74ln(Sa(t)) + 9.79$
	Strength change	$\Delta s(Sa(t)) = -7.33ln(Sa(t)) - 46.70$
Inoculated with Cons.	Weight change	$\Delta w(Sa(t)) = -2.29ln(Sa((t)) - 11.07$
	Porosity change	$\Delta \phi(Sa(t)) = 1.09ln(Sa(t)) + 6.45$
	Strength change	$\Delta s(Sa(t)) = -8.40ln(Sa(t)) - 70.59$
Abiotic H_2S	Weight change	$\Delta w(Sa(t)) = 0.40ln(Sa((t)) + 2.04$
	Porosity change	$\Delta \phi(Sa(t)) = 0.76ln(Sa(t)) + 4.07$
	Strength change	$\Delta s(Sa(t)) = -5.55ln(Sa(t)) - 36.50$
		Standard deviation (%)
Inoculated with *H.n.*	Weight change	$\sigma_w(Sa(t) = 0.12ln(Sa(t)) + 1.34$
	Porosity change	$\sigma_\phi(Sa(t)) = 2.50$
	Strength change	$\sigma_s(Sa(t)) = -1.40ln(Sa(t)) + 1.95$
Inoculated with *A.t.*	Weight change	$\sigma_w(Sa(t) = 0.35ln(Sa(t)) + 2.98$
	Porosity change	$\sigma_\phi(Sa(t)) = 2.70$
	Strength change	$\sigma_s(Sa(t)) = 0.87ln(Sa(t)) + 14.66$
Inoculated with Cons.	Weight change	$\sigma_w(Sa(t) = 0.37ln(Sa(t)) + 2.60$
	Porosity change	$\sigma_\phi(Sa(t)) = 3.08$
	Strength change	$\sigma_s(Sa(t)) = -1.50ln(Sa(t)) + 2.30$
Abiotic H_2S	Weight change	$\sigma_w(Sa(t) = 0.64$
	Porosity change	$\sigma_\phi(Sa(t)) = 2.73$
	Strength change	$\sigma_s(Sa(t)) = -0.90ln(Sa(t)) + 2.67$

Figures 5.5, 5.6, 5.7, 5.8 and 5.9 indicates that the dispersion of data from biotic samples increases with the exposure time. The largest standard deviation increase was associated to the presence of *A. thiooxidans* alone or within the consortium. Standard

deviation for control samples and those exposed to H_2S was constant during the exposure time. Standard deviation of control samples can be associated to uncertainties related to material (intrinsic uncertainty) and the test. Standard deviation of abiotic samples exposed to H_2S can be related to uncertainties coming from the chemical exposure. By comparing uncertainties at the end of the exposure, it is concluded that biodeterioration multiplies by about two or three the initial uncertainties (intrinsic, test and H_2S exposure).

In this section results of weight variations have been presented for samples inoculated in non aseptic and aseptic conditions. To verify the purity of samples inoculated in aseptic conditions during the whole experiment, one face of them was stamped on Agar at each sampling moment (Figure 5.11).

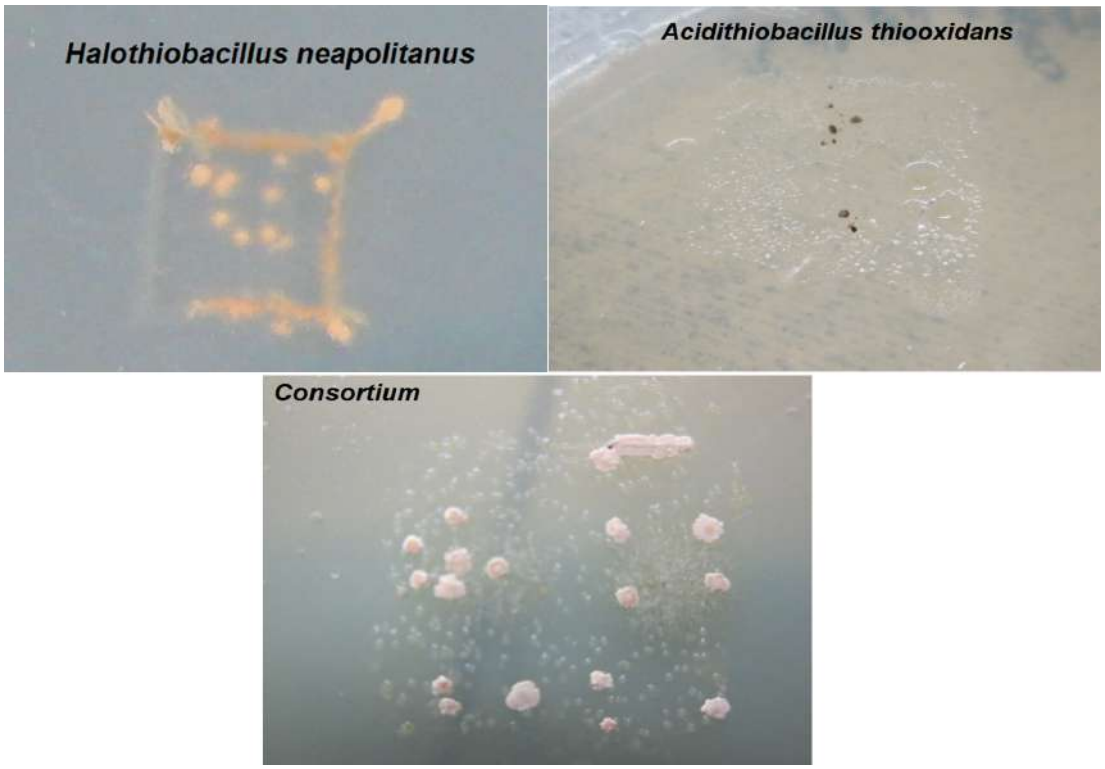

Figure 5.11: Verification of purity of strains by stamping one face of exposed samples upon Agar

Although addition of Triclosan showed an acceptable antimicrobial effect, it caused

a disaggregating effect. Little amounts of material losses were observed even in old samples and strength tests showed a capacity of about 15-25% that of ordinary mortar samples. For these reasons no further analyses were made to samples added with Triclosan.

5.3 Porosity variations in biodeteriorated samples

Average total porosity and its distribution were calculated and plotted from the average of three measurements for Hn, At, nt, ctrl and H_2S samples (inoculated in non aseptic conditions). Porosity tests for Hns, Ats and nts samples were not performed due to the negligible biodeterioration observed. Total porosity and typical distribution of pores in non-exposed (ctrl) samples were found to be similar to those reported in the literature [41] [42] [43]. In general, biodeterioration produced an increase in total porosity compared with that observed in control samples (Table 5.4). Also, porosity increase from biogenic activity was larger than that produced by chemical attack (H_2S). At early ages, in ctrl samples, 44% of the pores volume had sizes larger than 45000 nm (0.045 mm) which are believed to be placed on the surface. On the other hand, while 10-5000 nm pores' average volume increased up to 17% in exposed inoculated samples, it decreased up to 7% in control samples. The average volume of pores larger than 5000 nm increased up to 15% in inoculated samples while that of the control (ctrl) dropped up to 4%. Comparing the total porosity increase in samples exposed to H_2S (21%) with that of the inoculated samples (up to 32%) it is evident that biogenic attack was able to produce a porosity increase of about 11%.

Between days 23 and 98 (75 days) of exposure, Hn and At samples showed similar porosity changes (19% to 21%), probably due to the nearness of optimum pH in the surface of samples for each bacterium. In the same period, nt samples changed their porosity from 22% to 24%. However, while Hn and At maintained porosity around 19% between exposure days 0 and 23, the nt samples' porosity grew from 19% to 22% (Table 5.4). This could be explained by the fact that, in early exposure stages, consortium

Table 5.4: Total porosity variation in biodeteriorated samples inoculated in non aseptic conditions

Size range	**Day**	**Hn**	**At**	**nt**	H_2S	**ctrl**
10-5000nm	0	9%	9%	9%	9%	9%
	23	11%	13%	14%	9%	11%
	98	15%	15%	14%	10%	11%
	131	16%	17%	16%	15%	11%
>5000nm	0	9%	9%	9%	9%	9%
	23	6%	5%	7%	9%	5%
	98	7%	5%	10%	5%	4%
	131	13%	15%	12%	4%	4%
All (Total porosity)	0	19%	19%	19%	19%	19%
	23	19%	19%	22%	19%	17%
	98	21%	20%	24%	16%	17%
	131	29%	32%	28%	21 %	17%

was more aggressive, inhibiting the natural trend of cementitious material to react chemically and become more compact.

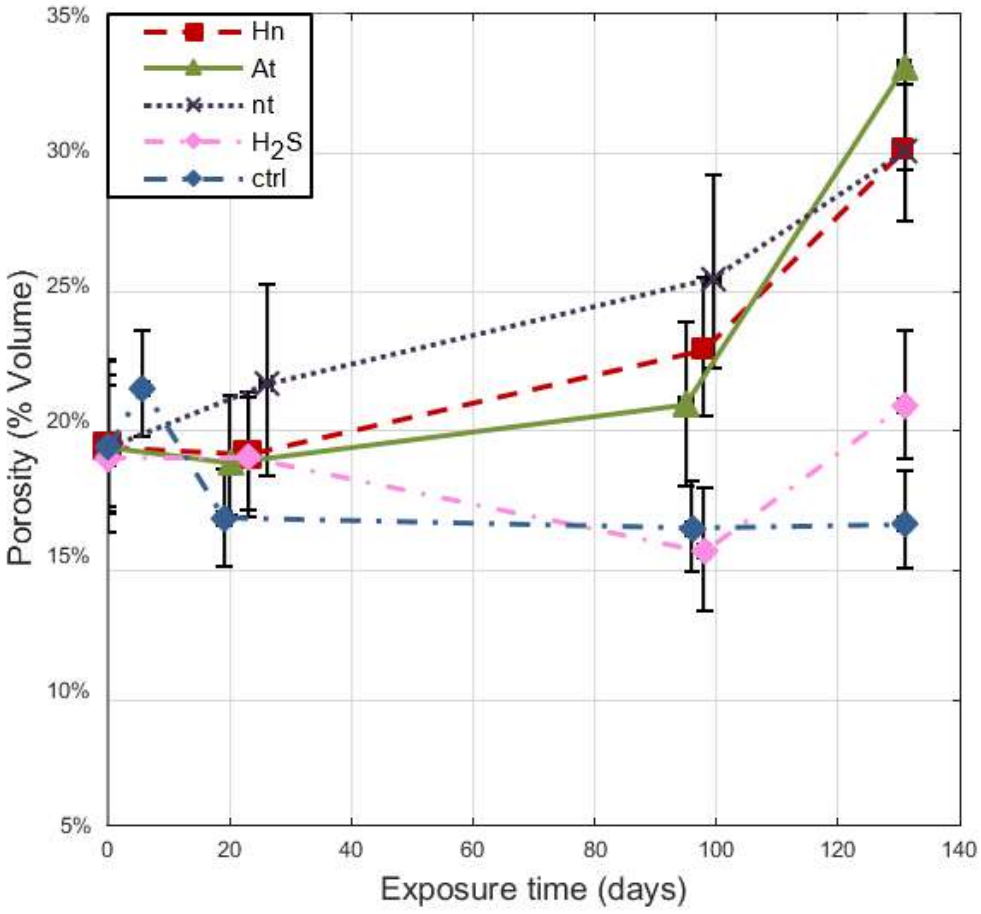

Figure 5.12: Total (open) porosity variation during exposure (inoculated in non aseptic conditions)

At the end of the experiment total porosity changes observed in inoculated samples were almost four times those observed in control samples. Severe deterioration could be associated with final total porosity values of 32% in At, 29% in Hn and 28% in nt (COV=0.13, 0.21 and 0.18) (Figure 5.12). It is evident that the effect from biogenic attack upon porosity is more important than that from chemical attack. As for the biogenic samples, it is possible that the competition between bacteria in the consortium could have inhibited biodeterioration leading to a minor porosity change in nt samples.

Also, it seems that porosity changes produced by chemical exposure are fairly similar to those observed in control samples during the first 100 days. For these reasons, it could be said that the most important bacterial growth occurred after three months of exposure.

It can be seen in Figures 5.13, 5.14 and 5.15 that more important changes in porosity are in the macropores range (size larger than 5000 nm). However, the peak shown around 6000 nm for 153 days of exposure does not have a rational explanation. For this, it is believed that such peak corresponds to cracking into samples as a result of manufacturing deficiencies. On the other hand, mesopores (10-5000 nm) showed less affectation.

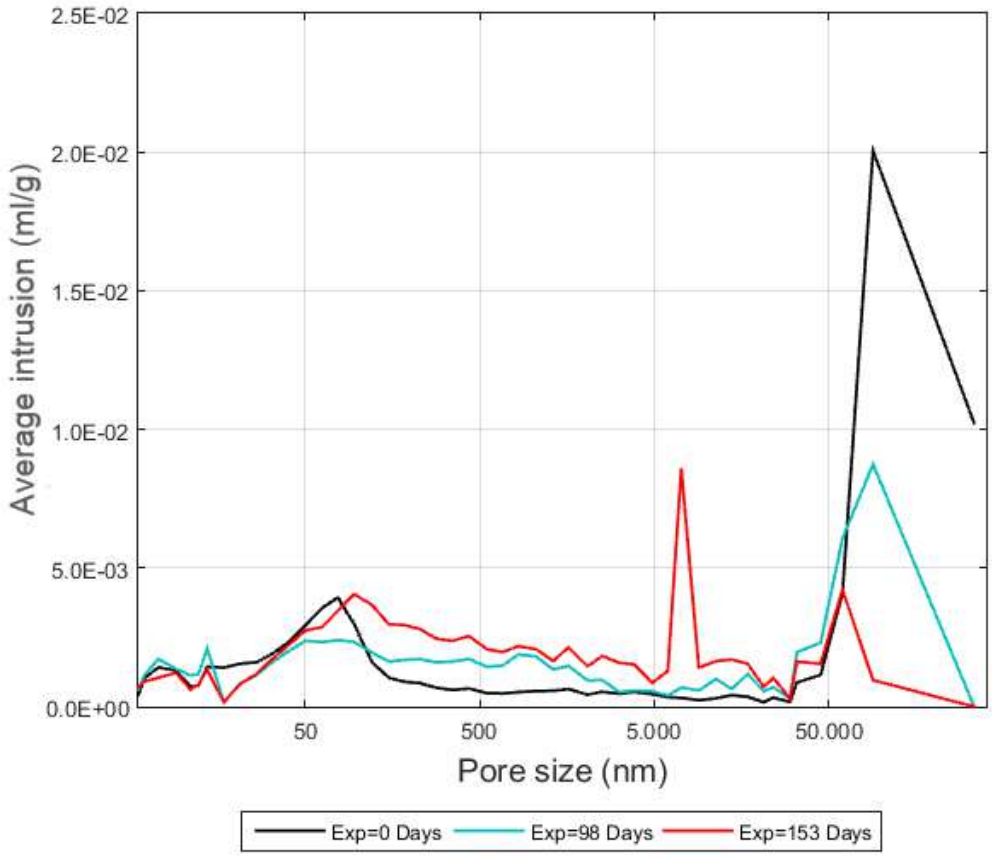

Figure 5.13: Average mercury intrusion of samples Hn during exposure inoculated in non aseptic conditions.

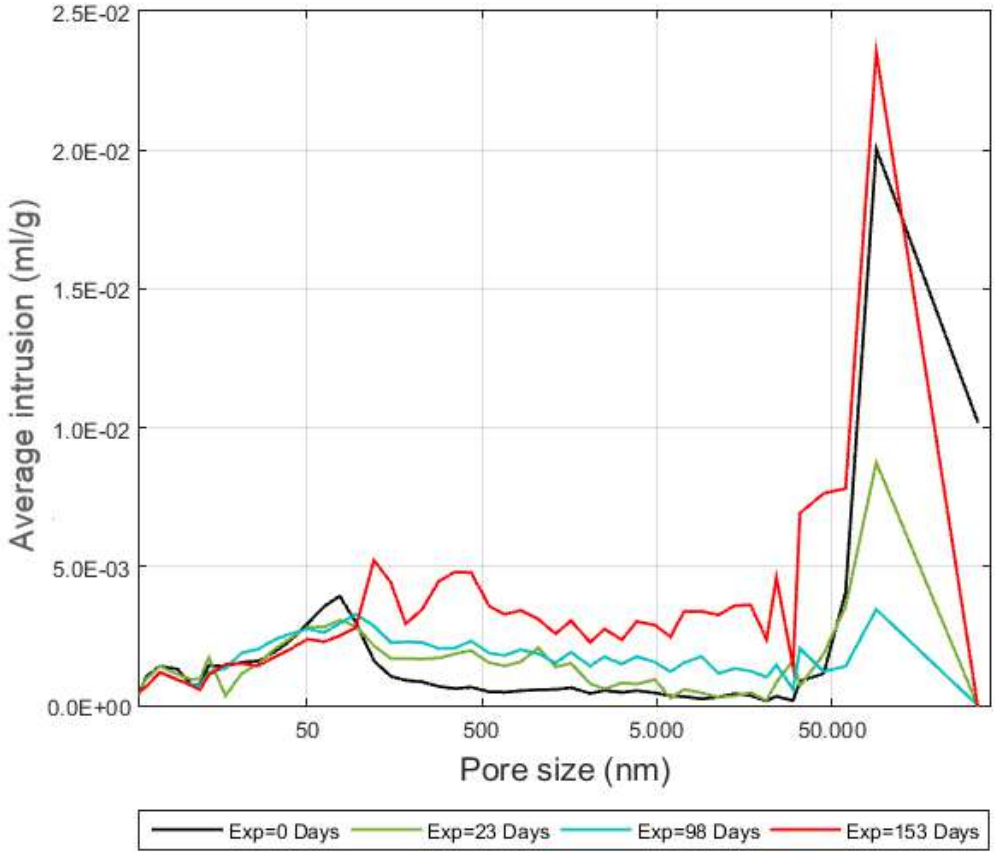

Figure 5.14: Average mercury intrusion of samples At during exposure inoculated in non aseptic conditions.

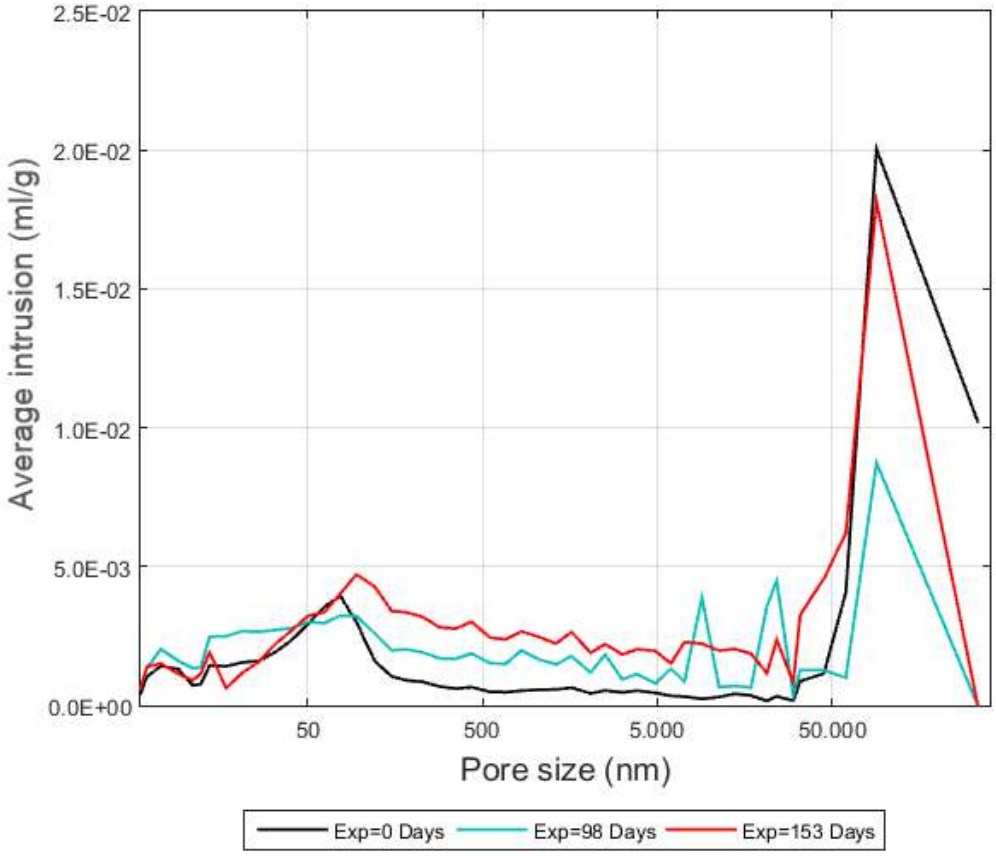

Figure 5.15: Average mercury intrusion of samples nt during exposure inoculated in non aseptic conditions.

As discussed previously, samples containing acidophilic bacteria (At and nt) showed more important porosity changes at the macropores range and less pronounced variations in the mesopores range (Figure 5.14 and Figure 5.15). Nevertheless, larger relative porosity changes in all pore sizes were observed in samples containing acidophilic bacteria. The highest intrusion peak resulted in big pores upon At samples (Figure 5.14).

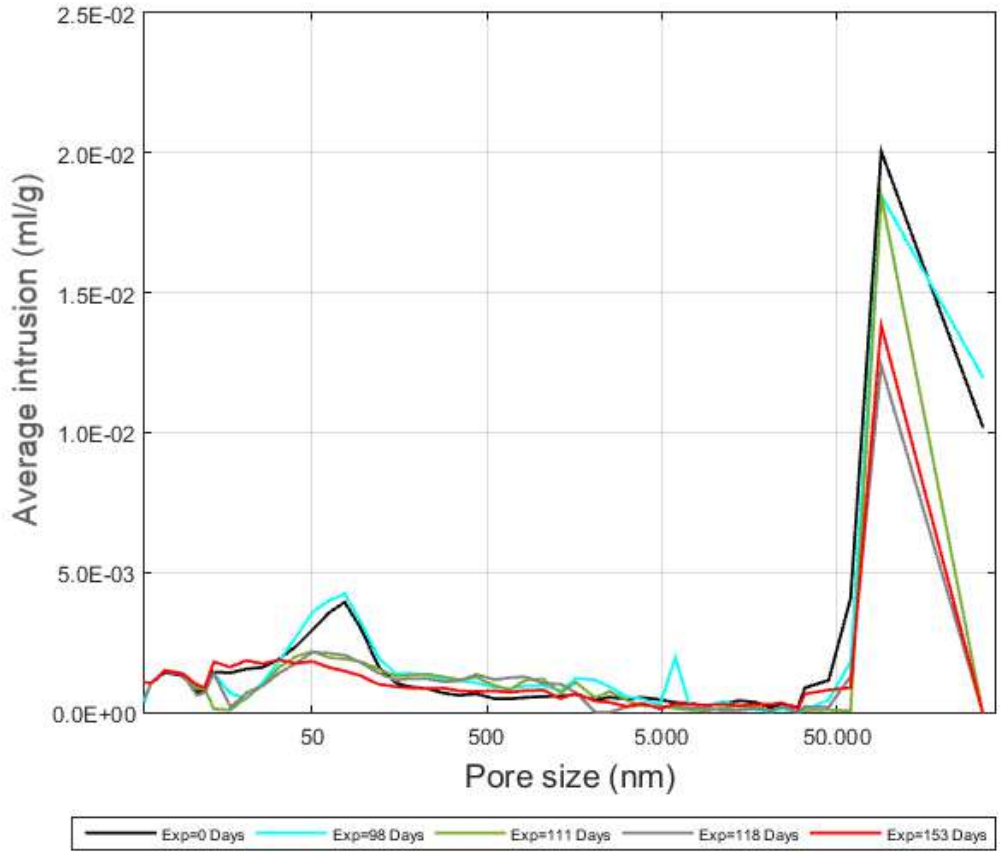

Figure 5.16: Average mercury intrusion of control samples in case of non aseptic conditions.

Figure 5.16 presents the porosity variation during the experiment for control samples. The general trend is to close all the pores with the time. This explains the reduction in total porosity (from 19 to 17%). Such behavior is caused by the natural chemical reaction of mortar while it is aging.

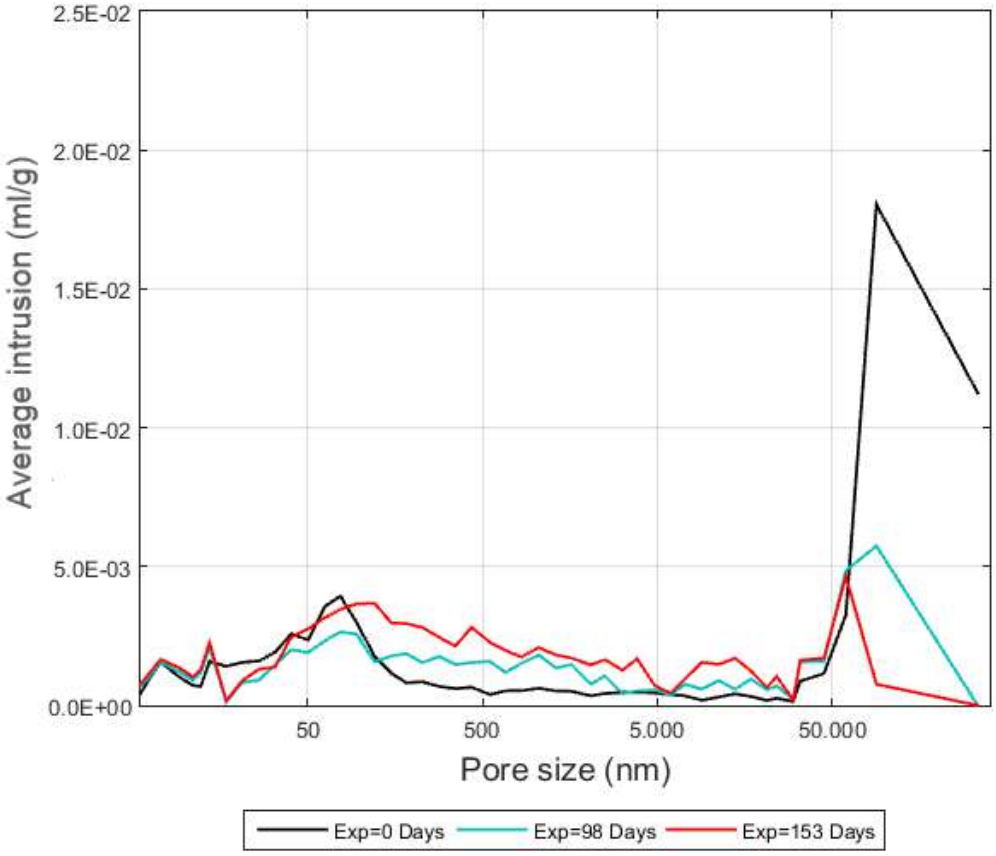

Figure 5.17: Average mercury intrusion of H_2S samples (case of non aseptic conditions).

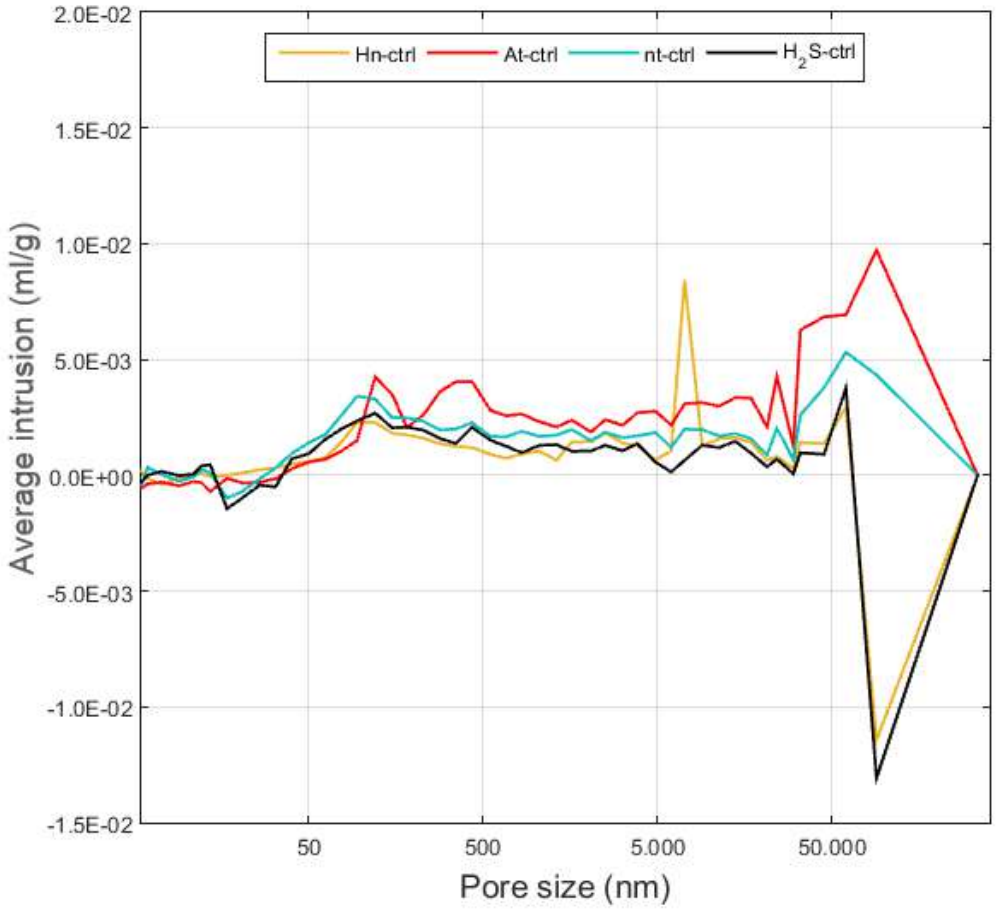

Figure 5.18: Average mercury intrusion with respect to control (case of non aseptic conditions).

Figure 5.18 has been constructed subtracting control samples mercury intrusion values from those of each type of sample. It is evident that chemical and biological attack augment the porosity specially that linked to large pore sizes. A comparison of Figure 5.13, 5.17. and 5.18. leads to conclude that the behavior of samples inoculated with *neutrophilic bacteria (Hn)* is highly similar to that of abiotic samples exposed to H_2S. This seems indicate that biogenic effects from *H. neapolitanus* have a low impact on the mortar damage.

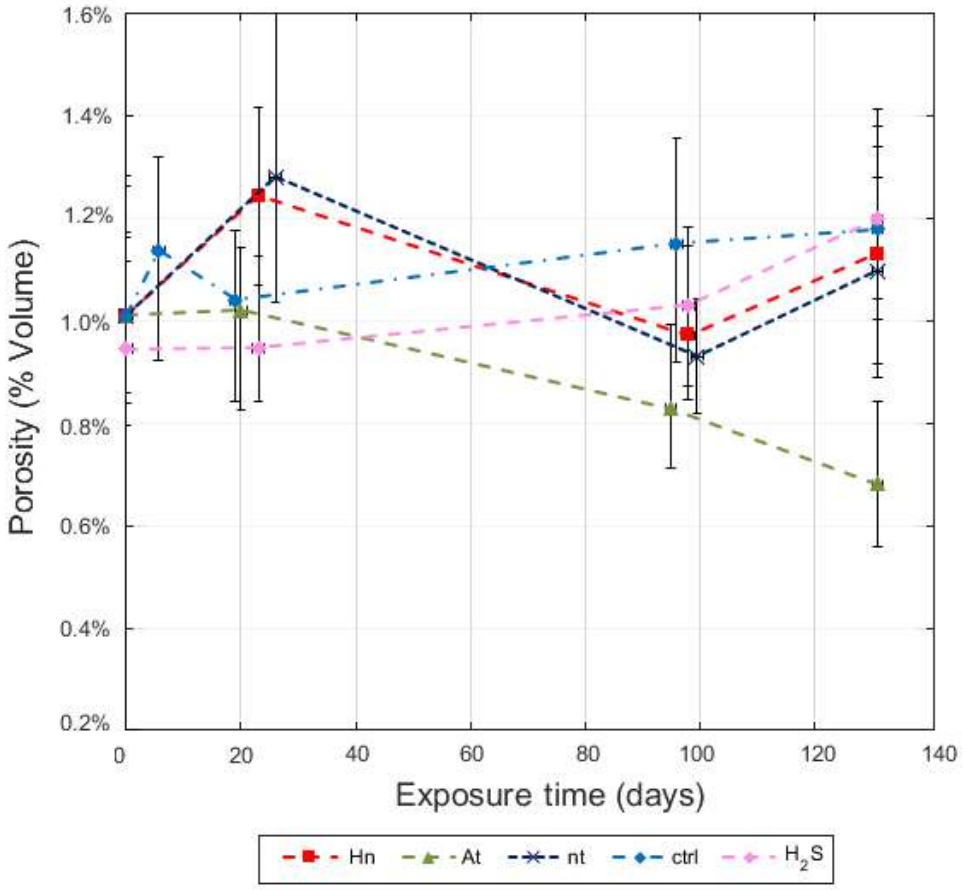

Figure 5.19: Volume variation in pores smaller than 10 nm (case of non aseptic conditions)

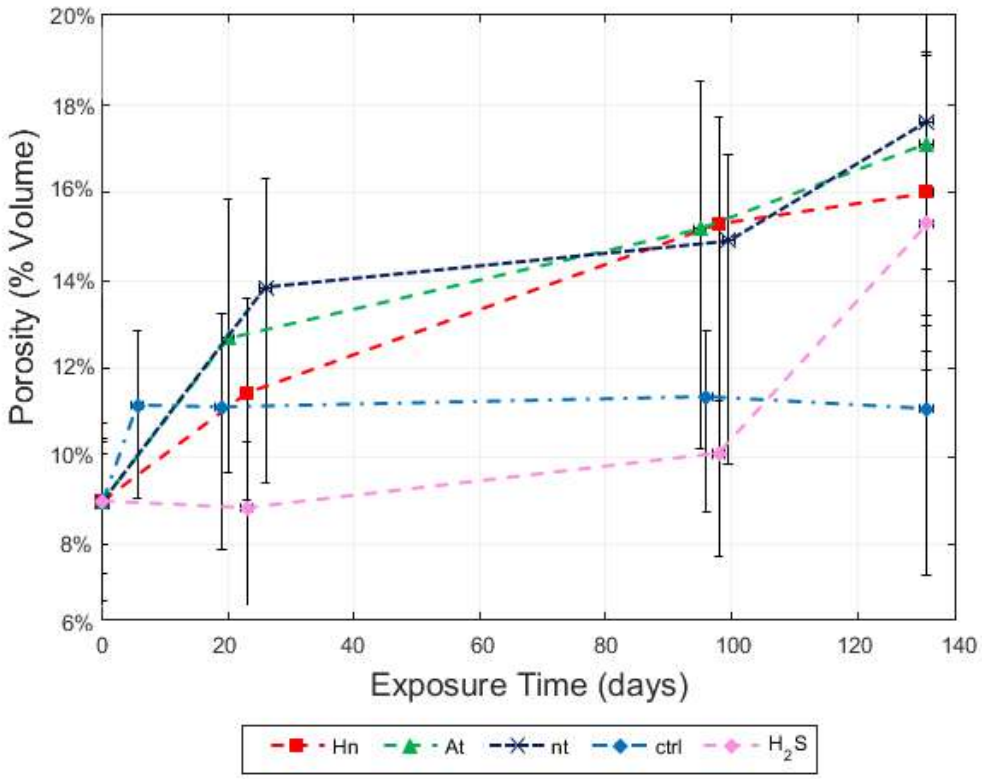

Figure 5.20: Volume variation in pores between 10 and 5000 nm (case of non aseptic conditions)

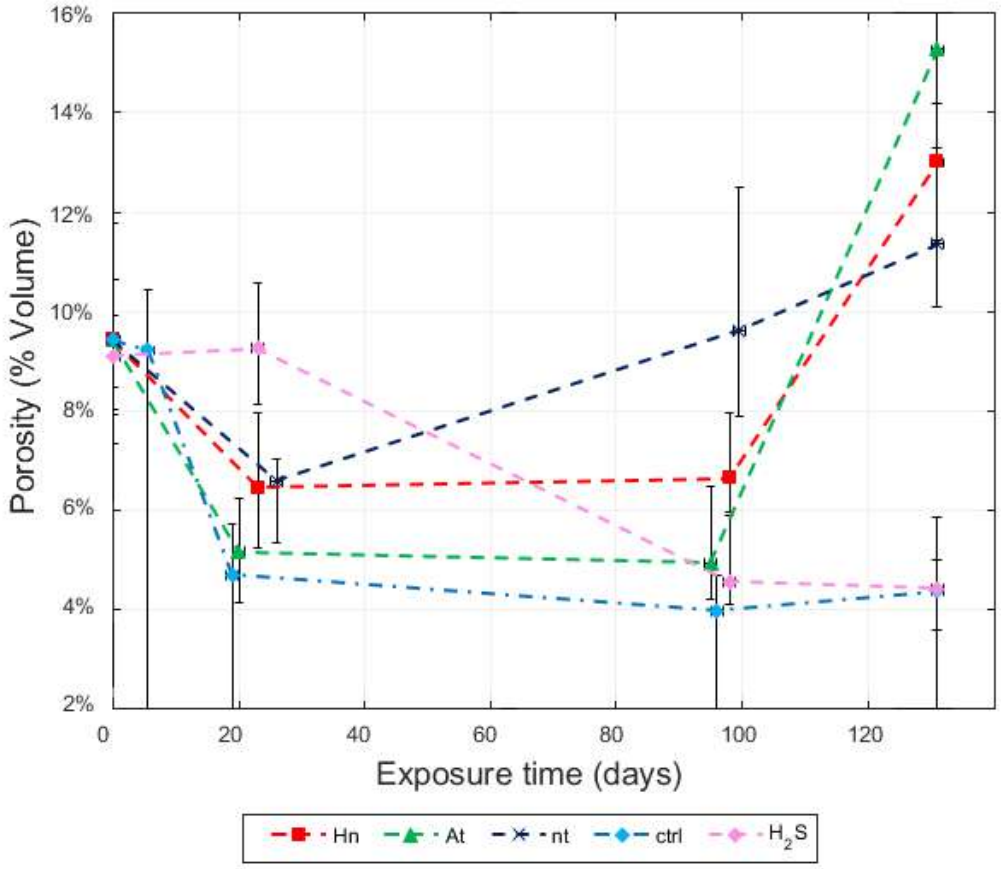

Figure 5.21: Volume variation in pores larger than 5000 nm (case of non aseptic conditions)

No changes in porosity were observed in small pores (sizes smaller than 10 nm) of samples after exposure to bacterial attack (Figure 5.19). This means that biodeterioration was not able to affect the gel pores and their dynamics. Largest changes in porosity were observed after 90 days of exposure. The existence of a bacterial adaptation period is evident (Figure 5.20 and 5.21).

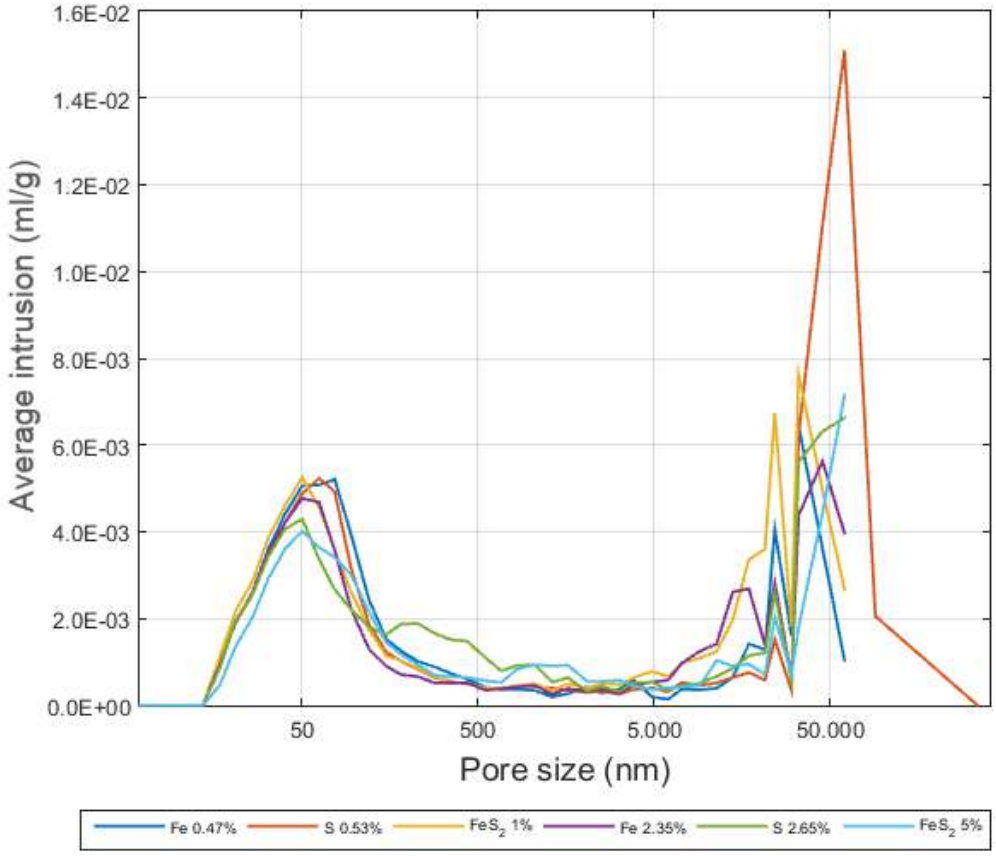

Figure 5.22: Average mercury intrusion of pyritic samples at the experiment initiation.

Porosity tests for pyritic samples were done only at the experiment initiation at time $t = 0$ (Figure 5.22). In virtue of laboratory limitations and the low influence of biodeterioration observed in weight tests after 150 days, no further assessments were done related to these samples. In any event, the following analysis can be useful for future works. From Figure 5.22, it can be seen that the larger the Fe amount the lower the total porosity. This is probably due to that iron oxidation (solid volume increase) tends to close the pores. Perhaps possible cracking due to the volume augment coming from iron oxides induced less empty cavities than that filled with corrosion products.

Conversely, the larger the S amount the larger the porosity which can be explained because the sulfur solubility. Cavities arisen from sulfur wash that is not bonded chemically are filled with water. When such water evaporates leaves additional empty spaces. For samples made with FeS_2 occurs the same as the Fe samples.

Samples inoculated in aseptic conditions were subjected to porosity tests too. At the end of the experiment (300 days), values of 0.087, 0.128, 0.114, 0.151, and 0.133 ml/g were measured in control samples, abiotic samples exposed to H_2S, and samples inoculated with *H. neapolitanus*, *A. thiooxidans* and the consortium respectively (Figure 5.28). The lower porosity variation in samples inoculated with *H. neapolitanus* is consistent with their small weight losses and the results reported for samples inoculated in non aseptic conditions. The larger porosity increase was observed for pores between 700 and 1500 nm in samples inoculated with *A. thiooxidans*. Interestingly, those show a pore volume increase for pore sizes around 1μm (1000nm), which is the average length of the *A. thiooxidans* bacillus. Samples inoculated with the consortium and abiotic samples exposed to H_2S showed an increase in pores between 7000 and 15000 nm suggesting the formation of new capillary pores.

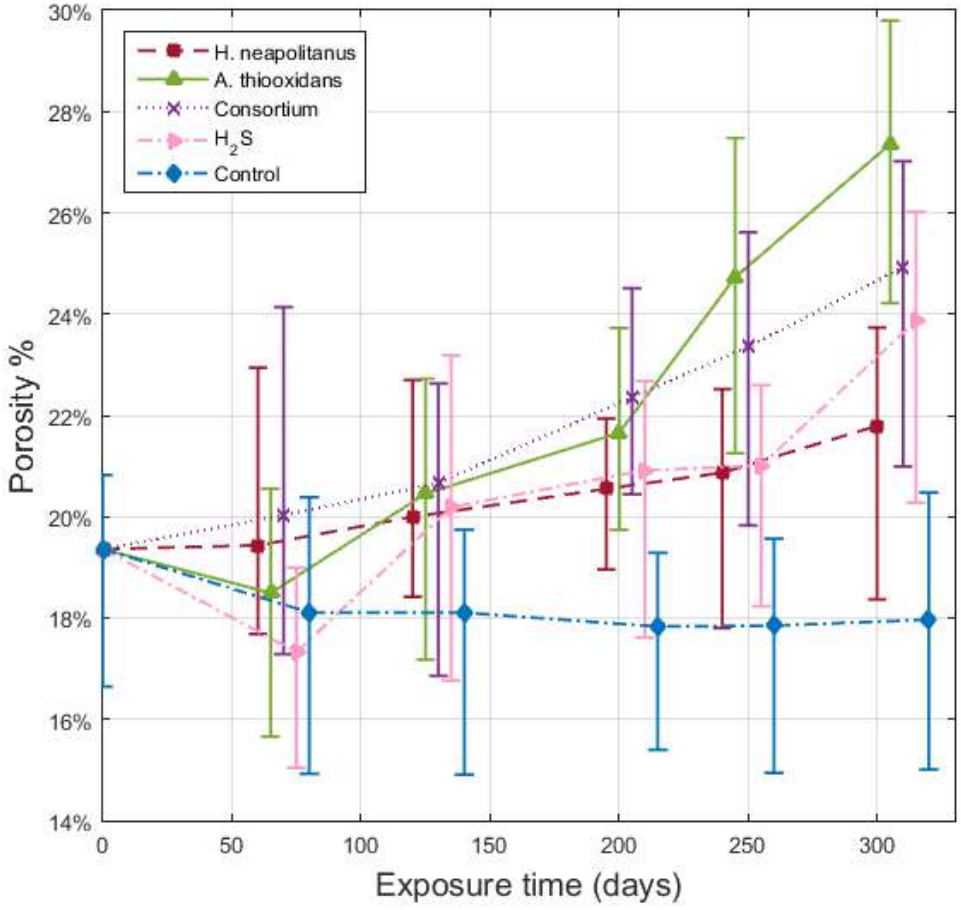

Figure 5.23: Porosity of samples inoculated in aseptic conditions

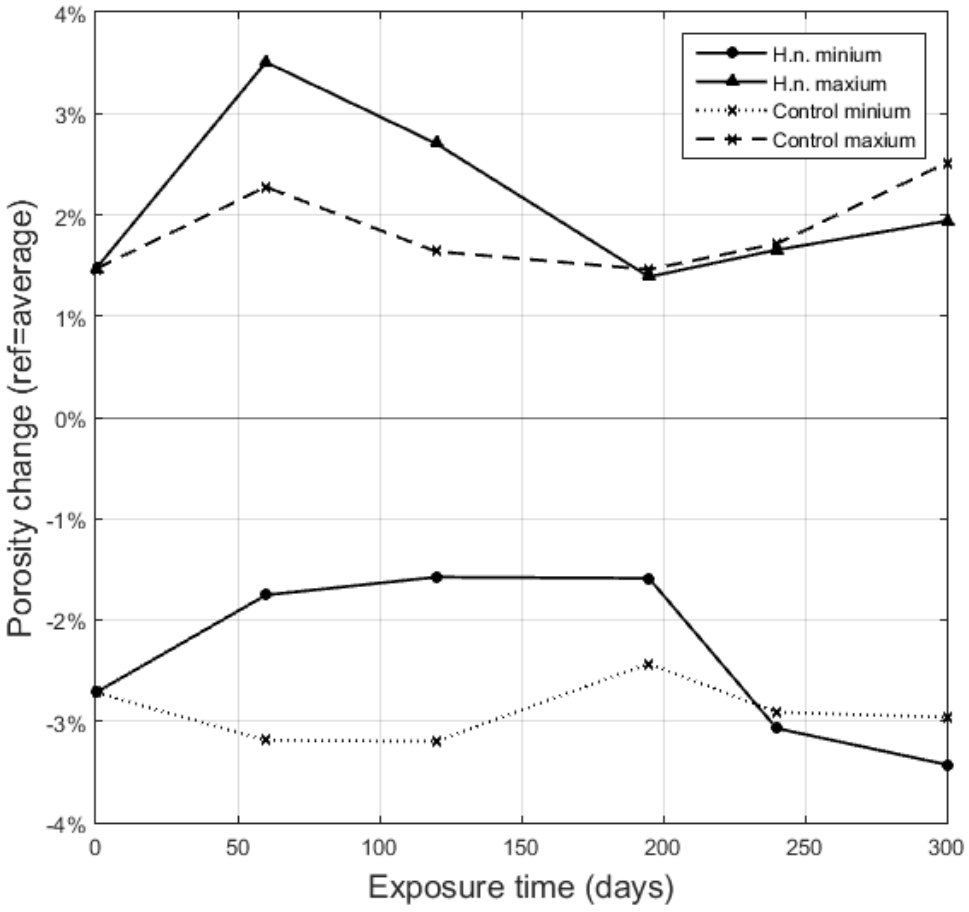

Figure 5.24: Gap between mean and extreme values for H.n. samples

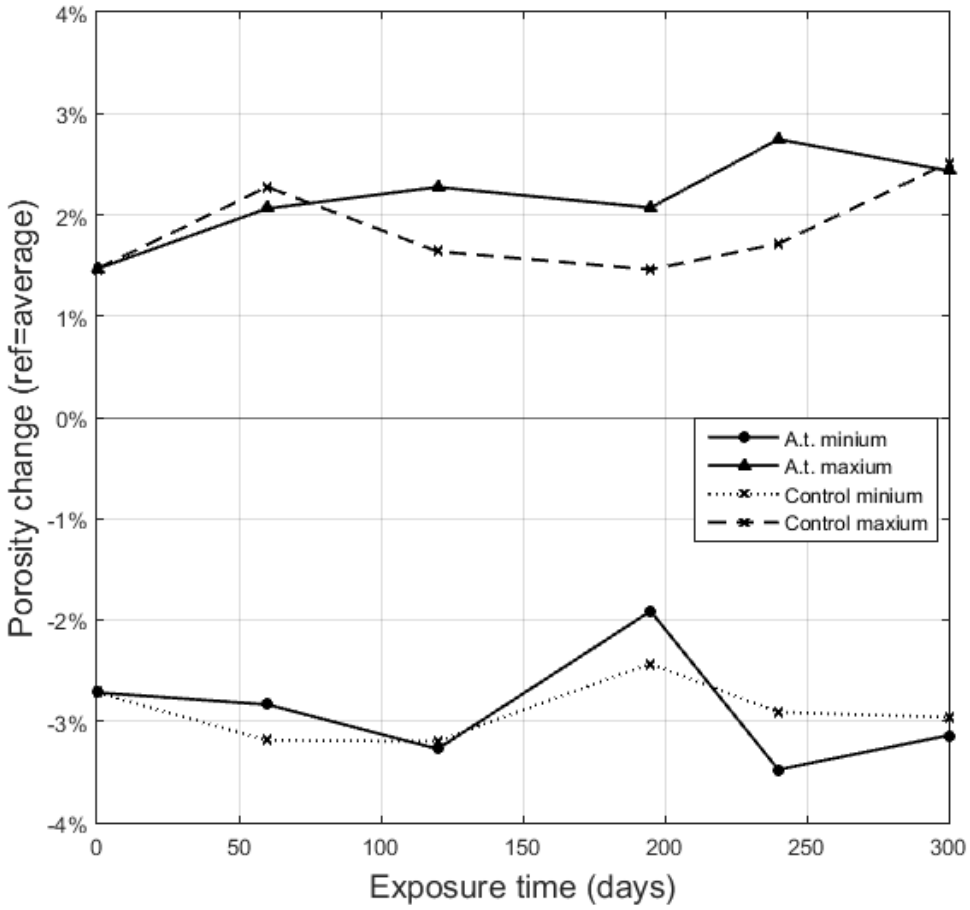

Figure 5.25: Gap between mean and extreme values for A.t. samples

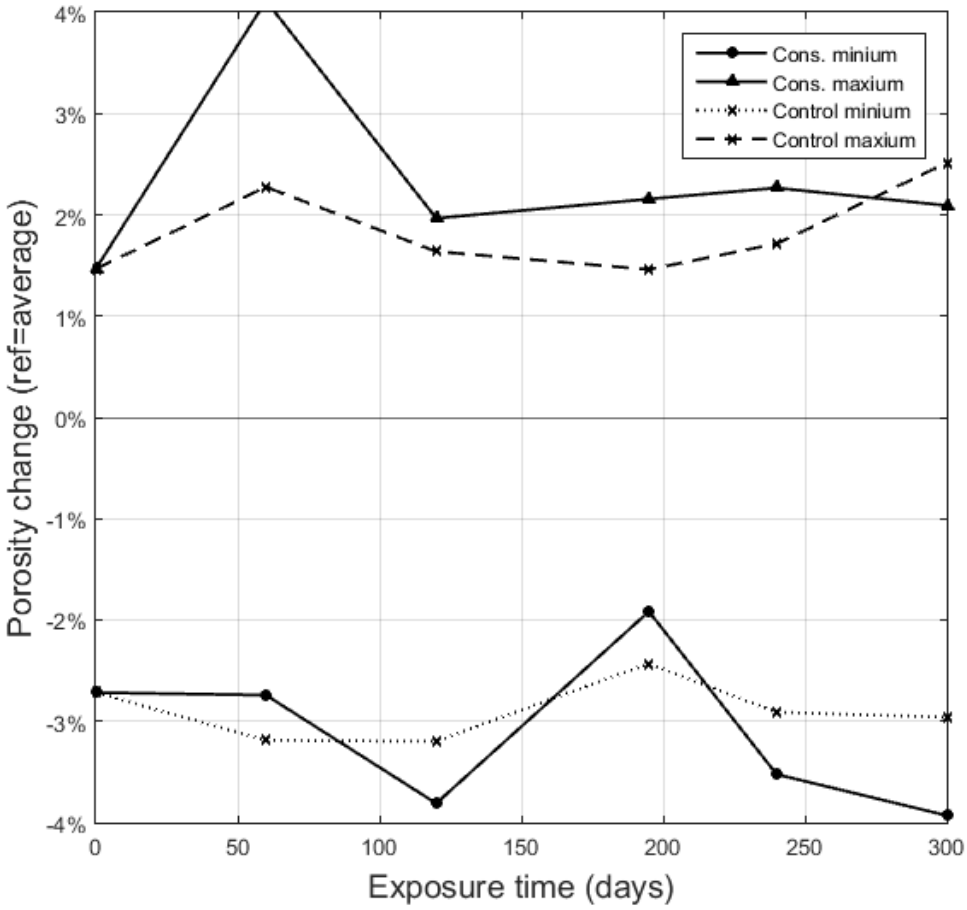

Figure 5.26: Gap between mean and extreme values for H.n.+A.t. samples

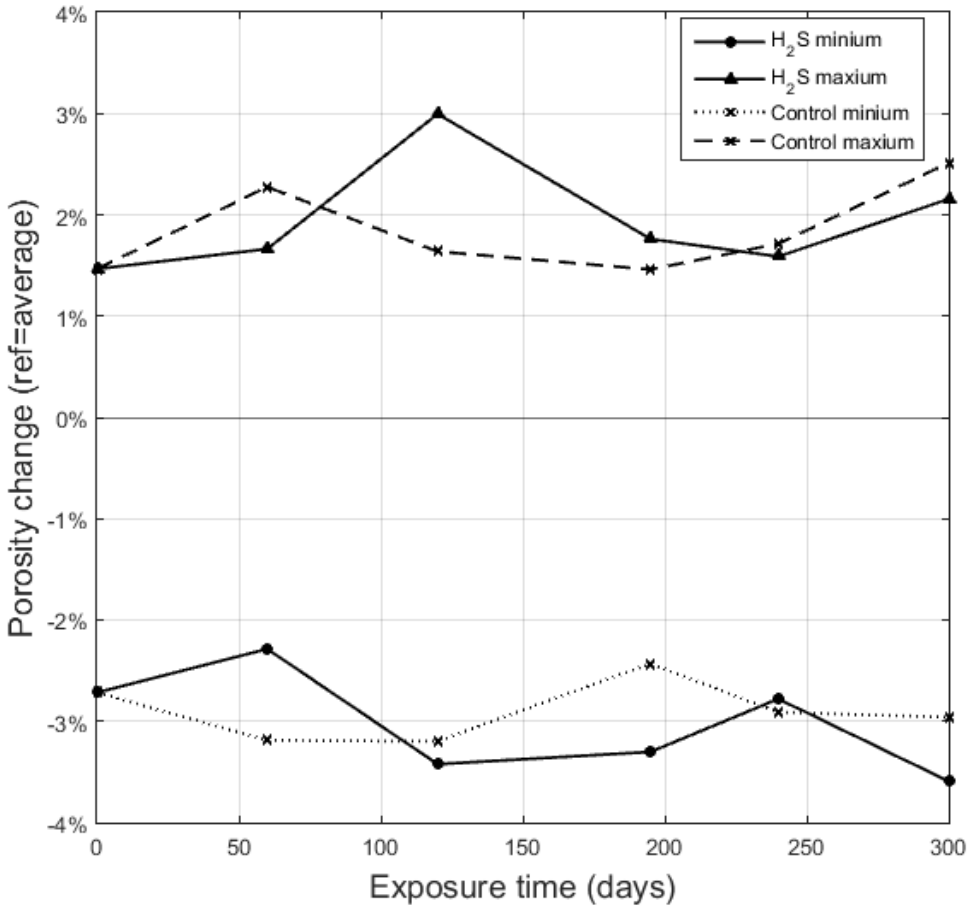

Figure 5.27: Gap between mean and extreme values for H_2S samples

Results from three samples of each experimental condition were averaged to determine the porosity at each exposure time. The gap between the mean value and minimum and maximum measured values were computed and drawn in Figures 5.23, 5.24, 5.25,5.26, 5.27. Gaps between 1 and 2% seem to be representative for all conditions. This signifies that the variability of exposed samples is highly similar to that of control samples, i.e. an inwardly comparison between all samples should have a minimal intrinsic error. From 50 to 200 days of exposure the maximum gaps observed were related to the H.n.+A.t., H_2S and H.n. samples. During this lapse, H.n. samples

showed the largest gaps both in minimum as in maximum values. A clogging process could produce such trend. Conversely, during the last 100 days of the experiment there was a minimal gap for all samples.

Average initial porosity of all samples was 19% (COV=0.12, computed using six samples randomly chosen from the population of available samples). After 300 days, the porosity of biotic samples increased significantly. Final porosities up to 27%, 25% and 22% (COV=0.10, 0.14 and 0.14) were measured in samples inoculated with *A. thiooxidans*, the consortium and *H. neapolitanus* respectively (Figure 5.23 and Figure 5.28)). Porosity in control samples was reduced up to 18% (COV=0.16) while in abiotic samples exposed to H_2S increased up to 24% (COV=0.13). Error bars were drawn using minimum and maximum values from 3 measures at each exposure time. Similar variability at each age was observed in all samples.

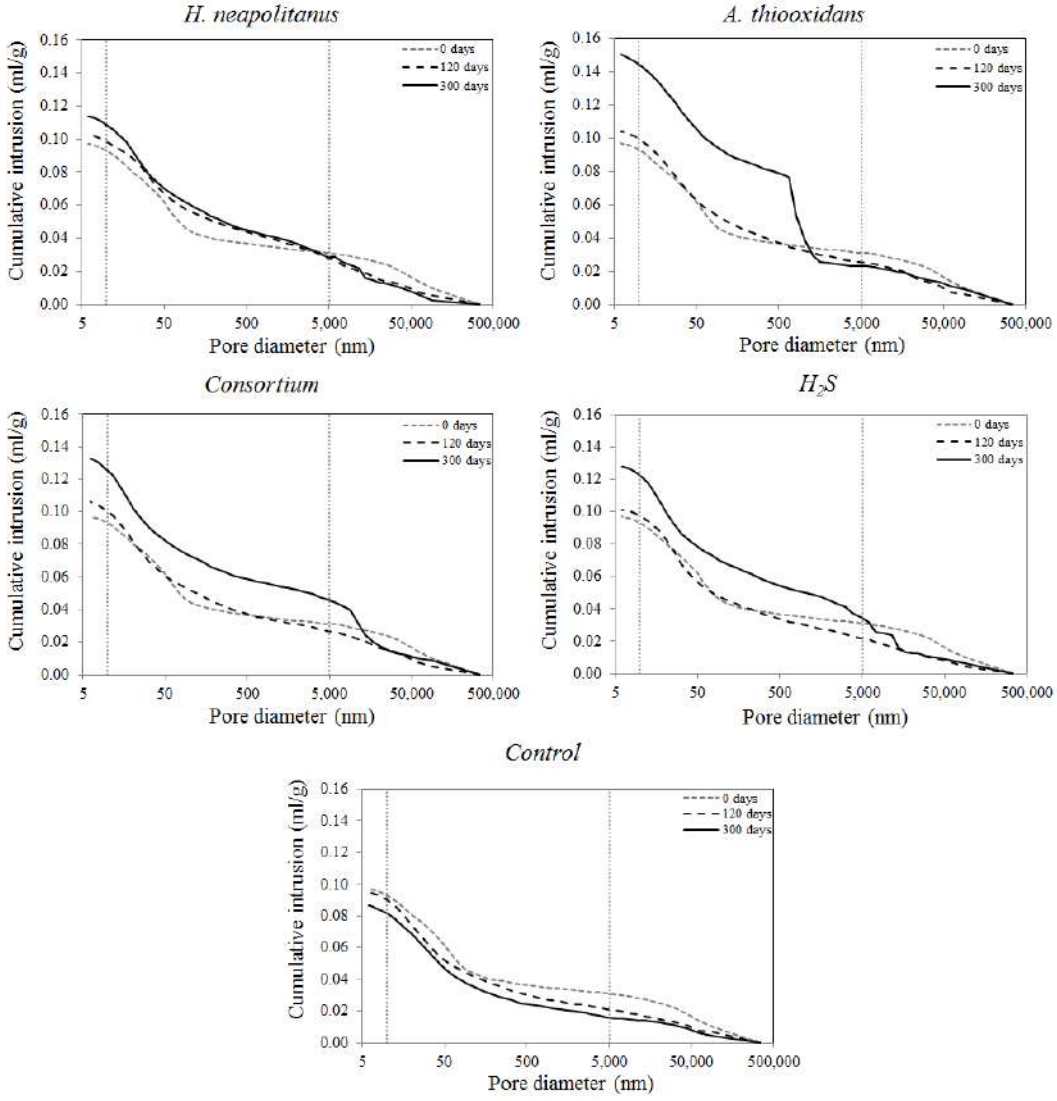

Figure 5.28: Cumulative mercury intrusion (average data) versus pore size in carbonated samples dried at 110^{o}C inoculated in aseptic conditions.

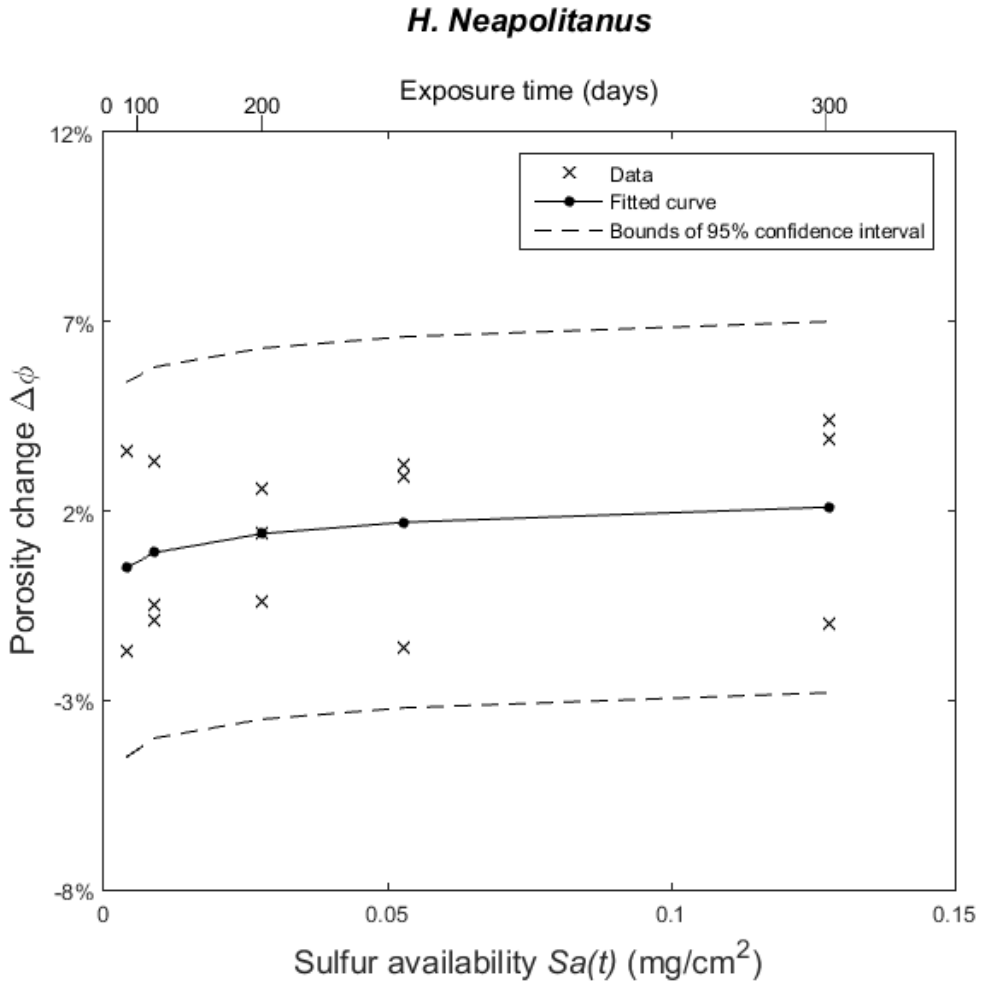

Figure 5.29: Comparison between proposed curves and measured data for porosity changes in carbonated samples dried at 110^{o}C - *H.Neapolitanus*

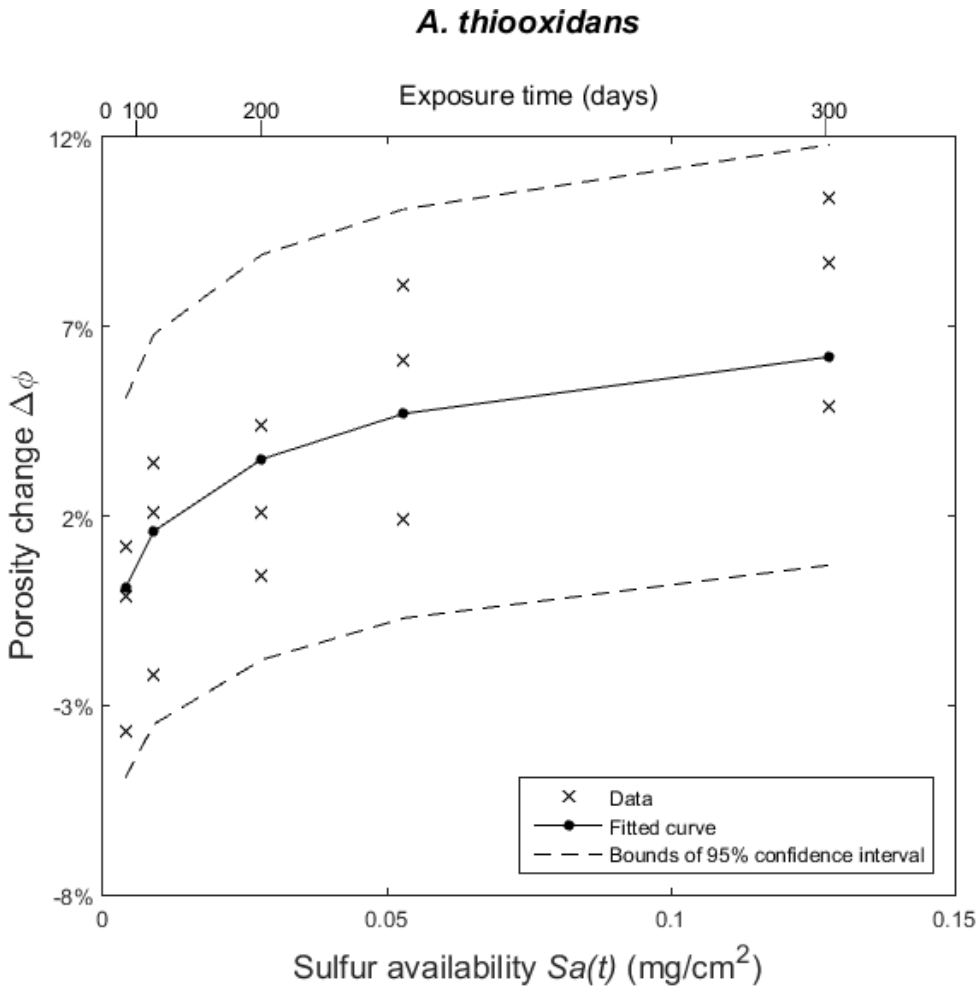

Figure 5.30: Comparison between proposed curves and measured data for porosity changes in carbonated samples dried at 110^{o}C - *A.Thiooxidans*

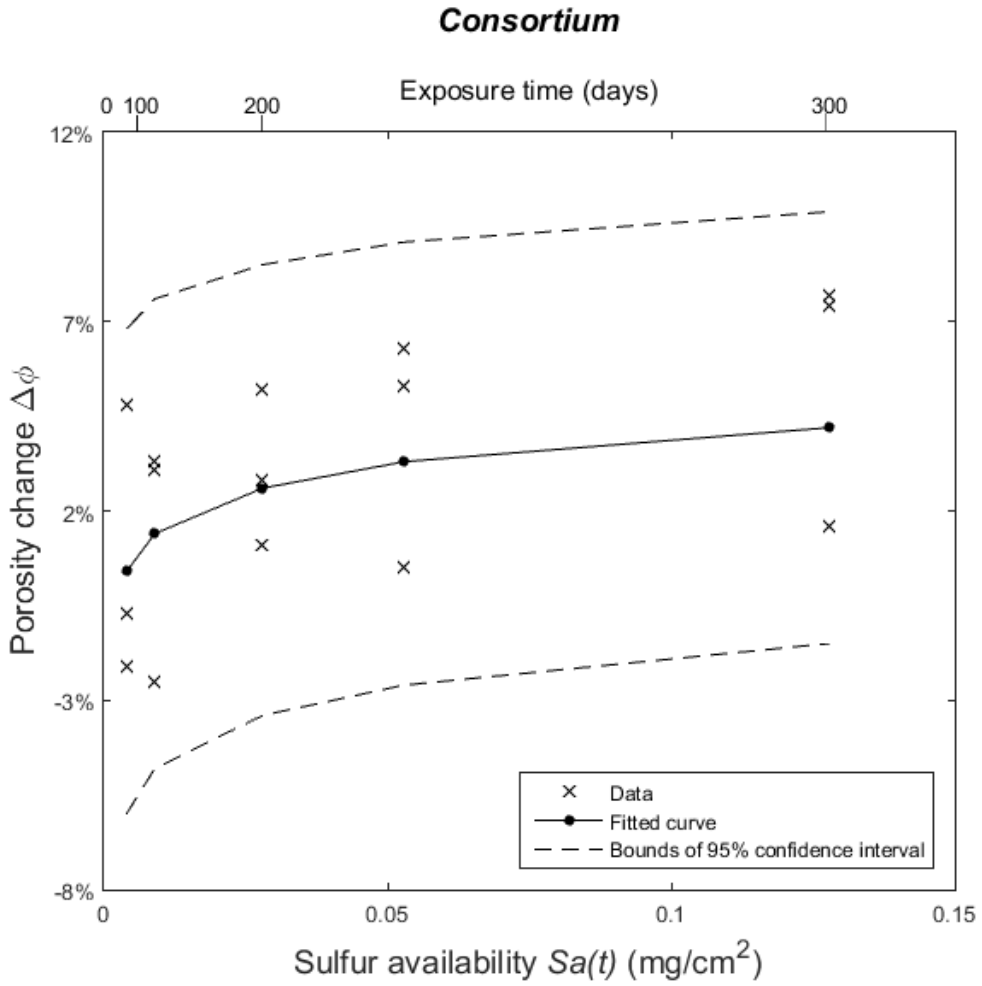

Figure 5.31: Comparison between proposed curves and measured data for porosity changes in carbonated samples dried at 110^{o}C - Consortium

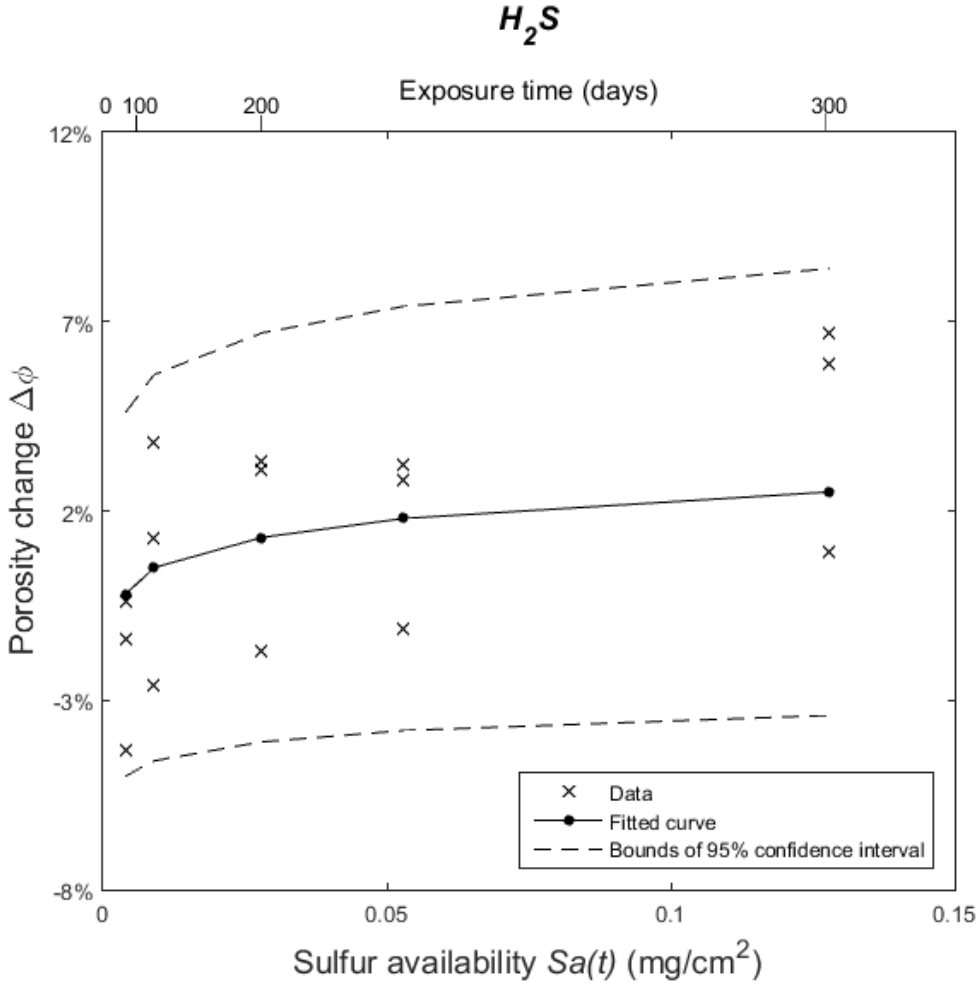

Figure 5.32: Comparison between proposed curves and measured data for porosity changes in carbonated samples dried at 110^{o}C - H_2S

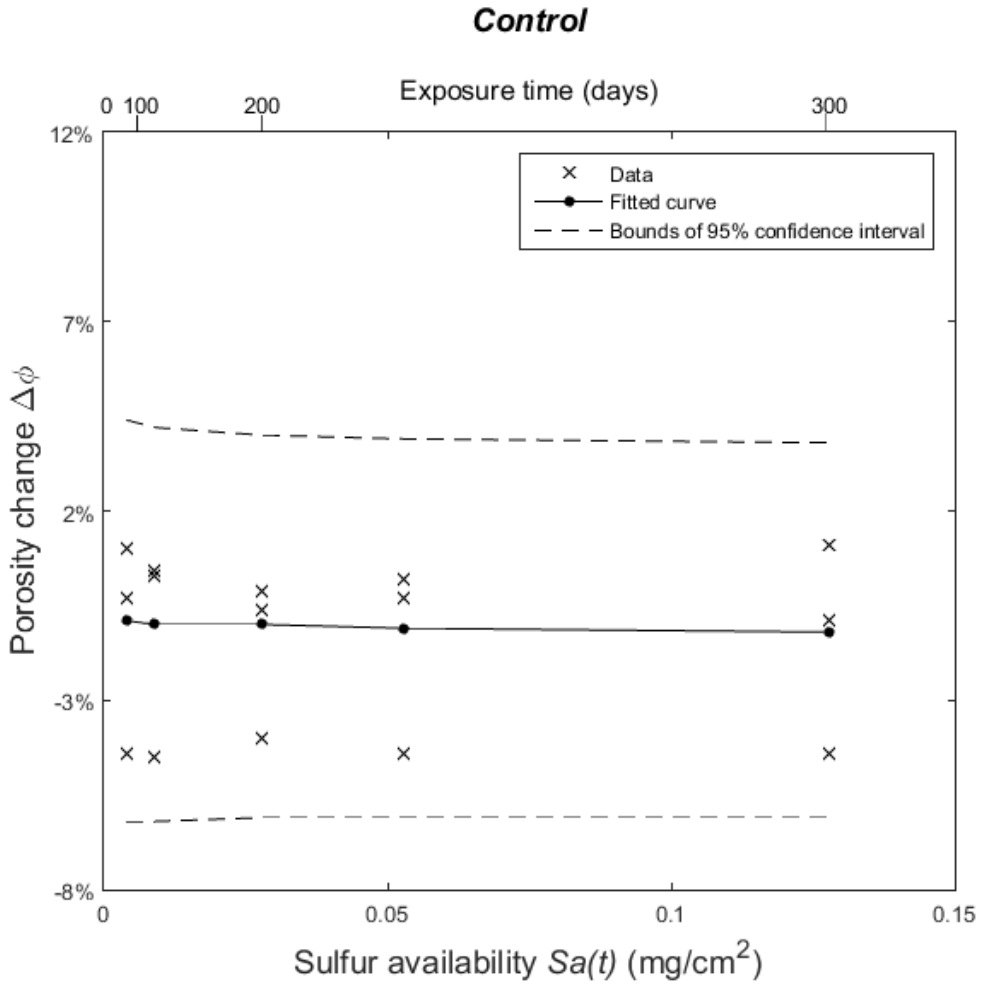

Figure 5.33: Comparison between proposed curves and measured data for porosity changes in carbonated samples dried at 110^{o}C - Control

The volume of micropores (0–10 nm) showed a visible change only for samples inoculated with the consortium (Table 5.5). This fact suggests that biodeterioration produced by the consortium was able to affect the smallest pore web. The volume of mesopores increased from 12.1% to 21.7% and from 12.1% to 14.8% in samples inoculated with *A. thiooxidans* and the consortium respectively. According to this, *A. thiooxidans* could be the responsible for the largest variations in mesopores while the consortium for those related to macropores. Also it has been reported that macropores

increase is associated to compressive strength decrease [40][42]. This fact could explain the greater strength drop observed in samples inoculated with the consortium in section 4.10. Also changes in macropores and mesopores could be related to changes in pores connectivity affecting the permeability and durability of the material.

Table 5.5: Initial and final porosities in pore ranges (from raw data, aseptic conditions)

Pore size description	Initial	Final (after 300 days of exposure)				
		H. n.	***A. t.***	**Cons.**	**H_2S**	**Control**
Micro: 0-10 nm	1.1%	1.3%	1.5%	1.8%	1.4%	1.4%
Meso: 10-5000nm	12.1%	15.0%	21.7%	14.8%	16.6%	13.4%
Macro: >5000nm	6.1%	5.5%	4.2%	8.3%	5.9%	3.2%
Average Porosity	19.4%	21.8%	27.4%	24.9%	23.9%	18.0%
Standard Deviation	2.4%	3.0%	2.9%	3.4%	3.1%	2.8%

The porosity increase was estimated as 5%, 4% and 3% for samples inoculated with *A. thiooxidans*, the consortium and those abiotic exposed to H_2S respectively (Figures 5.29, 5.30, 5.31, 5.32 and 5.33). Porosity increase of 2% and reduction of 2% were related to the samples inoculated with *H. neapolitanus* and control samples respectively. Figures 5.29, 5.30, 5.31, 5.32 y 5.33 leads to infer two trends of porosity changes depending on the sulfur availability. A rapid porosity increase for all exposed samples is observed for sulfur availability values $Sa(t)$ between $Sa_{lim} = 0.006 mg/cm^2$ and $0.030 mg/cm^2$. In general, larger changes in porosity are evident in acidic conditions (*A. thiooxidans*, consortium and chemical exposure) and almost negligible porosity variations are linked to neutral conditions (*H. neapolitanus*). Negligible porosity variation (0.1 to 0.7%) is associated to $Sa(t) \leq Sa_{lim}$ while from this value porosity change follows a logarithmic trend (Table 5.3). For practical purposes it can be assumed that there is no porosity variation ($\Delta\phi = 0$) if $Sa(t) < Sa_{lim}$. Due to the existence of only three measurements at each age, the standard deviation for each experimental condition has been computed as a unique value using the totality of data. As it expected, practically all experimental results are within the 95% confidence interval (Figures 5.29, 5.30, 5.31, 5.32 y 5.33).

Porosity measurements from samples inoculated in non aseptic conditions (up to 32%) resulted slightly larger than those inoculated in aseptic conditions (up to 27%).

Probably the mutualistic relationship among selected bacteria and other ubiquitous organisms present in the laboratory environment enhanced the biodeterioration processes.

5.4 Compressive strength variations in biodeteriorated samples

All samples were subjected to compressive strength test to evaluate the change in resistance as a result of microbial attack. Typical compressive test is shown in Figure 5.34. and Figure 5.35. Parallel cracks to load axis were associated to pressure-application uniformity. Average initial strength of 104-day-old samples was 32 MPa (COV 0.11). Samples exposed using SM inoculations showed a temporary increment of about 33% (day 66) from their initial strength. Conversely, samples exposed using MM inoculations had an early strength decrease of 14% after 26 days of exposure that was recovered later. Strength became almost negligible in samples inoculated with SM using non aseptic conditions after 153 days of exposure while MM samples and H_2S-only samples showed a strength loss up to 59% (COV=0.21) by the same time (Figure 5.36 and Figure 5.37). Behavior of samples exposed only to H_2S was similar to that of control samples until day 85, and then it switched to resemble the seawater-inoculated samples (Hns, Ats and nts). The similarity between H_2S samples and MM samples behavior seems to indicate that chemical effects of H_2S oxidation were much more important than those of biogenic activity in samples inoculated using salty media (Figure 5.37). Again, this suggests that bacterial growth could be inhibited in samples inoculated with salty media. On the contrary, it could also be argued that non-sterilization effects led to a slight contamination in the H_2S container, despite the fact that the ctrl and H_2S samples were kept isolated from other containers.

Figure 5.34: Typical compressive breaking of exposed samples

Figure 5.35: Deteriorated strength-tested sample after 84 days of exposure

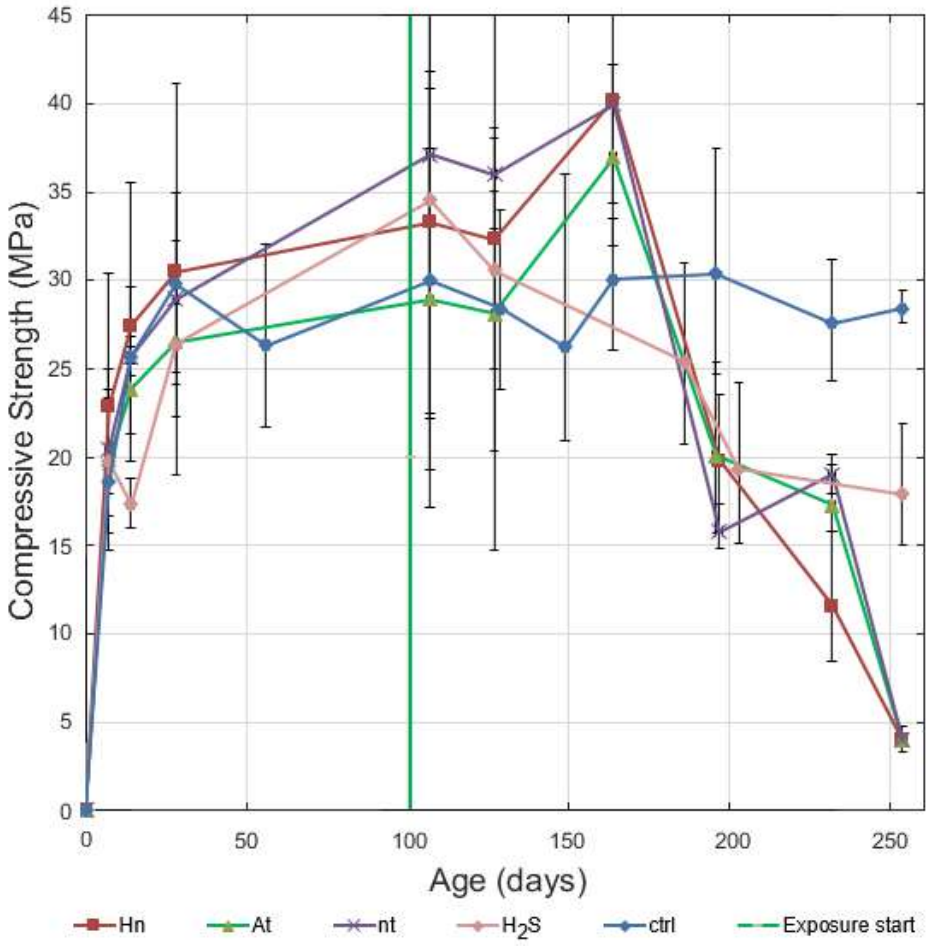

Figure 5.36: Strength variation during exposure of samples inoculated with SM in non aseptic conditions.

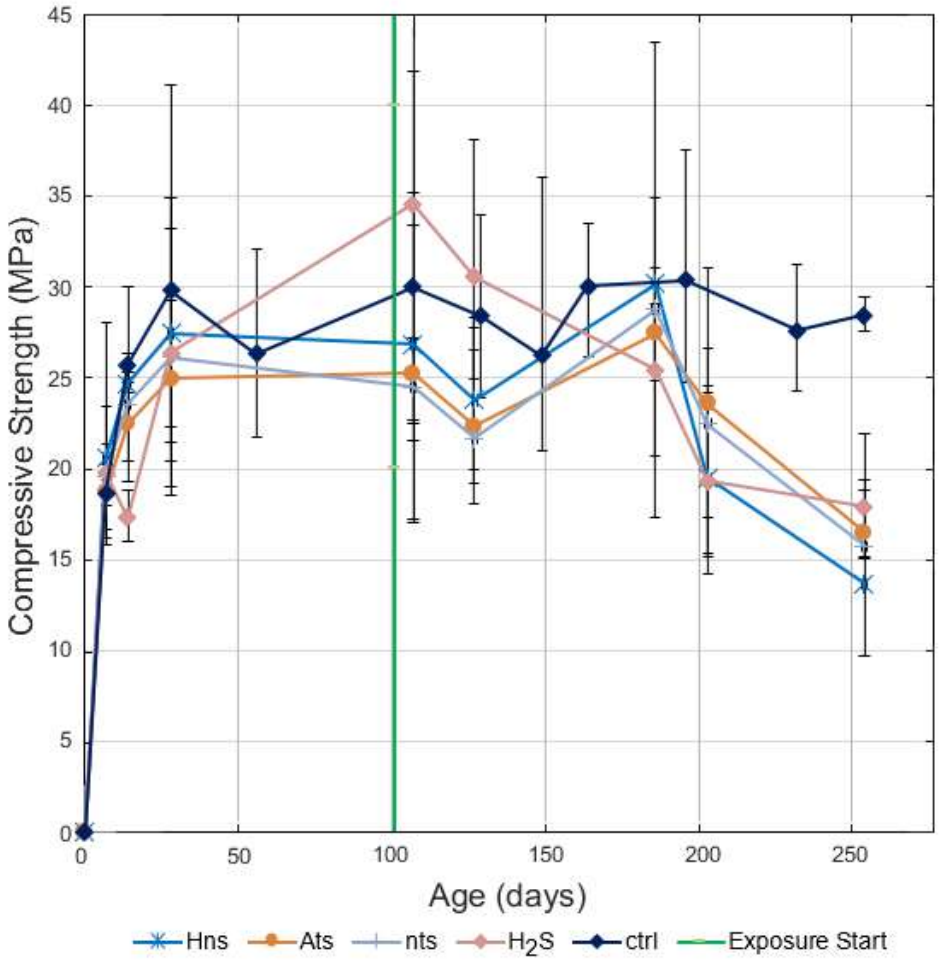

Figure 5.37: Strength variation after exposition of samples inoculated with MM using non aseptic conditions

Due to the low biodeterioration effects observed in pyritic samples, they were not tested periodically under compressive stress. The third column in table 5.6 shows the results of strength tests at the exposure time $t = 0$. The average strength of basic mortar was 23.4 MPa (COV 0.15). Fe addition increased the initial compressive strength of samples an average of 126%, while sulfur increased it an average of 107%. Pyrite addition resulted in a strength increase of 120%.

Samples inoculated in aseptic conditions were tested to determine their compressive

Table 5.6: Initial measured compressive strength of pyritic mortar samples

Mix	Addition	f´c	Overstrength
P1	0.47% Fe	31.8	136%
P2	0.53% S	25.4	109%
P3	1% FeS_2	28.2	121%
P4	2.35%Fe	27.2	116%
P5	2.65% S	24.5	105%
P6	5% FeS_2	27.8	119%
P7	0%	23.4	100%

strength. Typical compressive breaking of all tested samples showed cracks parallel to load axis revealing pressure-application uniformity. In general, the larger the sulfur availability the lower the compressive strength (Figure 5.38). Average initial strength was 30 MPa (COV=0.03) and 33 MPa (COV=0.02) for non-carbonated and carbonated 104-day-old samples, respectively. Abiotic carbonated samples (control) were used as the reference to compute the relative strength (Figures5.39, 5.40, 5.41, 5.42, 5.43 and 5.44.

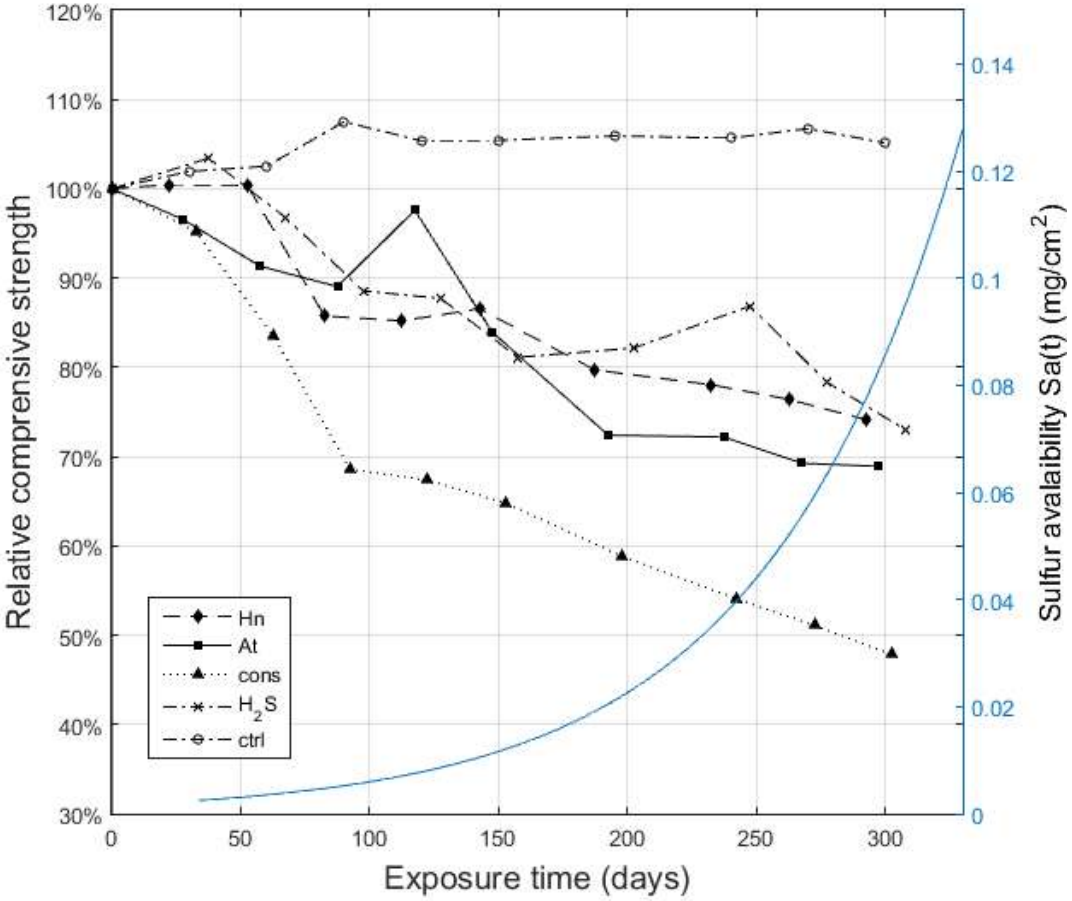

Figure 5.38: Strength variation trend versus sulfur availability trend for samples inoculated in aseptic conditions

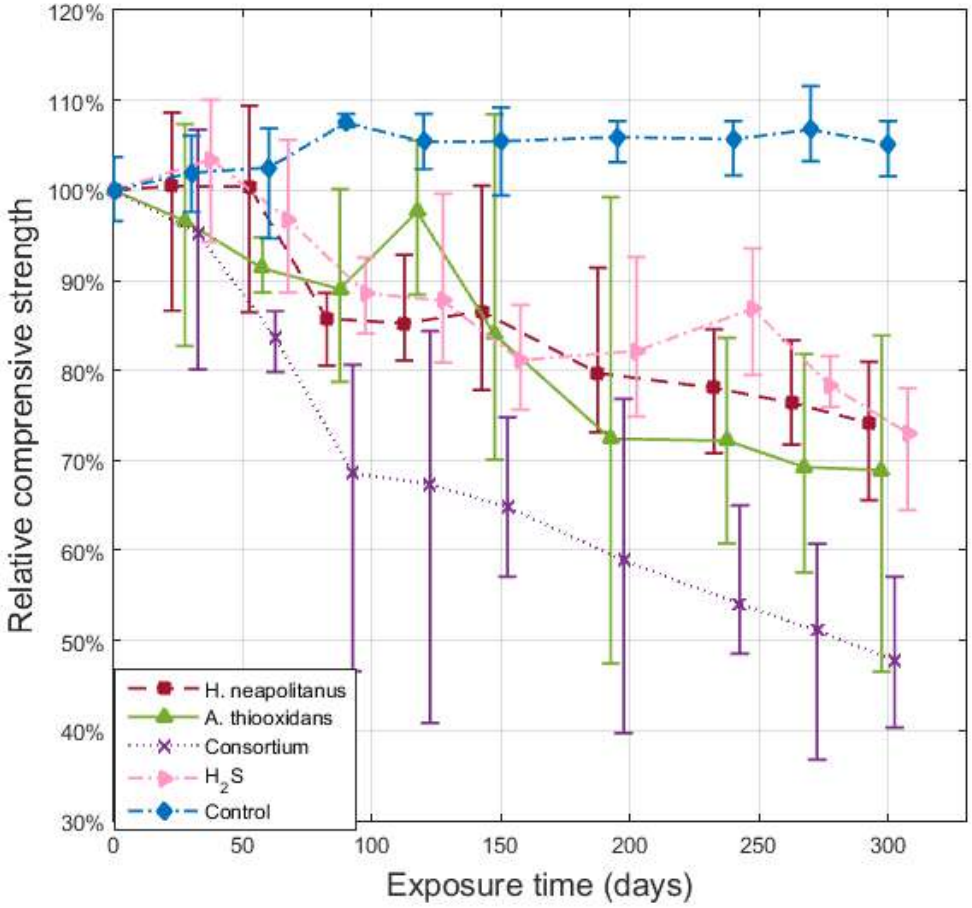

Figure 5.39: Strength variation of samples inoculated in aseptic conditions

After 300 days of exposure, samples inoculated with *H. neapolitanus*, *A. thiooxidans* and abiotic samples subjected to H_2S showed a strength loss equivalent approximately to 28% of their initial value. Control samples did not show important strength variations while samples inoculated with the consortium lost more than a half (52%, COV=0.13) of their initial strength (Figures 5.39, 5.40, 5.41, 5.42, 5.43 and 5.44). Furthermore, the most important strength loss was observed between days 60 and 90 for the same samples. These results confirm that the interaction among the microorganisms in consortium is a predominant factor for biodeterioration. By comparing the strength

of samples inoculated with *H. neapolitanus* (strength loss 25%, COV=0.08) and those abiotic samples coming from chemical exposure (strength loss 24%, COV=0.05), it is observed that the strength loss is caused mainly by the chemical effect of hydrogen sulfide over the mortar samples. Conversely, biogenic deterioration from *A. thiooxidans* (strength loss 32%,COV=0.20) and Consortium seems to contribute in a more important manner to relative strength changes . Error bars were drawn using minimum and maximum values from three samples per sampling time. The largest data variability at each age was observed in samples inoculated with *Acidithiobacillus thiooxidans* (Figures 5.40, 5.41, 5.42, 5.43 and 5.44).

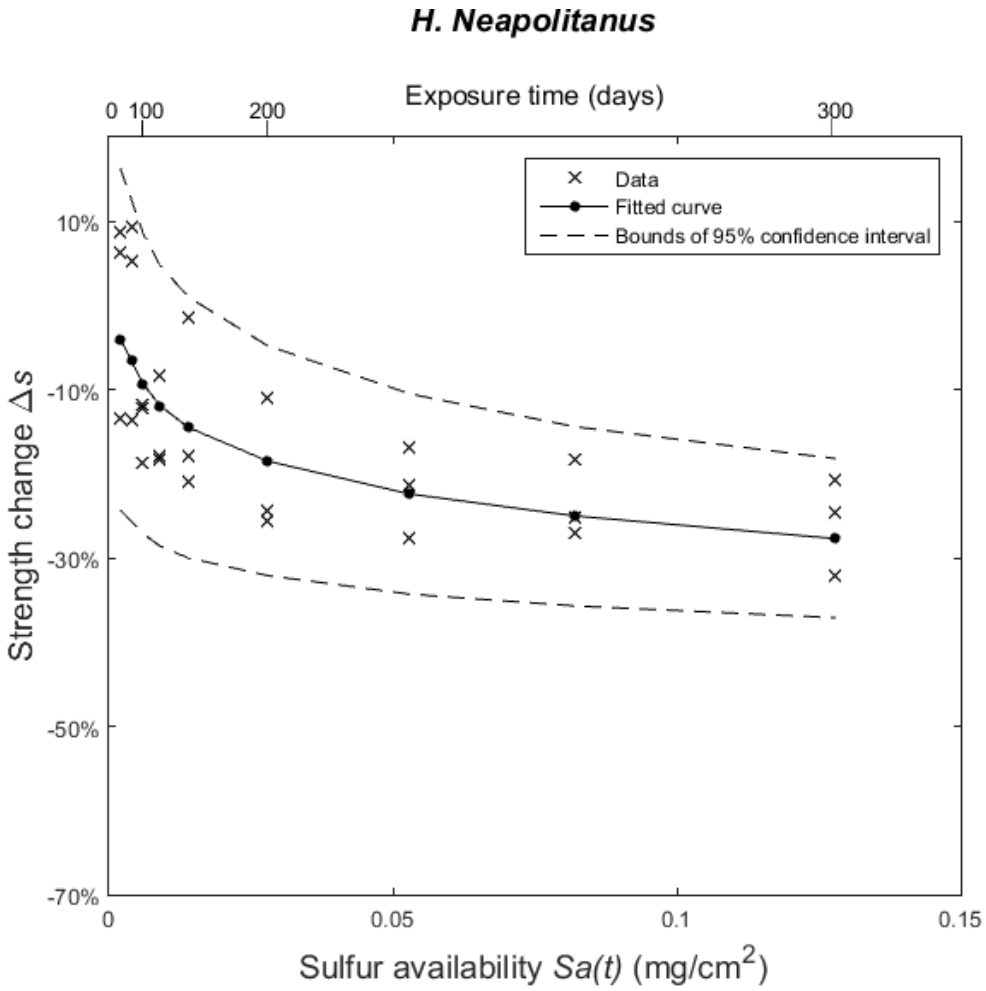

Figure 5.40: Comparison between proposed curves and measured data for strength changes in carbonated samples dried at 110^{o}C inoculated in aseptic conditions - *H.Neapolitanus*

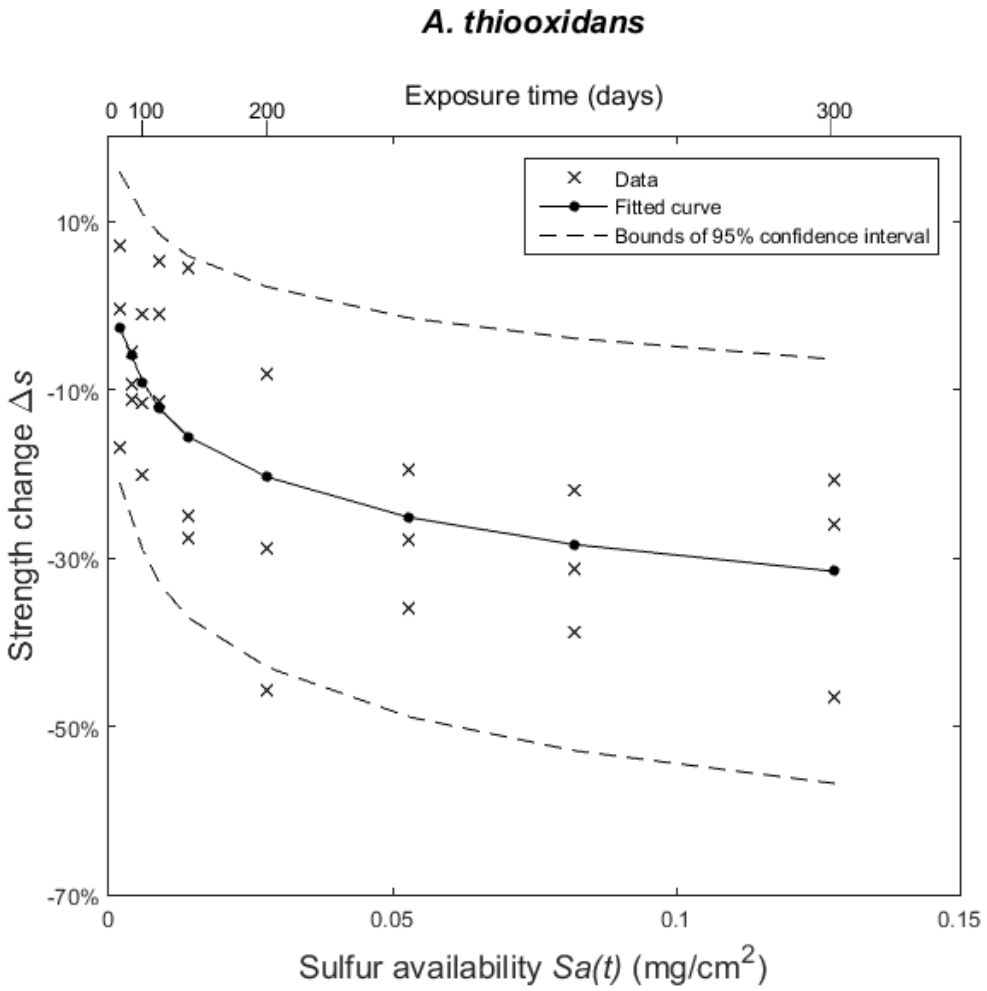

Figure 5.41: Comparison between proposed curves and measured data for strength changes in carbonated samples dried at 110^{o}C inoculated in aseptic conditions - *A.Thiooxidans*

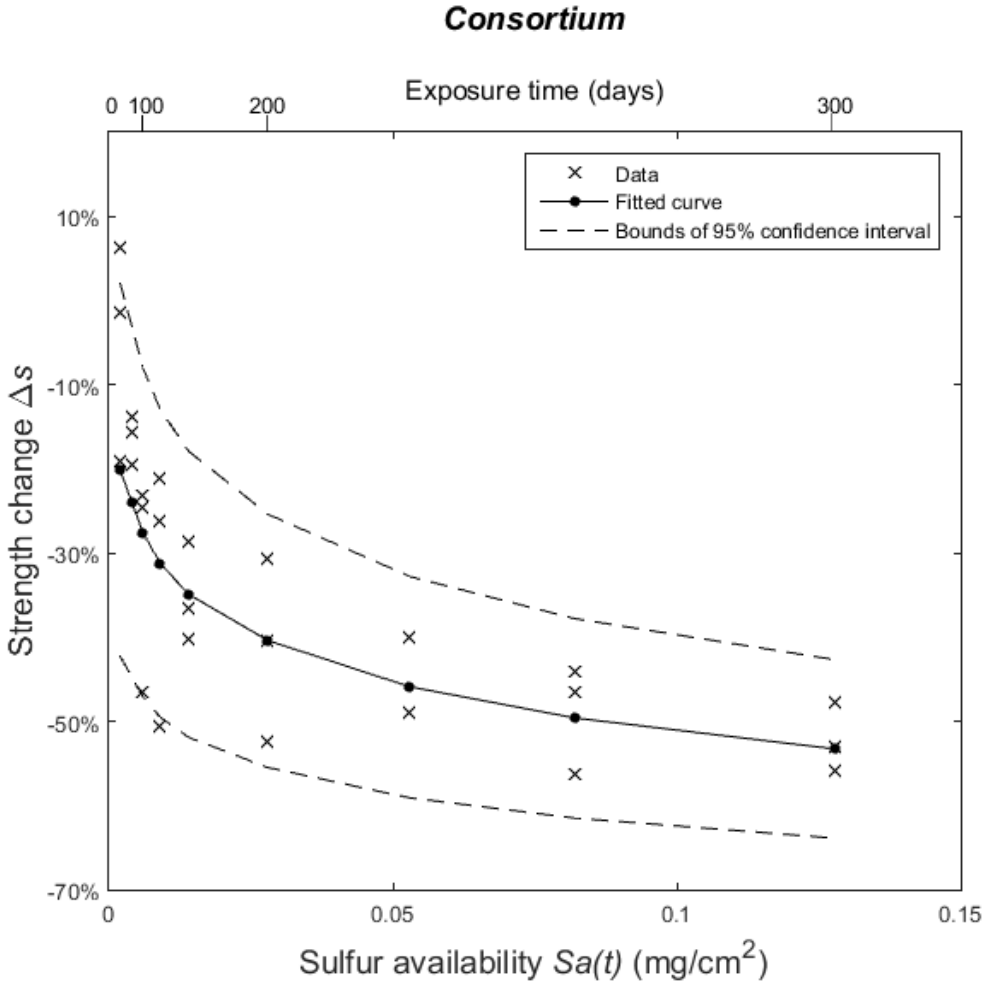

Figure 5.42: Comparison between proposed curves and measured data for strength changes in carbonated samples dried at 110°C inoculated in aseptic conditions - Consortium

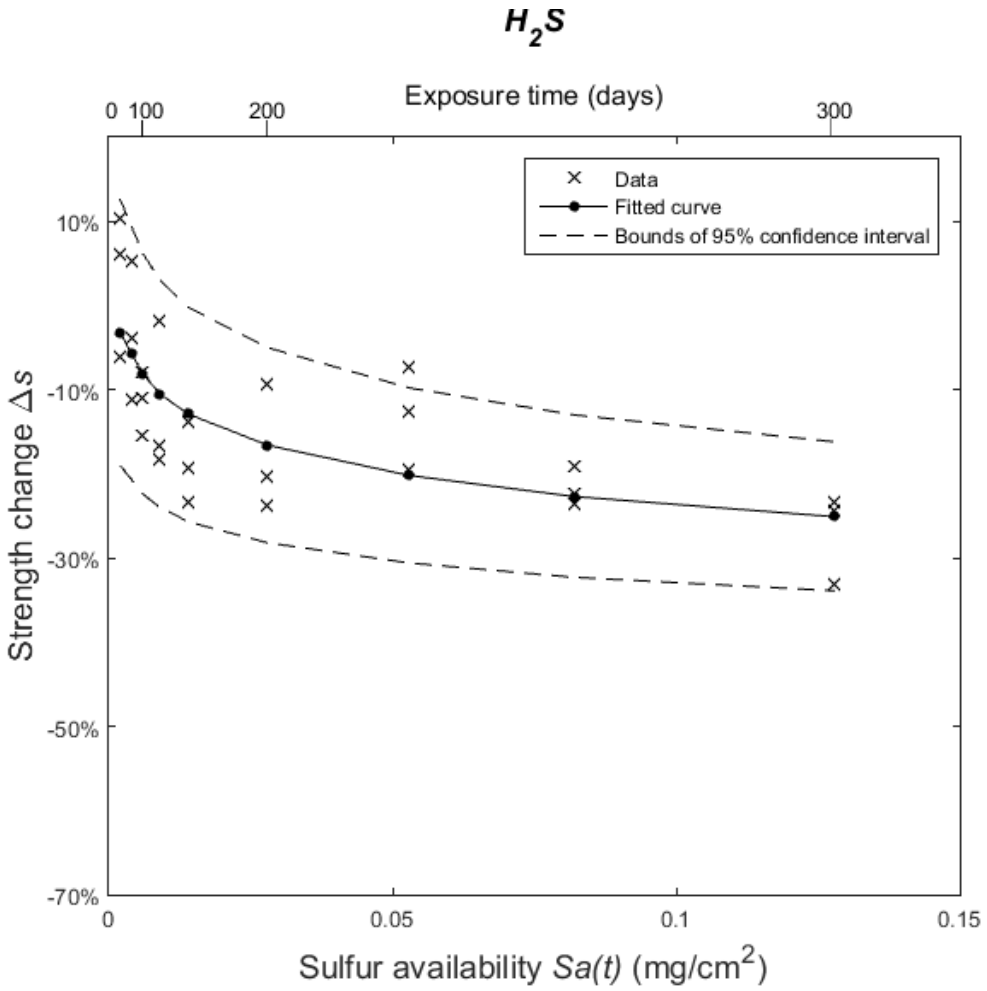

Figure 5.43: Comparison between proposed curves and measured data for strength changes in carbonated samples dried at 110^{o}C using aseptic conditions - H_2S

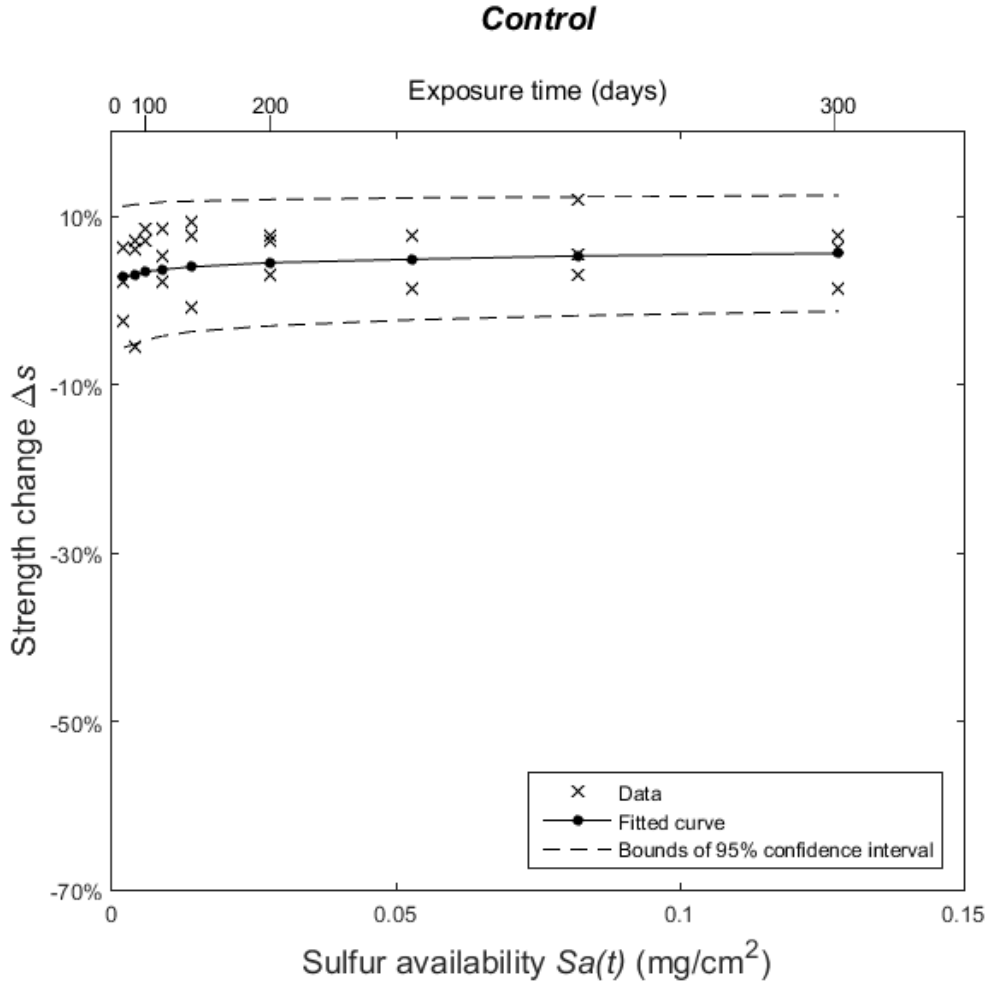

Figure 5.44: Comparison between proposed curves and measured data for strength changes in carbonated samples dried at 110^{o}C using aseptic conditions - Control

Negligible strength variation (0.5 to 5%) is associated to $Sa(t) \leq Sa_{lim}$ while a logarithmic trend is observed from this value (Figures 5.40, 5.41, 5.42, 5.43 and 5.44). For practical purposes it can be assumed that there is no strength variation ($\Delta s = 0$) if $Sa(t) < Sa_{lim}$ (Table 5.3). In general, the strength losses caused by the activity of the consortium doubled those produced by others conditions under the same sulfur availability. Again, as concluded for samples inoculated in non aseptic conditions, it is evident the larger influence of acidophilic bacteria (alone or within a consortium) in

the strength variation.

5.5 Strength-porosity relationship in biodeteriorated samples

It is well known that increased porosity causes an adverse effect on compressive strength [40][42]. As can be seen in Figure 5.45, Hn samples experienced a strength loss from 36 MPa to 12 MPa, while their porosity increased from 19% to 29%. Similarly, At and nt samples showed strength losses from 29 MPa to 17 MPa and from 36 MPa to 19 MPa, associated with porosity increments of 19% to 32% and from 19% to 28%, respectively. Control samples exhibited no apparent strength variation, while their porosity was reduced from 21% to 13%. The final putty-like consistency of samples Hn, At and nt on day 153 impeded testing them in relation to compressive strength and porosity, so that final strength was approximately fixed equal to 4 MPa.

The observed strength-porosity relationship is roughly similar in form to that reported in the literature. However, strength values measured in this study for medium to high degrees of biodeterioration (i.e. porosity between 20% and 30%) double or even triple those forecast using models existing in the literature (data not shown). Internal clogging of biodeterioration products or the failure of existing models for predicting strength at high-porosity values could be possible explanations of this difference.

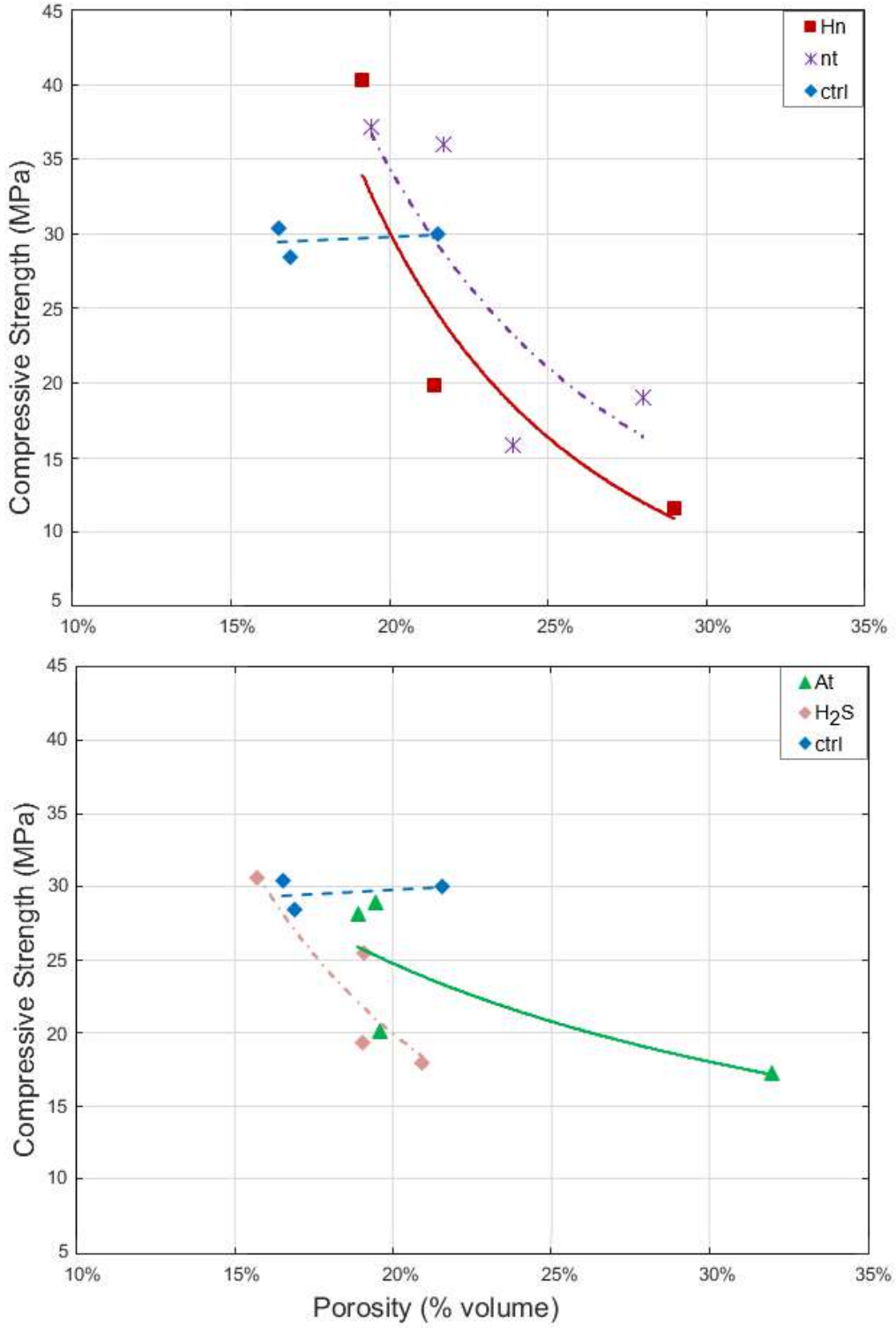

Figure 5.45: Strength and porosity variation in samples inoculated in non aseptic conditions. Each pair of data (porosity, strength) is measured at the same sampling time

While Figure 5.3 shows negligible weight losses during the first three months ($Sa(t) < Sa_{lim}$), Figure 5.36 indicates an important strength loss in the same lapse. Conversely during the last seven months, larger weight losses and smaller strength losses were observed. This fact seems to indicate that the major intensity of biogenic activity is related to larger weight loss and smaller strength variation. A rapid weight loss is linked to the overcoming of the bacterial lag phase while the bacterial growth is associated to a buffer effect in the strength deterioration. Apparently a positive effect in the compressive strength coming from clogging and deposition of biodeterioration byproducts in the inner mortar matrix is generated.

Figure 5.46 (down side) depicts the strength losses to weight losses relations modeled for biodeteriorated samples inoculated in aseptic conditions. The best fit of data was obtained using a logarithmic equation. An initial rapid strength loss (13 to 35%) for low weight losses (less than 2%) is observed followed by a slower strength loss (35 to 52%) for larger weight losses (2 to 7%) (Table 5.7). Straight lines (not shown) can be used for modeling the initial trend of the strength loss to weight loss (from origin to left edge of logarithmic line). These findings suggest that the most important strength deterioration could occur even when weight or thickness losses are not visible yet.

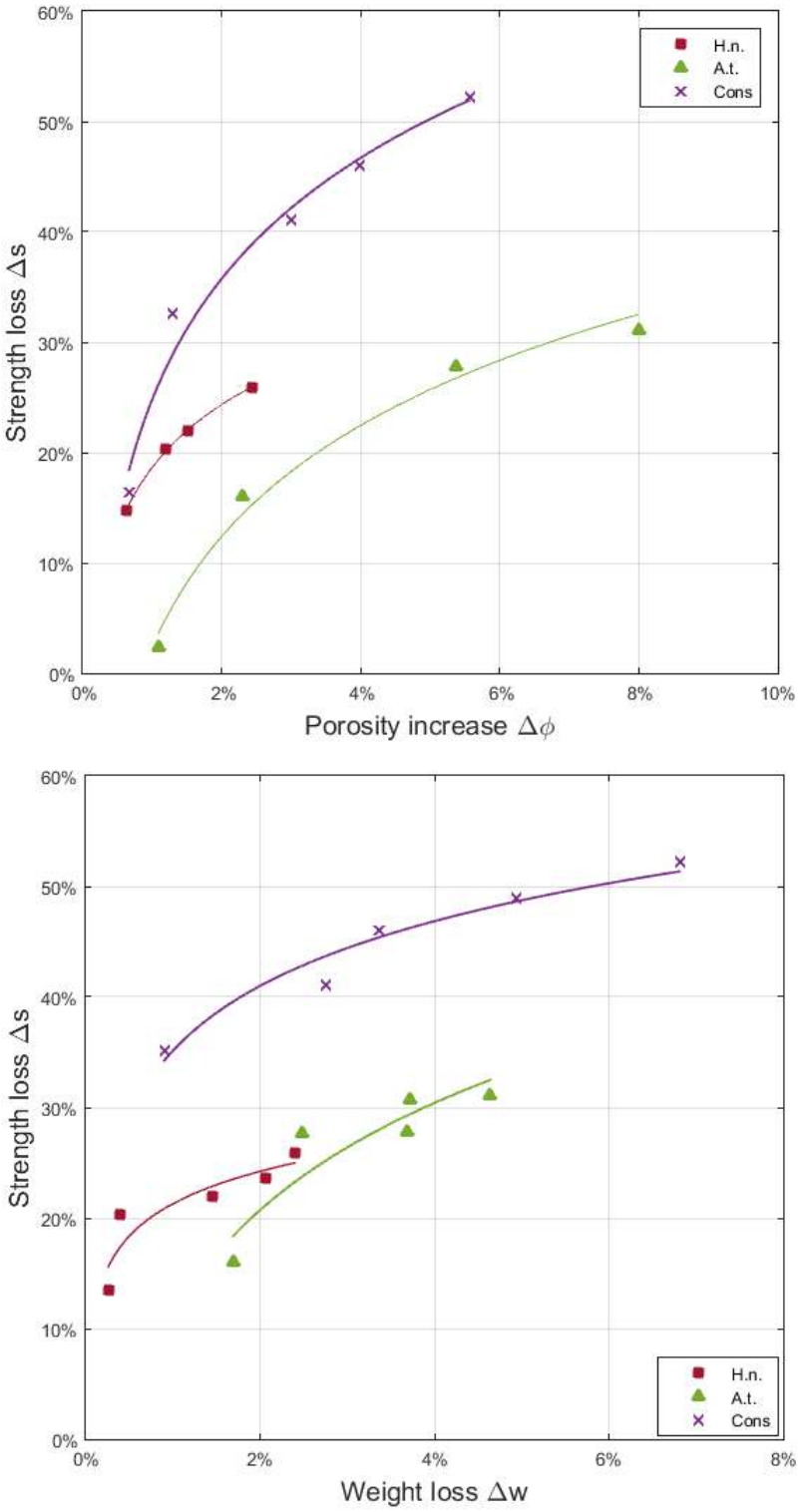

Figure 5.46: Strength losses associated to porosity and weight changes in biodeteriorated samples previously carbonated and dried at 110°C inoculated in aseptic conditions. Each pair of data (porosity increase, strength loss) or (weight loss, strength loss) is computed at the same sampling time

Table 5.7: Equations for relationships of changes in mechanical properties of biodeteriorated samples inoculated in aseptic conditions

Relationship	Samples	Equation	R^2
Strength loss (Δs) versus porosity increase ($\Delta\Phi$)	H.n.	Δs=0.0821ln($\Delta\Phi$)+0.5645	0.9987
Strength loss (Δs) versus porosity increase ($\Delta\Phi$)	A.t.	Δs=0.1453ln($\Delta\Phi$)+0.6923	0.9854
Strength loss (Δs) versus porosity increase ($\Delta\Phi$)	Cons.	Δs=0.1582ln($\Delta\Phi$)+0.9763	0.9749
Strength loss (Δs) versus weight loss (Δw)	H.n.	Δs=0.0422ln(Δw)+0.4073	0.8224
Strength loss (Δs) versus weight loss (Δw)	A.t.	Δs=0.1398ln(Δw)+0.7541	0.8297
Strength loss (Δs) versus weight loss (Δw)	Cons.	Δs=0.0845ln(Δw)+0.7405	0.9523

The trend of the relationship between strength and porosity of samples exposed to biodeterioration is similar to that reported in literature for cement pastes, mortars and concretes in no biodeteriorated samples [41][42][96][97][98]. In general, strength decreases when porosity increases. However, the relationship between strength and porosity changes depends on the experimental conditions (Figure 5.47). A similar compressive-strength-to-porosity slope was observed for samples inoculated with *A. thiooxidans* and those coming from chemical exposure. In contrast, a sharper slope was obtained for samples inoculated with *H. neapolitanus* and the consortium. These results suggest that concrete microstructure changes due to biodeterioration depend on the type of bacteria involved in the process. Indeed, the neutrophilic bacteria seem to have clogged the porous structure in a major proportion than acidophilic bacteria did. Best fit for compressive strength to total porosity relationship is shown in Table 5.8.

Attempts to find a correlation between strength variation and weight and porosity changes were not succesful. A strength loss versus Porosity change/Weight change ratio graph was plotted (not shown). Such graph showed a disperse point cloud with no apparent correlation. Best fit obtained using a linear trend was related to low values of coeficient of determination (lower than 0.56 in all the cases).

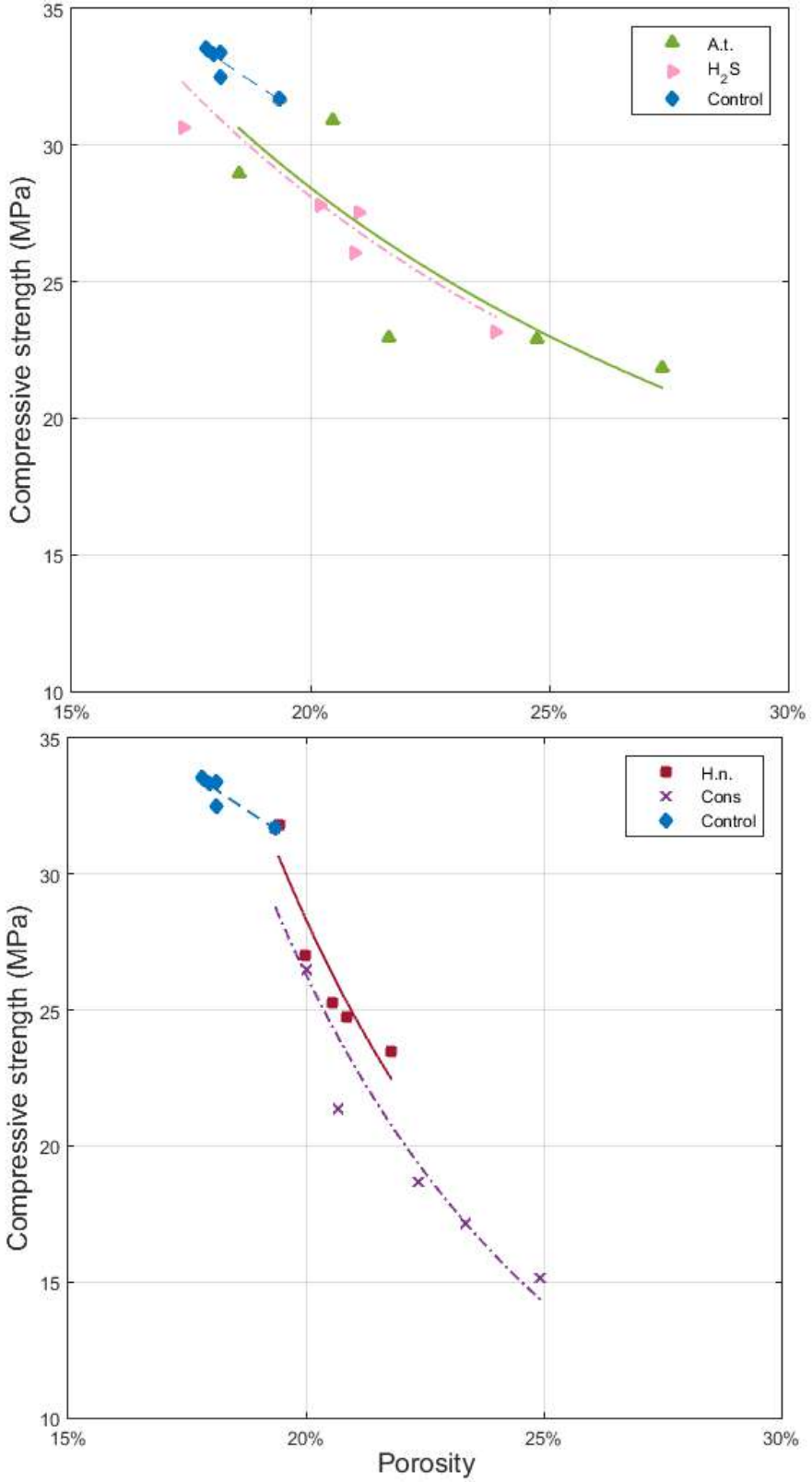

Figure 5.47: Compressive strength to total porosity relations associated to biodeterioration in samples carbonated and dried at 110°C inoculated in aseptic conditions

Table 5.8: Equations for relationships between Compressive Strength (s) in MPa and Total Porosity (ϕ) in % of biodeteriorated samples inoculated in aseptic conditions

Samples	Equation	R^2
H.n.	$s = 0.3680X^{-2.699}$	0.8973
A.t.	$s = 6.1649X^{-0.950}$	0.7128
Cons.	$s = 0.3152X^{-2.749}$	0.9275
H2S	$s = 5.9607X^{-0.964}$	0.8011
Control	$s = 10.5210X^{-0.671}$	0.8313

5.6 Summary and conclusions

- Samples inoculated with the consortium (H.n.+A.t.) showed the major signs of biodeterioration both in samples inoculated in non aseptic conditions as in samples inoculated in aseptic conditions. Weight losses up to 7 and 32%, porosity gains up to 8 and 13% and strength losses up to 52 and 100% were measured after 300 and 153 days of exposure in samples inoculated in aseptic and non aseptic conditions respectively.

- Apparently, acidophilic bacteria were able to produce the highest biodeterioration. However, in such case large error bars demand more study upon this preliminar conclusion. Conversely, samples inoculated with neutrophilic bacteria had a similar behavior to the abiotic samples subjected to H_2S. These results suggest that the ecology of the system influences in an important manner the biodeterioration effects. All the changes described in this work must be interpreted as average changes over the whole specimen volume (including deteriorated and not deteriorated zones).

- Effects of biodeterioration became more severe after about three months of exposure. Such lapse can be associated to the bacterial lag phase referred in the literature.

- In this study the samples were subjected only to a gaseous environment with low

to medium H_2S concentrations. These observations may indicate a major relative biodeterioration in here than in previous researches in which samples have been partially submerged. This effect could be explained by the fact that samples in this study had a high exposed-surface-to-mass-ratio. On the other hand, porosity and strength tests were undertaken in non-modified samples (tested as they were cast) ensuring more realistic results than when samples have been manipulated previously (cut and brushed as it has been made in other studies).

- Existence of sulfur compounds is of paramount importance in chemical and biological deterioration of sewers. In general, the larger the sulfur availability, the larger the biodeterioration or chemical effects. For this reason, the fitting of the curve for each biodeterioration effect has defined exclusively sulfur availability $Sa(t)$ as independent variable although other variables could be considered in future studies. Proposed fitting curves for weight, porosity and strength variation show a good correspondence with data. For Sa(t) values lower than $0.006 mg/cm^2$ all the biodeterioration effects can be neglected in practical applications. However, for larger values of Sa(t) all the biodeterioration effects should be modeled using logarithmic equations.

- From the relations between strength and weight and, strength and porosity, it is evident that the most important strength deterioration could occur even when weight or thickness losses are not visible yet. For this reason, it is important to consider the hidden effect of porosity changes when studying real surfaces within sewers.

- The higher dispersion of weight and strength measurements was observed in acidophilic and consortium samples. In the case of porosity measurements, all samples showed a similar dispersion through the time. It is possible that a part of such variations are related to the precision of the test procedures and the manufacturing processes applied in this study. However, the difference of dispersion between different biotic samples suggests that such effects are not important in

the case of this work.

Chapter 6

PROVISIONS TO CONTROL BIODETERIORATION IN STRUCTURAL DESIGN OF RC SEWERS

6.1 Introduction

The fundamentals of biodeterioration and results of the experiment of this study were previously presented. This chapter considers the inclusion of the effects of biodeterioration in a rational structural design practice.

Reinforced concrete sewers are usually exposed to highly varying and aggressive operative conditions during their lifetime. They are typically laid underground supporting important infill and traffic loads which can eventually produce soils settlements and structural material cracking [99]. Diluted and deposited solid matter and velocity variability of water running within the sewers modify the roughness of walls and bottom of the sewers [100]. Also the existence of gases such as carbon dioxide and hydrogen sulfide promote chemical deterioration of the sewers structure [66]. In addi-

tion, in coastal locations chloride diffusion can affect adversely the system's materials [101][102]. Furthermore, the byproducts coming from the growth of microorganisms existing in wastewater and moist walls of sewers accelerate the reinforced concrete deterioration [62]. The combination of the described mechanical, chemical and biogenic hazards can reduce the sewers service life cycle importantly [49].

Sewers failure affects adversely the efficiency of investment in sanitary infrastructure and, in many cases, leads to conditions in which the human health can be jeopardized [26]. Hereby appropriate design and management procedures are indispensable to optimize the sewers level service. As a help, modern techniques including design software aids and remote inspection systems are available for facilitating the design refinement and behavior tracing of sewers systems [37][71][103][104][105]. On the other hand, the consideration of chemical and biogenic aspects has been strongly recommended for the last years by several studies and standards. However, current design practice is still based on procedures which mainly focus on the mechanical performance of the system [104][106][107][108][109].

The literature about biodeterioration effects on reinforced concrete sewers is abundant. Weight and strength losses or porosity augment are some of the most important indicators related to early failure of sewers. Although there is evidence of 70 years old sewers systems which still keep an acceptable service level others have failed before the expected service lifetime][105][108][110][111]. Differences in performance of these systems can be mainly associated to variations in the wastewater quality, material quality, and wastewater flow characteristics. The legislation on the reduction of metals contaminants in sewers systems, promulgated in the 80's, brought important diminution of elements biologically toxic to biotic species present in sewers. This fact allowed major and faster proliferation of microorganisms capable to produce biodeterioration [71][37][112][113]. In addition, the increasing wastewater transport demand has produced important augments in caudal, velocity and turbulence of running water. These new conditions make to loss the protective (passive) layer of corroded material formed during years facilitating the biofilm renewal upon exposed surfaces. Once this

happens, the penetration of the front of corrosion in deeper layers of concrete matrix can occur [20][114][115].

To bring the previous fundamentals to a practical understanding, the following objectives are defined for this chapter:

- To summarize the fundamentals and procedures currently used in the structural design of sewers.
- To describe how biodeterioration affects the capacity of reinforced concrete sections.
- To use the results of the experimental work described previously to include the estimated thickness losses in a rational model for sewers design.
- To present recommendations for the use of adequate concrete covers to reduce the risk of collapse within a target expected lifetime.
- To present the chapter's conclusions and recommendations for future work.

6.2 Current practice in structural design of sewers

Most reinforced concrete sewers facilities are built underground. Hydraulic demands, structural stiffness of conduits, surrounding infills and soils heterogeneity, seismic events and overlaid traffic are important features to take into account when designing a sewer pipe [106]. [104]. Since hydraulic solicitations can be considered as not correlated to gravity loads and the seismic demands are not preponderant, related-to-hydraulic or seismic loads are not considered in this study. [116][117][118].

Fluid weight will vary depending on the hydraulic problems arisen from inadequate size or gradient of pipe, infiltration (from groundwater) and inflow (from surface runoff) [119][120]. Traffic (live) load magnitude is associated to the superficial cover quality (flexible or rigid pavements or unsurfaced cover), depth at which the pipe is set, class of vehicle (trucks, aircrafts or others) and direction of travel (parallel or perpendicular to

pipe axis). In general, the deeper the pipe is laid the lower the effects produced by traffic (Figure 6.2). Also the condition of the traffic behavior such as the coincidence of heavy wheels in narrow trench widths (passing mode) and its dynamic effects can increase the loads actually transmitted to the pipe. In current practice numerical simulation of such effects is achieved considering dimensional (load area) increase factors or equations and impact factors (Figure 6.3) [1][2].

In practice, the structural design of reinforced concrete sewers is based on two configurations for infill loads, leading to different loading conditions, trench and positive embankment (Figure 6.1)) [109][1]. In the trench case, due to the backfill settlement, friction forces at the backfill-in situ material interface will reduce the gravity effects upon the pipe. In the embankment case the soil placed on sides of the pipe will settle more than the soil above the pipe imposing larger effects from the soil above the pipe.

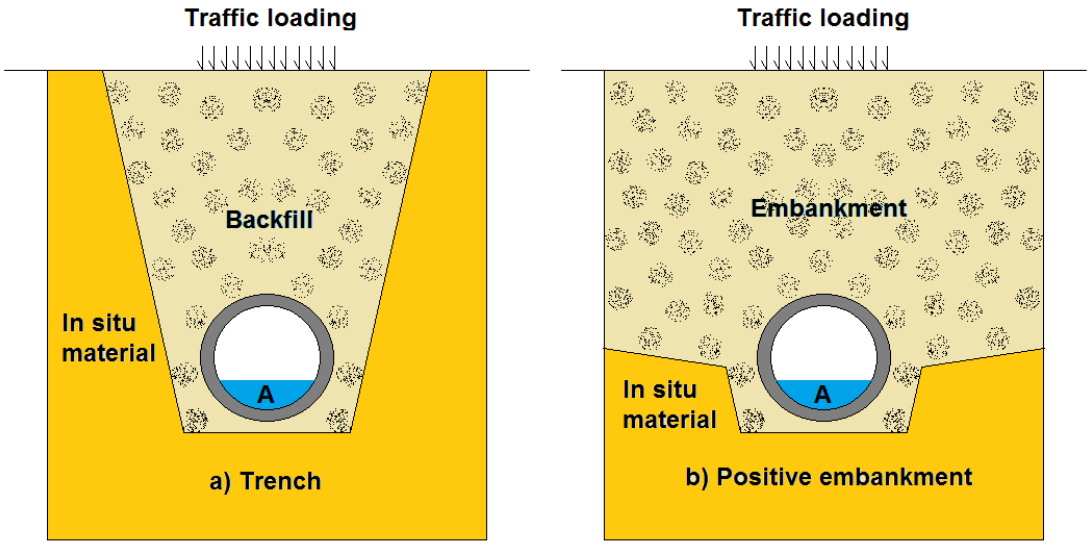

Figure 6.1: Installation and loading conditions for pipes set into excavated soils (adapted from [1][2])

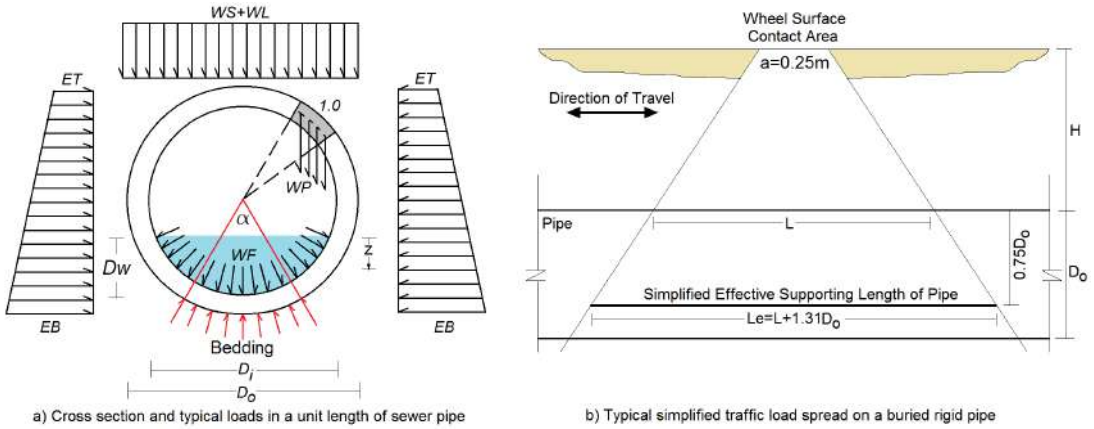

Figure 6.2: Typical loads demanding a sewer pipe. Bedding angle α value depends on the bedding material quality [3]

Typical structural design procedure includes determination of earth and live loads, selection of bedding characteristics, application of factor of safety and selection of material structural properties [1]. In this section, the description of structural demands and reinforced concrete sewers capacity are limited to those related to gravity effects and bending strength respectively. Gravity and fluid loads used in this work are computed as [1][2][3] (Figure 6.2):

$$WS = \frac{8C\gamma B^2 + {D_0}^2(4-\pi)\gamma}{8D_0} \tag{6.1}$$

$$C = \frac{1 - e^{-2ku\frac{H}{B}}}{2ku} \tag{6.2}$$

$$WP = 12(D_0 - D_i) \tag{6.3}$$

$$WF = 9.81z, 0 \leq z \leq Dw \tag{6.4}$$

$$WL = \frac{P(1+IM)}{A_s} \tag{6.5}$$

$$IM = 0.33(1 - 0.411H) \geq 0 \tag{6.6}$$

where WS=backfill pressure at the top of the pipe (kN/m^2), C=trench load coefficient, γ =backfill unit weight (kN/m^3), B=trench width (m), D_o=outer pipe diameter (m), D_i=inner pipe diameter (m), k=ratio of active unit pressure to vertical unit pressure, u=coefficient of friction between fill material and sides of trench, H=infill height placed upon the top of the pipe (m), ku=0.110 for saturated clay and 0.165 for sand or gravel, WP=pipe weight of an unit length arc (kN/m^2), WF=hydrostatic pressure at depth z(m) (kN/m^2), Dw(m)=submerged depth, WL=wheel load average pressure intensity (kN/m^2), P=total live load applied at the surface (kN), A_s=spread wheel load area at the outside top of the pipe (m^2) and IM=impact factor.

For pipes that laid under wide roads where high traffic volume is present, lateral earth pressure can be modeled using a linear load distribution. Minor and major load values ET and EB (kN/m^2) are computed using (Figure 6.2), then ET is given by:

$$ET = k\left(\gamma H + \frac{WLA_s}{A_w}\right) \text{ at the top of the pipe under embankments} \tag{6.7}$$

and EB is computed as:

$$EB = k\left(\gamma(H + D_0) + \frac{WLA_s}{A_w}\right) \text{ at the bottom of the pipe under embankments} \tag{6.8}$$

$$ET = EB = 0 \text{ for pipes laid on a trench} \tag{6.9}$$

This work deals only with the trench condition. For this reason, minimum and maximum lateral earth pressure (kN/m^2) $ET = EB = 0$.

For traffic loads, in the single dual wheel case, superficial dimensions (a,b) are amplified 1.15H and 1.00H times for granular soils and other soils respectively. . For two single dual wheel relations between A_s (spread load area) and A_w (wheel load area)

are more complex. Such relations can be found in the literature [1][2][3] (Figure 6.3). Figure 6.2 shows a section with the traffic loads spreading configuration along a pipe that is laid parallel to traffic direction using a simplified manner of computing the so called effective supporting length of pipe. In this work such simplified effective length is replaced by the use of a more rigorous analysis of interaction between the bedding and the pipe. The bedding angle α defines the arc length where the pipe is effectively supported. The value and form of the reaction pressure depend on the bedding material quality [1][3].

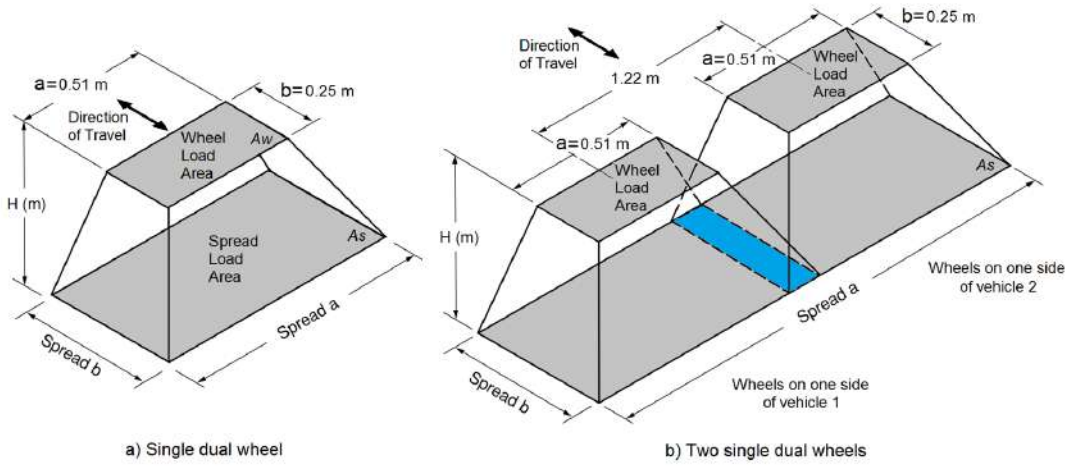

Figure 6.3: Spread load area configurations used in the evaluation of traffic loads (adapted from [1][3])

Sewer pipe strength is controlled mainly by bending moment and shear. Current design practice imposes large shear capacity avoiding fragile failure and leading the design to be governed by the bending moment capacity. For this reason, only bending moment capacity is considered in this work. Bending moment strength for singly reinforced normal weight concrete elements can be computed as [121]:

$$Mn = \rho f_y \left(1 - \frac{\rho f_y}{1.7 f'c}\right) bd^2 \tag{6.10}$$

where Mn is the nominal bending capacity (kN-m), ρ the reinforcement steel ratio, f_y

the steel yield strength (kN/m^2), $f'c$ the compressive strength of concrete (kN/m^2), b the cross section width (m), and d the internal lever arm (m) (Figure 6.4). No transversal reinforcement (stirrups or similar) are permitted. This practice leads to low reinforcement steel ratios which in turn guarantee a ductile failure and more efficient work during the life cycle of the structure.

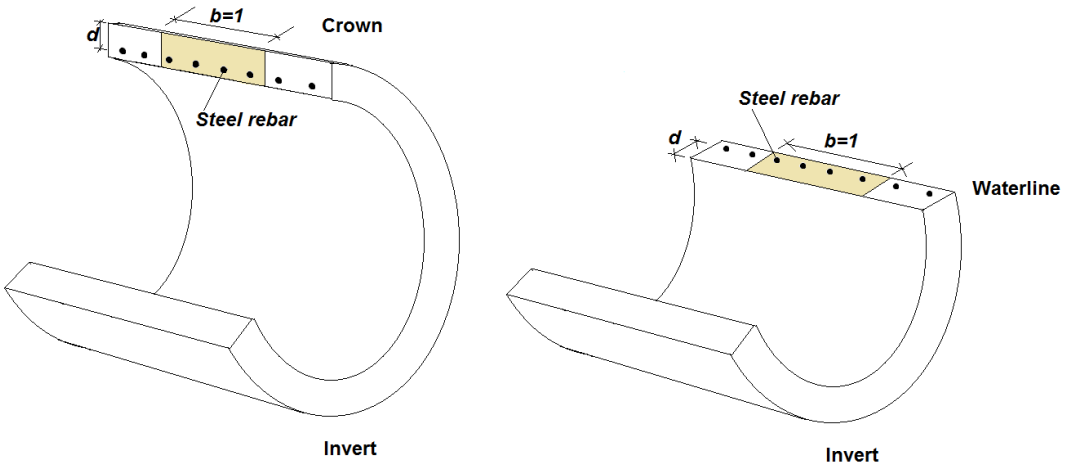

Figure 6.4: Analysis sections (crown and waterline) for structural design of RC sewers pipes

6.3 Biodeterioration effects upon reinforced concrete sewers

Biodeterioration is a surface phenomenon [60]. When a reinforced concrete element is subjected to aggressive biological attack, exposed surface is adversely affected leading to material losses (thickness reduction). Under this condition, reinforced concrete sections subjected to bending demands will loss progressively their capacity as shown in Figure 6.5. The high alkalinity of the concrete inhibits biological activity and current capacity keeps relatively invariant. However, the carbonation and presence of other environmental aggressive gases make the alkalinity concrete to lower allowing the pro-

liferation of biological species whose metabolic products deteriorate the concrete cover. At the beginning of such state a depassivation limit is reached and progressive concrete cover loss initiates. If aggressive gases are present, concrete cover will absorb them accelerating carbonation and allowing deeper penetration by diffusion [103]. Weakened superficial concrete layers will drop off due to their own weight and running water if present. Once the whole concrete cover has been removed, the steel reinforcement is exposed and a rapid capacity loss starts due to steel corrosion [122]. When the total reinforcement area has been corroded, the concrete section breaks off by bending stress.

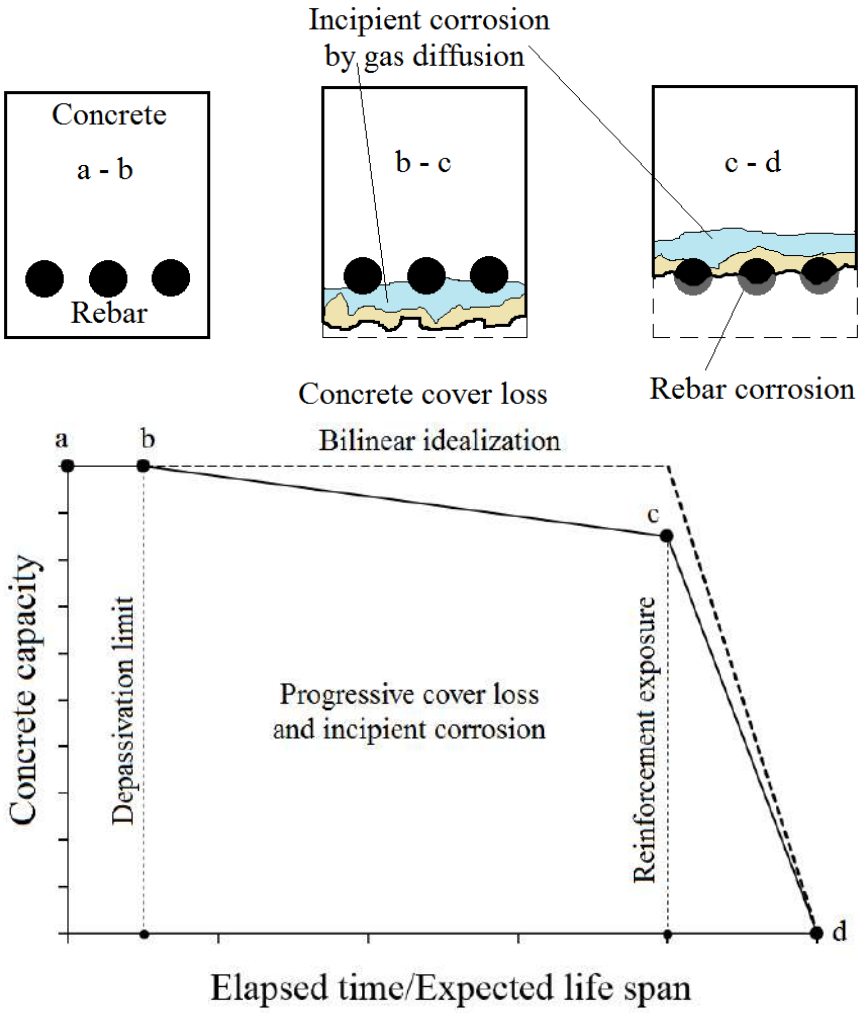

Figure 6.5: Bilinear idealization of capacity loss during biodeterioration

6. PROVISIONS TO CONTROL BIODETERIORATION IN STRUCTURAL DESIGN OF RC SEWERS

Concrete sewers maintenance and repair due to biodeterioration effects have proven to be very expensive [25][26]. Permeability and porosity augmentation and strength reduction produced by biodeterioration processes affect adversely structural durability. For this reason biodeterioration must be modeled as a time-variant solicitation throughout the structural lifetime [6].

The loss of thickness of concrete wall has the largest impact in practical applications. The reported values of concrete thickness loss vary between 0.21 mm/year [123], 2.59 mm/year [124], 5.37 mm/year [125], and 6.80 mm/year [126]. Moreover, thickness losses of about 14 mm/year have been observed in controlled laboratory environment [103]. Also the exposure history of the material has been found to be a key factor in thickness loss rates. For example, Wells and Melchers (2011) observed that new concrete coupons lost 0.05-0.80 mm/year while 70 years old coupons lost 1-7 mm/year [37].

Thickness losses have been found to be located mainly at the water line and crown [35]. Water line thickness losses can be two to four times larger than those at the crown [127]. Nevertheless, typical models of sewer failure consider three or four critical zones in a cross section of the pipe: at the left and right edges, at the top and seldom at the bottom [4][5]. In such places a reduction of thickness can be considered when studying the biodeterioration effects upon the structural integrity (Figure 6.6).

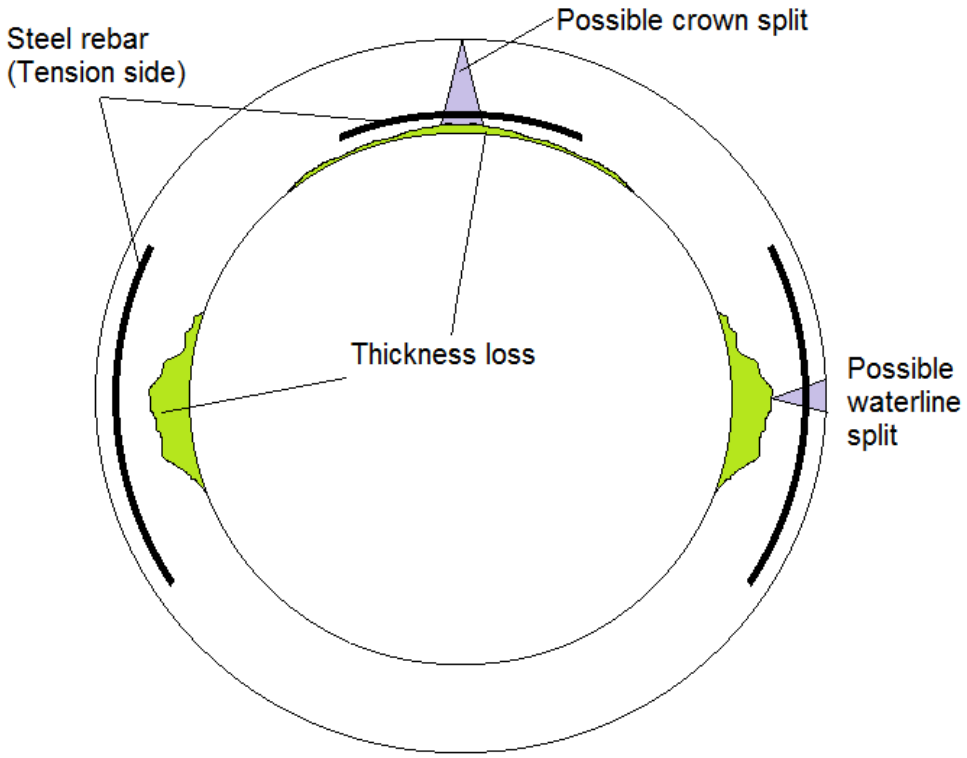

Figure 6.6: Typical breakings related to structural collapse in sewers [4][5]

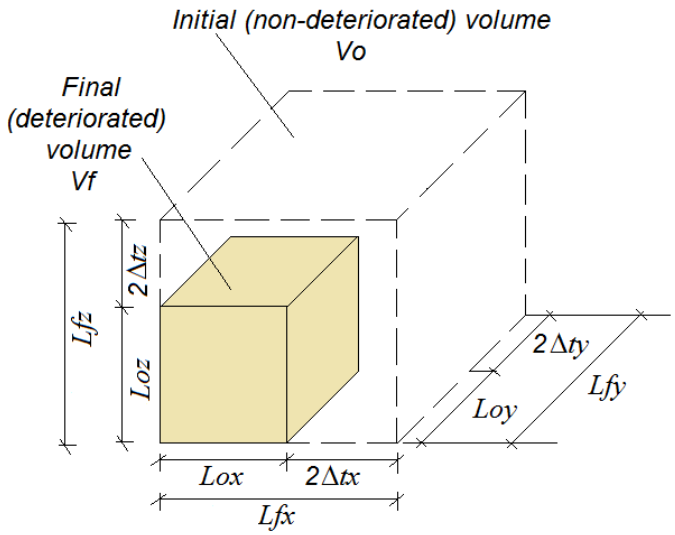

Figure 6.7: Theoretical relationship between initial and final volume of a biodeteriorated sample

To use the experimental results, relative weight loss and thickness loss were computed using (Figure 6.7):

$$\begin{aligned} L &= \frac{Wf - Wo}{Wo} \\ Vf &= Vo(1+L) \\ \Delta tx &= Lfx - Lox \\ \Delta ty &= Lfy - Loy \\ \Delta tz &= Lfz - Loz \\ L &= Vo - Vf = \Delta tx \cdot \Delta ty \cdot \Delta tz \end{aligned} \tag{6.11}$$

where L =relative sample weight loss, Wo =initial dry weight sample (g),Wf =final dry weight sample (g), Vo =initial sample volume (cc), Vf =final sample volume (cc), Lfx, Lfy, Lfz =final length side size (cm) in each perpendicular direction, Lox, Loy, Loz =initial length side size (cm) in each perpendicular direction. The accu-

mulated sulfur amount (sulfur availability) was related to the computed thickness loss at each sampling time as shown in Figure 6.8. To do so, the thickness loss related to the the weight loss measured at each sampling time was associated to the sulfur availability value computed for the same moment. Also, the expected continuous concentration (mean value) of hydrogen sulfide is shown in the upper horizontal axis.

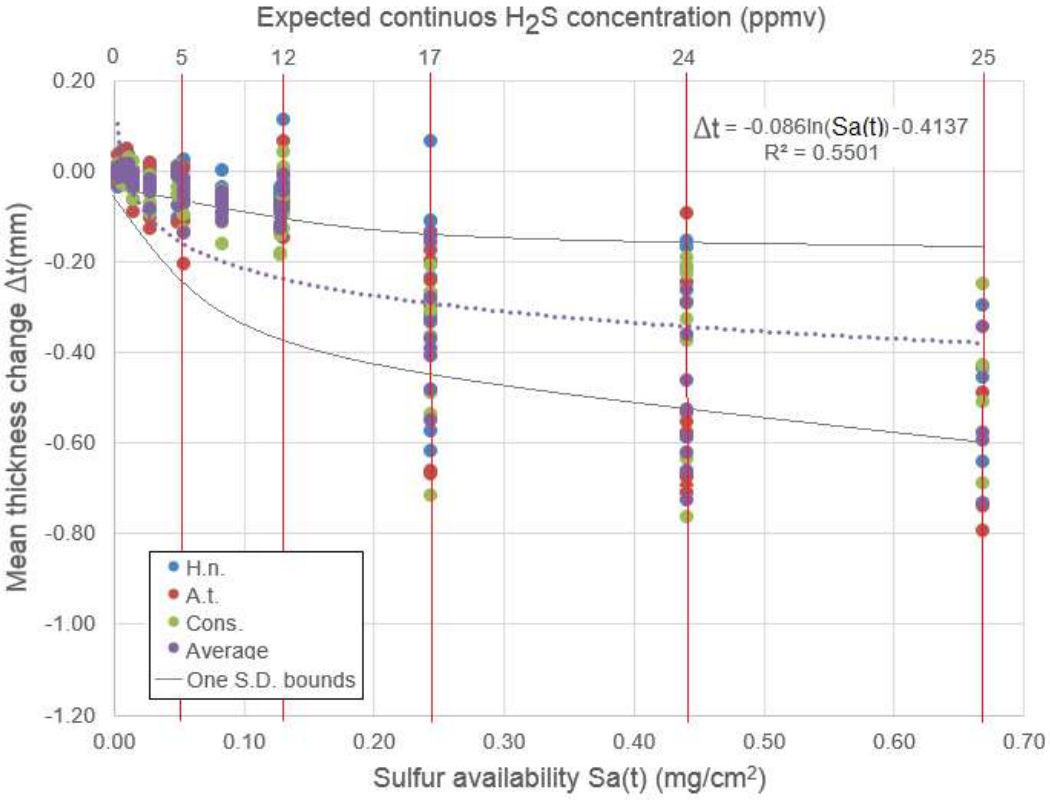

Figure 6.8: Average thickness loss produced by biodeterioration computed and fit from data. One Standard Deviation (S.D.) bounds are shown.

After 300 days of sulfur exposure up to $0.128 mgS/cm^2$ ($0.154 mgS/cm^2/year$) samples showed thickness losses of 0.260 mm. Using lineal interpolation, a thickness loss rate of 0.312 mm/year was computed. Resultant thickness loss versus sulfur availability rate can be approximated to $0.260/0.128 = 2.03 mm * cm^2/mgS$. This loss was measured from samples not brushed. In real conditions an enhancer effect of biodeterio-

ration can be possible due to the continuous removal of deteriorated layers produced by erosion at waterline and material dropped from crown. Previous thickness losses values are consistent with those reported in other researches [123]. However, sulfur amounts required in this experiment to produce such effects are considerably lower than those reported in literature. Typical sulfur concentrations between 6 and $26 gS/m^2/d$ have been associated to reported thickness losses [128]. The higher deterioration rate found in this experiment can be explained by several reasons: it exists lower biological competition due to the existence of only two pure strains; the exposed surface to volume ratio of samples is larger than in previous studies; there is an experimental scale effect and; there are no toxic compounds existing in typical wastewater. In any event, it seems that such laboratory enhancer effects are largely counteracted by the biological competition and the existence of toxic elements within the real sewers.

6.4 Consideration of biodeterioration effects in structural design of sewers

The effect of biodeterioration in the structural behavior of sewers depends highly on variable deterioration patterns. Factors such as age, pipe characteristics (size, length, materials), existence of underground water, chemical and physical soil properties, proximity of other installations, sewer slope, anoxic slim layer thickness, sulfide production, and quality and quantity of sewer water can vary widely imposing larger uncertainty to the analysis and design of sewers [110][119]. However, during the last years, rational procedures to include the effects of concrete corrosion in the structural design have been proposed [3]. Such procedures are based on reasonable and practical methods such as addition of sacrificial thickness and control of allowable cracks widths in the inner walls of sewers [129]. In the first case, the use of sacrificial layer thickness varying from 13 to 125 mm are suggested for concretes made using different aggregate types. Other methods such as mitigation of hydrogen sulfide emissions, self-cleansing procedures, chemical treatment and syntetic coatings adhesion have been proposed and applied to

reduce the biodeterioration effects [130].

Verification of corrosion rates models is of paramount importance. Material heterogeneity seems to have been a key factor in accomplished service time of sewers. For example early models fit rather well up to the first 20 years of service but have forecasted thickness losses of about one fourth to one third of those measured 15 years later [110]. These reasons remark the evident need of continuous research related to the structural design of sewers based on the thickness losses approach.

Thickness losses produced by biodeterioration impose a higher probability of failure in structural design of sewers pipes compared with that obtained from the use of procedures considering exclusively physical and mechanical approaches. To confront this hazard typical factors of safety of 1.0 and 1.3 are used for reinforced concrete pipes with and without sacrificial layer respectively [3]. Despite this methodology's appeal for designers, the uncertainty associated to the load-capacity relations is still not understood completely.

In this work, a typical sewer pipe is analyzed using the direct stiffness method, in which the thickness loss at the water line and the crown are reduced in successive stages. Frame elements are jointed to form a quasi-cylindrical duct. To compute the inner forces and nodal displacements in the pipe, a MATLAB® code was developed and validated using the software SAP2000® (Figure 6.9) [131][132][133][134][135][136]. SAP2000 software has been successfully used to study the behavior of tubular structures, sewers pipes and infrastructure components [132][133][134][135][136]. Joints of lower elements (bedding) were supported upon springs to simulate the bearing conditions. The constant of every spring was computed multiplying the modulus of subgrade reaction by the afferent area around the joint [5][137][138]. The model used in the MATLAB code shown in Figure 6.10 resulted appropriated to simulate the inner forces distribution.

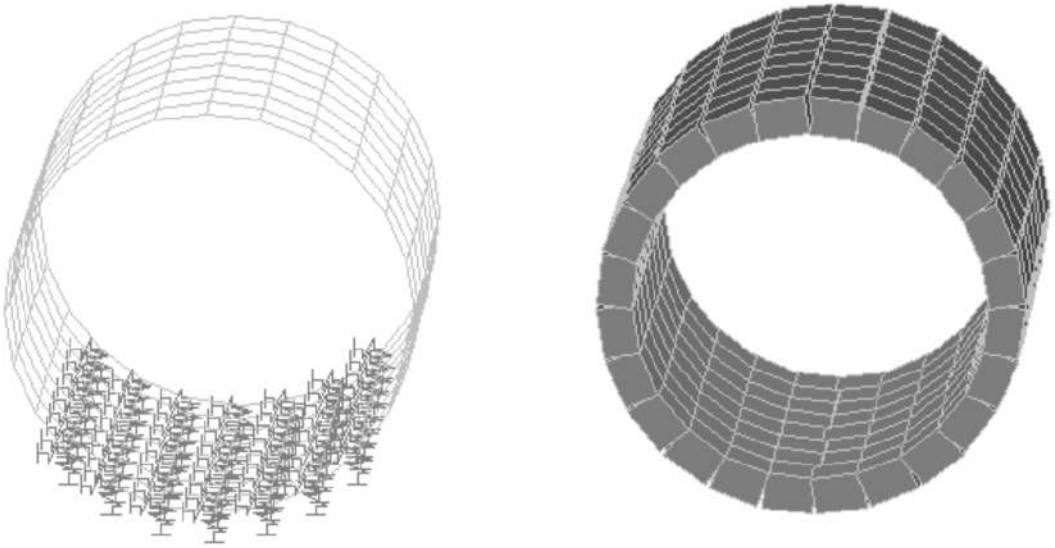

Figure 6.9: Model used for validation (SAP2000)

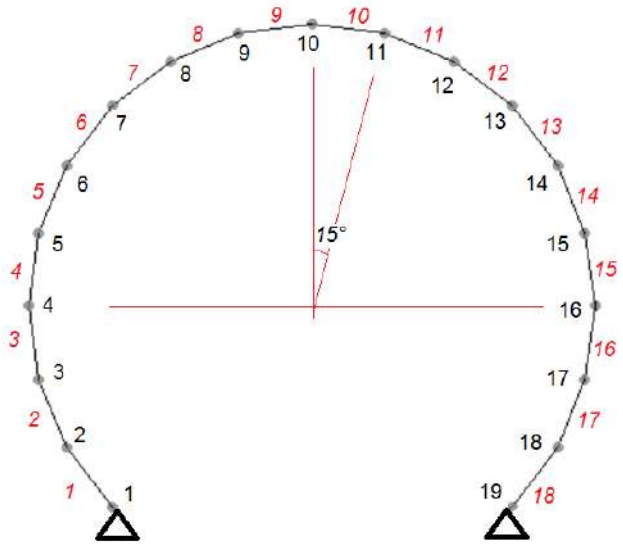

Figure 6.10: Model used for MATLAB® code design. Up: Validation using SAP2000®; Down: Crown at point 10, waterline at points 4 and 16

To take into account the progressive thickness loss during the pipes life span the use of a conditioning lapse for corrosion initiation between 0.9 to 3 years (walls acidification

and biofilm formation with 0 mm/year thickness loss) followed by a linear thickness loss has been proposed [71][139]. High variability of thickness losses reported in literature and the findings of this work let to consider a corrosion initiation lapse of three years and a linear thickness loss mean value of $0.31 mm/year$ in the crown zone for an average 12 ppmv H_2S concentration. Here it is supposed that the biodeteriorated layer will be continuously removed allowing deeper deterioration. Reliable data for waterline zone were not found so it was considered that its thickness loss can vary from 2 to 4 times that of the crown zone [127]. To model the sulfur availability influence, a reference value of $2.03 mm - cm^2/mgS$ corresponding to a continuous flow of 12±4 ppmv H_2S was chosen. Multiples of that value, 10, 30, 50, 100 and 423 ppmv H_2S rates of mean sulfur availability were considered using a linear trend. Such values were selected to cover a wide range of real H_2S concentrations reported in literature [139][140]. Standard deviation (from daily average data) was fit from values reported in field studies shown in Table 6.1.

Table 6.1: Real H_2S concentrations (ppmv) reported in literature. All the information has been taken from the work of Wells and Melchers (2015) [139]

Average	Minimum	Maximum	COV (%)
125	26	222	90.4%
423	107	828	38.5%
1.5	0	4.3	73.3%
6	0	17.6	53.3%
2.7	0	19.4	88.8%
2.2	0	59.9	131.8%

To consider the uncertainty related to biodeterioration, pipe geometrical characteristics, loads and bending capacity probability distributions are used. Load mean values are calculated as stated in section 6.2. Mean values of geometrical characteristics are taken as nominal commercial values required by the ASTM standards [141]. Bending capacity value at time τ is computed rewriting equation 6.10 as:

$$Mn(\tau) = \rho(\tau) \cdot fy \left(1 - \frac{\rho(\tau) \cdot fy}{1.7 f'c}\right) b \cdot d(\tau)^2 \tag{6.12}$$

with

$$d(\tau) = do - \frac{\Delta t(\tau)}{1000} \tag{6.13}$$

and

$$\Delta t(\tau) = r \cdot Sa(\tau) \tag{6.14}$$

The ratio steel at time τ is defined as:

$$\rho(\tau) = \begin{cases} \frac{As}{bdo} & \text{if } d(\tau) \geq do + d_b \\ \frac{As_r}{bd(\tau)} & \text{if } 2do - d_b < d(\tau) < 2do + d_b \\ 0 & \text{if } d(\tau) \leq 2do - d_b \end{cases} \tag{6.15}$$

In previous expressions $Sa(\tau)$ is the sulfur availability (mgS/cm^2) at time τ , $\Delta t(\tau)$ the thickness loss (mm) at time τ, r the thickness loss versus sulfur availability rate ($mm - cm^2/mgS$), $d(\tau)$ the available inner lever arm (m) at time τ , do the available inner lever arm (m) at time $\tau = 0$, As the initial rebar area (m^2), d_b the mean bar diameter (m), and As_r the reduced rebar area due to corrosion (m^2). The width $b = 1.0$ is considered to be a deterministic value. As_r value is computed using sulfuric acid diffusion following the model proposed by Bastidas et al (2009) [49].

The probability of failure associated to the sewer pipe system can be determined from [142][143]:

$$g(\vec{X}) = g(\vec{X}_R, \vec{X}_S) = g(Sa(\tau), \rho(\tau), d(\tau)) \tag{6.16}$$

$$P_f = P\left[g(\vec{X}) \leq 0\right] = \int_{g(\vec{X})\leq 0} \cdots \int f(x)\left(\vec{x}\right) d\vec{x} \tag{6.17}$$

being $\vec{X}_R, \vec{X}_S$ the system resistance (i.e. bending moment capacity, equations 6.12) and the effect of loads demanding the system (i.e. demanded bending moment, the equations

in section 6.2 and Figure 6.2) respectively. Probability of failure of the problem was estimated using Monte Carlo's simulations [142][143]. To apply Monte Carlo's method, a synthetic sample composed of N random numbers ($\vec{X}_R, \vec{X}_S$) is generated separately at each time $\tau = 0, 1, 2, , T$. Then, for each pair of numbers ($\vec{X}_R, \vec{X}_S$), at a given time $\tau = \tau_i$, a $g(\vec{X}(\tau_i))$ value is computed. If $g(\vec{X}(\tau_i)) \leq 0$ the structure has failed. Finally the probability of failure of the system can be approximated to:

$$P_f \approx \frac{n(\tau_i)}{N} \tag{6.18}$$

where $n(\tau_i) \leq N$ is the number of failures of the system for a given time τ_i .

6.5 Numerical application

Current commercial pipes have nominal diameters varying from 225 to 3600 mm and typical length of 2440 mm. In most cases adjacent pipes are usually connected using a flexible ring capable of allowing movements in the joint. This configuration facilitates the stresses relief due to accommodation during a seismic event. Moreover, when good quality beddings are used, settlements will hardly occur. For these reasons the structural analysis has considered two realistic conditions with no seismic effects: empty pipe and pipe in service with no settlements. In the first case no loads from water pressure are included. The second case involves all the loads defined in section 5.2. Similarly, the geometry of pipe sections is modified to take into account thickness losses in each analysis condition.

This example considers a reinforced concrete pipe (2.13 m inner diameter, 2.57 outer diameter) that will be built under a road with high truck traffic into a 3.60 m x 8.07 m (width x depth) trench. Ordinary granular material will be used in backfill and bedding. Under pipe invert a granular cradle 50 cm thick will be compacted. No sacrificial thickness will be considered. The reinforcement configuration is determined from the results of a classic design (considering a factor of safety of 1.30). Random variables related to the problem are shown in Table 6.2. The effects of biodeterioration

in the performance are considered by evaluating the probability of failure of the system.

Table 6.2: Suggested values for Monte Carlo simulation

Variables	Mean	$\mathbf{cv}_x(COV)$	Distribution	REF.
Concrete compressive strength, *f'c* (MPa)=	$x_k/(1\text{-}1.56\text{cv}_x)$	0.19	Lognormal	[143]
Reinforcement steel strength, *fy* (MPa)=	$x_k\ /(1\text{-}1.56\text{cv}_x)$	0.10	Lognormal	[144]
Steel elastic modulus, *Es* (MPa)=	x_d =200000	0.06	Lognormal	[144]
Extreme fiber to rebar center distance, *c* (mm)=	x_d =(25;50;75;100)	0.10	Lognormal	[145]
Reinforcement steel area, *As* (cm^2/m)=	x_d =(7;9;11;13)	0.05	Lognormal	[141]
Soil unit weight, $\gamma(kN/m^3)$=	x_d =20	0.10	Lognormal	[143]
Backfill height, *H* (m)=	x_d =[3:5]	-	Uniform	
Traffic (live) load, *P* (kN)=	$x_k\ /(1\text{-}1.56\text{cv}_x)$	0.25	Lognormal	[3]
Sulfur availability, Sa(mg/cm^2/year)*=	x_d =(0.26;0.44;0.85;3.33)	(0.86;0.83;0.75;0.39)	Lognormal	

xd: design value, *xk*: characteristic value, cv_x: coefficient of variation
*Depends on exposure conditions

Characteristic values *xk* used in this example are:

- *f'c* (MPa)= 28
- *fy* (MPa)= 420
- *P* (KN)= 223

The pipe specifications are adopted from the design of sewers requirements stated in ASTM standards [141][145][146][147]. Although triple cage is specified, elliptical cage is not taken into account when computing the bending strength (Figure 6.11).

The MATLAB® code was run to generate 1000 iterations using Montecarlo's method for every variable each time $\tau = \tau_i$. A time window of 100 years was covered.

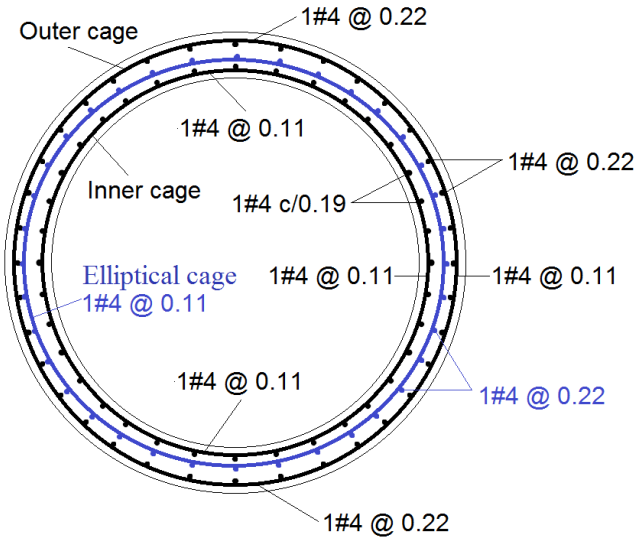

Figure 6.11: Example of typical steel reinforcement. No detailing steel reinforcement is shown

In the next section it is demonstrated that the larger the sulfur availability the larger the probability of failure. Accepting as a practical value a probability of failure of pd=0.10, the mean expected lifetime of the sewer pipe is about 30, 19, 12 and 6 years for 30, 50, 100 and 423 ppmv H_2S concentrations respectively when using an extreme fiber to rebar center distance, c=2.5 cm. On the other hand, if c=5.0 cm expected life augment up to 56, 36, 19 and 8 years respectively. These results are more critical to those reported in the literature due mainly to the effect of rates of corrosion used in each case [6][148][149].

6.6 Proposal of methodology for considering biodeterioration effects in structural design of sewers

Figure 6.12 summarizes the proposal to include the findings of this study in the structural design of sewers. The process can be summarized as follows:

- To select the parameters such as diameter, material characteristics, hydrogen

sulfide concentration and load values to be used as a seed from which values of capacity and demand will be computed for each time t.

- To compare the capacity to the demand value for each time t. If capacity is lower that demand there will be a failure event.
- To repeat the process described N times and compute the probability of failure using the count of failure events.
- To plot the probability of failure versus time curves and define the target values for design.

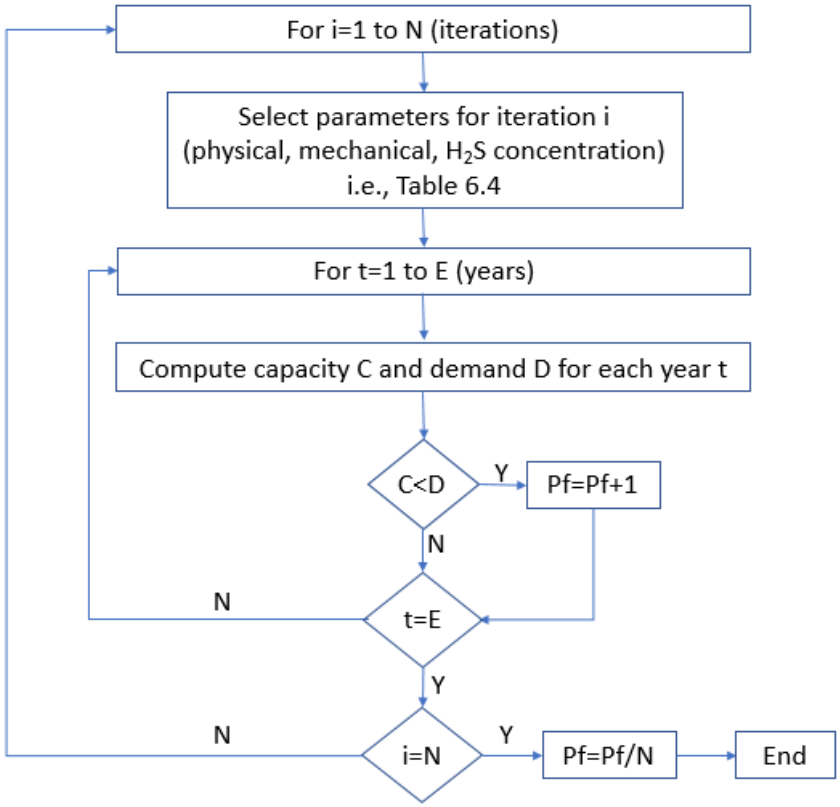

Figure 6.12: Methodology for proposal application

Following what has been reported in the literature, in this work the sulfur availability and the protective cover have been selected as the most influential parameters [6].

For this reason, in practical situations, it is sufficient to forecast the hydrogen sulfide concentrations and assign and appropriate concrete cover to ensure a satisfactory service life span. Nevertheless, an adequate compressive strength is recommended because it is correlated to high density and low porosity which guarantees a better durability. Besides, resistance under typical gravity loads or other physical demands will be sufficiently secure due to the larger structural sections required by the corrosion control. On the other hand, the Design Service Life (DSL) for sewers is computed using the findings and proposals of some statistical studies related to the sewers behaviour upon the time [6][149]. From this analysis the DSL values can be fit as shown in Table 6.3.

Table 6.3: Design Service Life (DSL) for given total concrete covers

H_2S conc. (ppmv)	**Cover (cm)**	**DSL (years)**	**Cover (cm)**	**DSL (years)**	**Cover (cm)**	**DSL (years)**	**Cover (cm)**	**DSL (years)**
30	3.5	41	5.5	63	7.5	84	12.5	180
50	3.5	27	5.5	42	7.5	53	12.5	87
100	3.5	15	5.5	23	7.5	29	12.5	47
423	3.5	7	5.5	9	7.5	11	12.5	17

In sewers laying under highways and other important assets the use of DSL=100 years is recommended [150]. However, although there are many sewers exceeding such goal, also an important amount of sewers failing between lapses of 3 and 60 years has been reported [151][152]. When considering the biodeterioration effects an adequate management has to be planned for reducing the risk of collapse from corrosion. Nevertheless, when this is not possible, the best choice is to delay the collapse adding additional (sacrificial) material. In such event a maximum DSL=25 years is recommendable and achievable. In any case, the minimum concrete cover was computed to guarantee a 15, 20 and 25 years span. Table 6.4 contains the recommended values applicable to average concentrations up to 100 ppmv H_2S and mean diameters of pipe from 100 to 250 cm. The use of these guidelines will demand a higher initial investment but reduce maintenance costs. The concrete volume will augment between 104 and 123% with respect to that of a typical sewer pipe. On the other hand, a flow capacity reduction up to 10% could affect the service level of pipes working close to the

whole flow capacity. In the case of hydrogen sulfide concentrations lower than 30 ppm no sacrificial cover is needed for DSL up to 35 years.

Table 6.4: Recommended minimum concrete cover for DSL=15,20 and 25 years (mean diameter from 100 to 250 cm)

H_2S conc. (ppmv)	DSL (years)	Sacrificial cover (mm)	Total cover (mm)*	Final to initial Area ratio	Typical conditions
50	15	0	25	100%	Tropical zones
	20	0	25	100%	
	25	6	31	98%	
100	10	10	35	97%	Critical exposure
	20	22	47	94%	
	25	37	62	90%	

*Considering a minimum legal concrete cover of 25 mm [141]

According to Table 6.4, when concentrations vary from 50 to 100 ppmv H_2S a concrete cover ranging from 31 to 62 mm must be placed. In addition, when designing, it is important to check the rebar efficiency on bending moment capacity due to the reduction of the internal lever arm if the original section thickness is kept. Nowadays, a typical 19 mm sacrificial thickness is specified for outer diameters larger than 1.05 m [3]. This value is similar to that proposed here for H_2S concentrations up to 100 ppmv and a DSL of 20 years. For concentrations below 30 ppmv H_2S a minimum concrete cover of 25 mm is recommended. Finally, in absence of in situ statistical data to determine design concentrations, lineaments given in [106][128] can be used.

6.7 Conclusions and recommendations for future work

The following are the conclusions related to the proposed objectives of this chapter:

- Typical structural design of buried sewers requires the confrontation of demands and available resistance. Traffic and infills loads are the most important demands which are considered not to be correlated with the capacity. However, their variability has to be included when designing a pipe. On the other hand, biodeterioration affects exclusively the resistance reducing the thickness wall and the

strength of superficial concrete and increasing the risk of corrosion of steel reinforcement. For these reasons, a comprehensive analysis including the randomness of demands and resistance must be done.

- Inside sewers pipes, biodeterioration destroys the cohesiveness of superficial concrete layers. Softened layers are continuously washed by running water or drop off allowing a deeper penetration of hazardous microorganisms and the exposure of steel reinforcement. Then, presence of corrosive gases such as CO_2 and H_2S leads to reinforcement depassivation and consequent corrosion which will rapidly take the affected section to the collapse.

- A conditioning lapse for corrosion initiation of three years and a linear thickness loss mean value of 0.31 mm/year in the crown zone for an average 12 ppmv H_2S concentration were considered. A thickness loss in waterline zone of 2 to 4 times that of the crown zone was used. Also a loss rate of $2.03 mm - cm^2/mgS$ corresponding to a continuous flow of 12±4 ppmv H_2S ($0.128 mgS/cm^2$) was used. Besides, multiples of that value, equivalent to 10, 30, 50, 100 and 423 ppmv H_2S rates were considered in the computations following a linear trend.

- When H_2S concentrations oscillate between 50 and 100 ppmv, inner concrete covers ranging from 31 to 62 mm must be used to guarantee a design service life up to 25 years. For concentrations below 30 ppmv H_2S a minimum concrete cover of 25 mm is recommended. On the other hand, according to the results of this work, the currently recommended sacrificial thickness (19 mm) will protect the inner walls from biodeterioration during 20 years if the H_2S concentrations are lower than 100 ppmv.

- In reinforced concrete sewers the biodeterioration effects increase the risk of structural collapse. Due to the rapid SOB proliferation in H_2S-rich environments, biodeterioration becomes critical when the availability of sulfur increases within sewers. Biodeterioration affects adversely the durability increasing the probability of failure and reducing the expected service life time. It causes thickness losses

at the inner fibers located on the side walls and crown of the pipe. These losses reduce the bending moment capacity and modify the demanding forces distribution along the pipe section. Progressive concrete cover losses and cracking expose the reinforcement steel to corrosion sharpening even more this decay trend.

- This work has focused on average hydrogen sulfide concentrations (i.e. continuous flow). There is evidence that hydrogen sulfide peaks can be more dangerous to the concrete health than a steady supply. It is recommendable to adapt the model for taking into account H_2S peaks more than a mean concentration.

Chapter 7

CLOSURE

7.1 Conclusions

The following conclusions are valid for the two main objectives of this thesis:

- In this work the relationships resulted from biodeterioration between strength, weight loss and porosity have been investigated simultaneously in a comprehensive manner, while previous research only studied weight loss.

- Biodeterioration increased porosity and depressed strength and weight in high surface/volume mortar samples. Samples used in this work were not cut as reported in previous researches. This particularity gave a more realistic measurement of porosity due to the uniformity of the samples' surfaces. The samples' high surface/volume ratio allowed an apparent acceleration of biodeterioration. Besides, the fact that the samples were not submerged as in previous works calls for care when comparisons with other studies are done.

- The biogenic and chemical deterioration can potentiate the physical damage due to the chemical reactions leading to the structural breaking of the concrete matrix. It has been observed that biogenic deterioration (biodeterioration) is usually faster and catastrophic than pure chemical or physical deterioration. In this work acidophilic bacteria (*Acidithiobacillus thiooxidans*), alone or within a consortium,

produced the most severe mortar biodeterioration. Conversely *Hallothiobacillus neapolitanus*, when alone, were unable to deteriorate importantly the mortar samples. In all the cases, the inoculated samples showed larger deterioration effects than abiotic samples exposed to H_2S.

- In reinforced concrete sewers the biodeterioration effects increase the risk of structural collapse. Due to the rapid SOB proliferation in H_2S-rich environments, biodeterioration becomes critical when the availability of sulfur increases within sewers.

- Biodeterioration affects adversely the durability increasing the probability of failure and reducing the expected service life time. The thickness losses reduce the bending moment capacity and modify the demanding forces distribution along the pipe section. Once the reinforcement is exposed to the corrosive environment the collapse is reached rapidly.

- The results suggest that the ecology of the system influences in an important manner the biodeterioration effects. In all the cases the major deterioration was observed in samples inoculated with mixed cultures. Also the samples inoculated in non aseptic conditions produced a deterioration several times greater than those inoculated in aseptic conditions. On the other hand, although the amount of available sulfur was larger in the first case, samples subjected only to H_2S did not show important differences from each other. These facts lead to conclude that the biogenic effects were responsible for the important difference in deterioration between cultures inoculated in non aseptic and aseptic conditions.

- All the changes described in this work must be interpreted as average changes over the whole specimen volume (including deteriorated and not deteriorated zones)

Regarding to the effects produced by biodeterioration upon mortar samples inoculated in non aseptic conditions and exposed to hydrogen-sulfide-rich environments:

- Weight losses of up to 32%, porosity augmentation up to 32% and total strength loss were observed in only five months. With respect to other reports in the literature, these results are only comparable to a weight loss of 37% after one year of exposition. This fact confirms the more severe deterioration observed in this work

Regarding to the effects produced by biodeterioration upon mortar samples inoculated in aseptic conditions and exposed to hydrogen-sulfide-rich environments:

- Weight losses up to 7%, porosity augmentation up to 27% and strength losses up to 48% were observed after 10 months of exposure. Pure acidophilic bacteria were able to produce a high biodeterioration mainly depicted by weight loss (5%) and porosity augment (7%). Conversely samples inoculated with pure neutrophilic bacteria had a similar behavior to the abiotic samples subjected to H_2S.

- The big difference between the behavior of samples inoculated in non aseptic and aseptic and the possible extrapolation to real sewers environments can be explained as follows. In the case of samples inoculated in aseptic conditions, it exists much lower biological competition, there is an experimental scale effect and, there is no wastewater toxicity in the experiment. In addition, in a typical sewer, the continuous removal of deteriorated layers produced by erosion at waterline and material dropped from crown might enhance even more the observed aggressiveness. However, all this enhancer effects seem to be counteracted by the biological competition among a large amount of species and the toxicity in wastewater. As seen, this is a complex issue which requires more investigation.

- Mean expected lifetime of a sewer pipe depends importantly upon the hydrogen sulfide concentration. The larger the H_2S concentration, the shorter the service life time is. To guarantee a service lifetime of 25 years it is recommendable to use inner concrete covers of 25, 31 and 62 mm for 30, 50 and 100 ppmv H_2S concentrations respectively. For high concentration (423 ppmv H_2S) use of sacrificial cover is not recommended.

7.2 Recommendations for future work

- This thesis has focused on average hydrogen sulfide concentrations (i.e. continuous flow). There is evidence that hydrogen sulfide peaks can be more dangerous to the concrete health than a steady supply. It is recommendable to adapt our model for taking into account H_2S peaks more than a mean concentration.

- As expressed in this document, it is not clear yet how the biological competition affects the laboratory-in situ measurements relationship. Similarly, the relation between the lab-controlled measurements of bacterial growth and those taken in situ affected by the wastewater toxicity has to be investigated. It is recommendable to design and apply experiments where the previous challenges can be undertaken.

- In this work only sulfur availability has been considered when modeling biodeterioration effects. It is recommendable to evaluate the contribution of other parameters or processes in the capacity loss such as the diffusion processes or the effect of water velocity.

- There is a lack of experimental evidence related to the relation of thickness losses in different parts of the sewers walls. It is necessary to develop studies tending to determine the crown to waterline thickness losses ratio in typical sewers.

REFERENCES

[1] American Concrete Pipe Association. **Concrete Pipe Design Manual**, 2011. xxv, 142, 143, 145

[2] AASHTO. **AASHTO LRFD Bridge Desig Specifications**, 2012. xxv, 142, 143, 145

[3] Concrete Manufacturers Association. **Concrete Pipe and Portal Culvert Handbook**, 2012. xxv, 143, 145, 152, 153, 158, 162

[4] JP Davies, BA Clarke, JT Whiter, and RJ Cunningham. **Factors influencing the structural deterioration and collapse of rigid sewer pipes**. *Urban water*, **3**(1):73–89, 2001. xxv, 148, 149

[5] G. Becker, H. Boduroglu, S. Camarinopoulos, S. Frondistou-Yannas, a. Gedikli, V. G. Kallidromitis, D. Kampranis, and C. Sanna. **Structural Assessment and Upgrading of Sewers Based on Inspection Results**. *Journal of Infrastructure Systems*, **15**(December):321–329, dec 2009. xxv, 148, 149, 153

[6] M Mahmoodian and A.M. Alani. **Multi-Failure Mode Assessment of Buried Concrete Pipes Subjected to Time-Dependent Deterioration , Using System Reliability Analysis**. *J Fail. Anal.and Preven.*, **13**:634–642, 2013. xxvii, 8, 10, 148, 159, 160, 161

[7] P Mehta and P. J. M. Monteiro. *Concrete: Microstructure, Properties, and Materials*. McGraw-Hill, 2006. 1

[8] M. Sanchez-Silva and David V. Rosowsky. **Biodeterioration of Construction Materials: State of the Art and Future Challenges**. *Journal of Materials in Civil Engineering*, **20**(5):352–365, may 2008. 2, 3, 13

[9] Emilio Bastidas-Arteaga, Mauricio Sánchez-Silva, Alaa Chateauneuf, Moema Ribas Silva, and M. Ribas Silva. **Coupled reliability model of biodeterioration, chloride ingress and cracking for reinforced concrete structures**. *Structural Safety*, **30**(2):110–129, mar 2008. 2, 8, 11

[10] Willem De Muynck, Anibal Maury Ramirez, Nele De Belie, and Willy Verstraete. **Evaluation of strategies to prevent algal fouling on white architectural and cellular concrete**. *International Biodeterioration & Biodegradation*, **63**(6):679–689, 2009. 3

[11] Ana Miller, Amélia Dionísio, and Maria Filomena Macedo. **Primary bioreceptivity: a comparative study of different Portuguese lithotypes**. *International biodeterioration & biodegradation*, **57**(2):136–142, 2006. 3

[12] Virginie Wiktor, F De Leo, C Urzì, René Guyonnet, Ph Grosseau, and Eric Garcia-Diaz. **Accelerated laboratory test to study fungal biodeterioration of cementitious matrix**. *International Biodeterioration & Biodegradation*, **63**(8):1061–1065, 2009. 3, 32

[13] Marcia A Shirakawa, SM Selmo, MA Cincotto, CC Gaylarde, S Brazolin, and Walderez Gambale. **Susceptibility of phosphogypsum to fungal growth and the effect of various biocides**. *International biodeterioration & biodegradation*, **49**(4):293–298, 2002. 3

[14] B Prieto, B Silva, N Aira, and L Álvarez. **Toward a definition of a bioreceptivity index for granitic rocks: Perception of the change in appearance of the rock**. *International biodeterioration & biodegradation*, **58**(3):150–154, 2006. 3

REFERENCES

[15] James Hiller and James Scullin. **Mold-Understanding the Basics**. In *Forensic Engineering*, pages 74–83. ASCE, 2003. 3

[16] Rhena Schumann, Norbert Häubner, Steffi Klausch, and Ulf Karsten. **Chlorophyll extraction methods for the quantification of green microalgae colonizing building facades**. *International Biodeterioration & Biodegradation*, **55**(3):213–222, 2005. 3

[17] Christine C Gaylarde and Peter M Gaylarde. **A comparative study of the major microbial biomass of biofilms on exteriors of buildings in Europe and Latin America**. *International biodeterioration & biodegradation*, **55**(2):131–139, 2005. 3

[18] Emilio Bastidas-Arteaga, M Sanchez-Silva, and A Chateauneuf. **Structural reliability of RC structures subject to biodeterioration, corrosion and concrete cracking**. In *10th International Conference on Applications of Statistics and Probability in Civil Engineering,Tokyo:Japan, ICAPS 10*, pages 183–190, 2007. 8

[19] Angela Bielefeldt, Ma. Guadalupe D. Gutierrez-Padilla, Serguei Ovtchinnikov, Joann Silverstein, and Mark Hernandez. **Bacterial Kinetics of Sulfur Oxidizing Bacteria and Their Biodeterioration Rates of Concrete Sewer Pipe Samples**. *Journal of Environmental Engineering*, **136**(7):731–738, jul 2010. 8, 9, 13, 14

[20] Shiping Wei, Zhenglong Jiang, Hao Liu, Dongsheng Zhou, and Mauricio Sanchez-silva. **Microbiologically induced deterioration of concrete - A Review**. **1007**:1001–1007, 2013. 8, 141

[21] Hector A Videla. *Manual of Biocorrosion*. CRC Press, 1996. 8

[22] K Cho and T Mori. **A newly isolated fungus participates in the corrosion of concrete sewer pipes**. *Water Science and Technology*, **31**(7):263–271, 1995. 8, 14

[23] Robert E Melchers and RJ Jeffrey. **Probabilistic models for steel corrosion loss and pitting of marine infrastructure**. *Reliability Engineering & System Safety*, **93**(3):423–432, 2008. 8

[24] Robert E Melchers. **The effect of corrosion on the structural reliability of steel offshore structures**. *Corrosion Science*, **47**(10):2391–2410, 2005. 8

[25] Ramesh Kumar, P Gardoni, and M Sanchez-Silva. **Effect of cumulative seismic damage and corrosion on the life-cycle cost of reinforced concrete bridges**. *Earthquake Engineering & Structural Dynamics*, **38**(7):887–905, 2009. 8, 148

[26] Mauricio Sanchez-Silva, Georgia-Ann Klutke, and David V. Rosowsky. **Life-cycle performance of structures subject to multiple deterioration mechanisms**. *Structural Safety*, **33**(3):206–217, may 2011. 8, 140, 148

[27] Christine Lors, Mohamad Hajj Chehade, and Denis Damidot. **pH variations during growth of *Acidithiobacillus thiooxidans* in buffered media designed for an assay to evaluate concrete biodeterioration**. *International Biodeterioration & Biodegradation*, **63**(7):880–883, oct 2009. 9, 13, 14

[28] Silke Ehrich, Laure Helard, Roger Letourneux, Jaques Willocq, and Eberhard Bock. **Biogenic and chemical sulfuric acid corrosion of mortars**. *Journal of materials in civil engineering*, **11**(4):340–344, 1999. 9

[29] Wolfgang Sand. **Importance of hydrogen sulfide, thiosulfate, and methylmercaptan for growth of *thiobacilli* during simulation of concrete corrosion**. *Applied and Environmental Microbiology*, **53**(7):1645–1648, 1987. 9

[30] Satoshi Okabe, Mitsunori Odagiri, Tsukasa Ito, and Hisashi Satoh. **Succession of sulfur-oxidizing bacteria in the microbial community on corroding concrete in sewer systems.** *Applied and environmental microbiology*, **73**(3):971–80, feb 2007. 9, 10, 14, 75

[31] Mark Alexander, Alexandra Bertron, and Nele De Belie. *Performance of cement-based materials in aggressive aqueous environments*. Springer, 2013. 9, 10, 12, 53

[32] J Monteny, Nele De Belie, E Vincke, Willy Verstraete, and Luc Taerwe. **Chemical and microbiological tests to simulate sulfuric acid corrosion of polymer-modified concrete**. *Cement and Concrete Research*, **31**(9):1359–1365, 2001. 9, 13

[33] CU Parker and Joyce Prisk. **The oxidation of inorganic compounds of sulphur by various sulphur bacteria**. *Microbiology*, **8**(3):344–364, 1953. 9, 12

[34] Robert L Starkey. **Concerning the physiology of *Thiobacillus thiooxidans*, an autotrophic bacterium oxidizing sulfur under acid conditions**. *Journal of bacteriology*, **10**(2):135–163, 1925. 9, 13, 14

[35] Jes Vollertsen, Asbjørn Haaning Nielsen, Henriette Stokbro Jensen, Tove Wium-Andersen, and Thorkild Hvitved-Jacobsen. **Corrosion of concrete sewers–the kinetics of hydrogen sulfide oxidation.** *The Science of the total environment*, **394**(1):162–170, may 2008. 9, 148

[36] Orli Aviam, Gabi Bar-Nes, Yehuda Zeiri, and Alex Sivan. **Accelerated biodegradation of cement by sulfur-oxidizing bacteria as a bioassay for evaluating immobilization of low-level radioactive waste**. *Applied and environmental microbiology*, **70**(10):6031–6036, 2004. 9

[37] P A (Tony) Wells and Robert E Melchers. **Microbial corrosion of sewer pipe in Australia - Initial field results**. In *18th Intrenational Corrosion Congress 2011*, pages 1–12, 2011. 10, 41, 140, 148

[38] A BEELDENS, Joke Monteny, Elke Vincke, Nele De Belie, D VAN GEMERT, and Willy Verstraete. **Biogenic sulphuric acid corrosion: a microscopic investigation. Concrete for extreme conditions.** In *Proceedings of the International Congress on Challenges of Concrete Construction, Dundee, 5-11 September 2002/RK Dhir, J. McCarthy & MD Newlands (eds.)*, 2002. 10

[39] Robin E Beddoe and Horst W Dorner. **Modelling acid attack on concrete: Part I. The essential mechanisms**. *Cement and Concrete Research*, **35**(12):2333–2339, 2005. 10

[40] Ming-fang Ba, Chun-xiang Qian, Xin-jun Guo, and Xiang-yang Han. **Effects of steam curing on strength and porous structure of concrete with low water/binder ratio**. *Construction and Building Materials*, **25**(1):123–128, 2011. 10, 115, 130

[41] Xudong Chen, Shengxing Wu, and Jikai Zhou. **Influence of porosity on compressive and tensile strength of cement mortar**. *Construction and Building Materials*, **40**:869–874, mar 2013. 10, 89, 134

[42] Rakesh Kumar and B Bhattacharjee. **Porosity, pore size distribution and in situ strength of concrete**. *Cement and concrete research*, **33**(1):155–164, 2003. 10, 44, 89, 115, 130, 134

[43] Carcaño Rómel Solís and Eric I Moreno. **Análisis de la porosidad del concreto con agregado calizo**. *Revista de la Facultad de Ingeniería Universidad Central de Venezuela*, **21**(3):57–68, 2006. 10, 89

[44] Ángela Maria Hincapié Henao and Yesid de Jesús Montoya Góez. **La microestructura de los prefabricados de concreto**. *Revista Universidad EAFIT*, **41**(140):95–105, 2012. 10

[45] E Bastidas-Arteaga, M Sanchez-Silva, Ph Bressolette, A Chateauneuf, and W Raphael. **Assessment of the coupled effect of corrosion-fatigue on the reliability of RC bridges**. In *Bridge Maintenance, Safety Management, Health Monitoring and Informatics-IABMAS'08: Proceedings of the Fourth International IABMAS Conference, Seoul, Korea, July 13-17 2008*, pages 1302–1309. CRC Press, 2008. 11, 13

[46] Jon H Tuttle and Holger W Jannasch. **Occurrence and types of Thiobacillus-like bacteria in the sea**. *Limnol. Oceanogr*, **17**(4):532–543, 1972. 11

[47] RC Tilton, AB Cobet, and GE Jones. **MARINE THIOBACILLI: I. ISOLATION AND DISTRIBUTION**. *Canadian journal of microbiology*, **13**(11):1521–1528, 1967. 11

[48] Francesco Crescenzi, Antonella Crisari, Edoardo D'Angel, and Alessandro Nardella. **Control of acidity development on solid sulfur due to bacterial action**. *Environmental science & technology*, **40**(21):6782–6786, 2006. 11

REFERENCES

[49] Emilio Bastidas-Arteaga, Philippe Bressolette, Alaa Chateauneuf, and Mauricio Sánchez-Silva. **Probabilistic lifetime assessment of RC structures under coupled corrosionfatigue deterioration processes**. *Structural Safety*, **31**(1):84–96, jan 2009. 11, 140, 156

[50] Yunping Xi and Zdenek P Bazant. **Modeling chloride penetration in saturated concrete**. *Journal of Materials in Civil Engineering*, **11**(1):58–65, 1999. 11

[51] Ayman Ababneh, Farid Benboudjema, and Yunping Xi. **Chloride penetration in nonsaturated concrete**. *Journal of Materials in Civil Engineering*, **15**(2):183–191, 2003. 11

[52] Jianjun Zheng and Xinzhu Zhou. **Analytical solution for the chloride diffusivity of hardened cement paste**. *Journal of Materials in Civil Engineering*, **20**(5):384–391, 2008. 11

[53] Jianjun Zheng and Xinzhu Zhou. **Three-phase composite sphere model for the prediction of chloride diffusivity of concrete**. *Journal of Materials in Civil Engineering*, **20**(3):205–211, 2008. 11

[54] Clair N Sawyer, Perry L McCarty, and Gene F Parkin. **Chemistry for environmental engineering and science**. 2003. 12

[55] Mark Dopson and D Barrie Johnson. **Biodiversity, metabolism and applications of acidophilic sulfur-metabolizing microorganisms**. *Environmental microbiology*, **14**(10):2620–2631, 2012. 12

[56] MT Madigan, JM Martinko, and Jack Parker. **Brock Biology of Microorganisms. Southern Illinois University Carbondale**, 2000. 12

[57] Ernest O. Nnadi and Juan Lizarazo-Marriaga. **Acid Corrosion of Plain and Reinforced Concrete Sewage Systems**. *Journal of Materials in Civil Engineering*, **25**(9):1353–1356, sep 2013. 12, 75

[58] Henriette Stokbro Jensen, Asbjørn Haaning Nielsen, Thorkild Hvitved-Jacobsen, and Jes Vollertsen. **Modeling of hydrogen sulfide oxidation in concrete corrosion products from sewer pipes.** *Water environment research : a research publication of the Water Environment Federation*, **81**(4):365–73, apr 2009. 12

[59] MG Donoso, A Méndez-Vilas, JM Bruque, and ML González-Martin. **On the relationship between common amplitude surface roughness parameters and surface area: Implications for the study of cell–material interactions**. *International Biodeterioration & Biodegradation*, **59**(3):245–251, 2007. 12

[60] M. O'Connell, C. McNally, and M.G. Richardson. **Biochemical attack on concrete in wastewater applications: A state of the art review**. *Cement and Concrete Composites*, **32**(7):479–485, aug 2010. 12, 146

[61] H S Jensen, a H Nielsen, T Hvitved-Jacobsen, and J Vollertsen. **Survival of hydrogen sulfide oxidizing bacteria on corroded concrete surfaces of sewer systems.** *Water science and technology : a journal of the International Association on Water Pollution Research*, **57**(11):1721–6, jan 2008. 12

[62] H S Jensen, a H Nielsen, P N L Lens, T Hvitved-Jacobsen, and J Vollertsen. **Hydrogen sulphide removal from corroding concrete: comparison between surface removal rates and biomass activity.** *Environmental technology*, **30**(12):1291–6, nov 2009. 12, 38, 140

[63] David J Giannantonio, Jonah C Kurth, Kimberly E Kurtis, and Patricia A Sobecky. **Molecular characterizations of microbial communities fouling painted and unpainted concrete structures**. *International biodeterioration & biodegradation*, **63**(1):30–40, 2009. 13

[64] D J Roberts, D Nica, G Zuo, and J L Davis. **Quantifying microbially induced deterioration of concrete : initial studies**. *International Biodeterioration & Biodegradation*, **49**:227–234, 2002. 13, 14

[65] B I Cayford, G W Tyson, J Keller, and P L Bond. **Microbial community composition of biofilms associated with sewer corrosion**. In *6th International Conference on Sewer Processes and Networks*, number 60, 2010. 13, 14

[66] Shiping Wei, Mauricio Sanchez, David Trejo, and Chris Gillis. **Microbial mediated deterioration of reinforced concrete structures**. *International Biodeterioration & Biodegradation*, **64**(8):748–754, dec 2010. 14, 139

[67] Mark Hernandez, Eric A Marchand, Deborah Roberts, and Jordan Peccia. **In situ assessment of active Thiobacillus species in corroding concrete sewers using fluorescent RNA probes**. *International Biodeterioration & Biodegradation*, **49**(4):271–276, 2002. 14

[68] Donovan P Kelly and Ann P Wood. **Reclassification of some species of Thiobacillus to the newly designated genera *Acidithiobacillus* gen. nov., *Halothiobacillus* gen. nov. and *Thermithiobacillus* gen. nov.** *International Journal of Systematic and Evolutionary Microbiology*, **50**(2):511–516, 2000. 14

[69] R.P. P George, S. Ramya, D. Ramachandran, and U. Kamachi Mudali. **Studies on Biodegradation of normal concrete surfaces by fungus Fusarium sp.** *Cement and Concrete Research*, **47**:8–13, may 2013. 14

[70] Ji-dong Gu, Tim E Ford, Neal S Berke, and Ralph Mitchell. **Biodeterioration of concrete by the fungus Fusariuml**. *International Biodeterioration & Biodegradation*, **41**:101–109, 1998. 14

[71] T Wells and R E Melchers. **An observation-based model for corrosion of concrete sewers under aggressive conditions**. *Cement and Concrete Research*, **61-62**:1–10, 2014. 14, 140, 155

[72] WWj Umbreit and TF Anderson. **A study of *Thiobacillus thiooxidans* with the electron microscope**. *Journal of bacteriology*, **44**(3):317, 1942. 14

[73] Ryoki Asano, Takako Sasaki, and Yutaka Nakai. **Isolation and characterization of sulfur oxidizing bacteria from cattle manure compost**. *Animal Science Journal*, **78**(3):330–333, 2007. 15

[74] Owen D Osborne, Allan Pring, and Claire E Lenehan. **A simple colorimetric FIA method for the determination of pyrite oxidation rates**. *Talanta*, **82**(5):1809–1813, 2010. 29

[75] Mitsuo Manaka. **Comparison of rates of pyrite oxidation by dissolved oxygen in aqueous solution and in compacted bentonite**. *Journal of mineralogical and petrological sciences*, **104**(2):59–68, 2009. 29, 30

[76] M Kevin Parfitt, Daniel J Jones, and R Gary Garvin. **Structural, construction, and procedural failures associated with long-term pyritic soil expansion at a private elementary school in Pennsylvania**. *Journal of Performance of Constructed Facilities*, **25**(1):56–66, 2010. 29, 30, 31

[77] Y Wakizaka, K Ichikawa, Y Nakamura, and S Anan. **Deterioration of concrete due to specific minerals**. *Proc. Aggregate*, pages 331–338, 2001. 30

[78] Achour Bellaloui, Gilbert Nkurunziza, and Gérard Ballivy. **Caractérisation en laboratoire du potentiel expansif de granulats de remblais de fondation**. *Canadian geotechnical journal*, **39**(1):141–148, 2002. 30, 31

[79] María Fernanda Serrano Guzmán and Diego Darío Pérez Ruíz. **Agregados no convencionales para la preparación de concretos ecológicos**. 2011. 30

[80] M Floyd, MA Czerewko, JC Cripps, and DA Spears. **Pyrite oxidation in Lower Lias Clay at concrete highway structures affected by thaumasite, Gloucestershire, UK**. *Cement and Concrete Composites*, **25**(8):1015–1024, 2003. 30

[81] Mourice A Czerewko, Stephen A Cross, Philip G Dumelow, and Amon Saadvandi. **Assessment of pyritic Lower Lias mudrocks for earthworks**. *Proceedings of the Institution of Civil Engineers-Geotechnical Engineering*, **164**(2):59–77, 2011. 30, 31

[82] Thomas Schmidt, Andreas Leemann, Emanuel Gallucci, and Karen Scrivener. **Physical and microstructural aspects of iron sulfide degradation in concrete**. *Cement and Concrete Research*, **41**(3):263–269, 2011. 30

REFERENCES

[83] Gérard Ballivy, Patrice Rivard, Caroline Pépin, Marc G Tanguay, and Alexandre Dion. **Damages to residential buildings related to pyritic rockfills: field results of an investigation on the south shore of Montreal, Quebec, Canada**. *Canadian Journal of Civil Engineering*, **29**(2):246–255, 2002. 30

[84] Diana M Ossa and Marco A Márquez. **Biooxidación de sulfuros mediante cepas nativas de acidófilos compatibles con *Acidithiobacillus ferrooxidans* y *thiooxidans*, mina de oro el Zancudo,(Titiribí, Colombia)**. *Revista Colombiana de biotecnología*, **7**(2):55–66, 2005. 31

[85] Willem De Muynck, Nele De Belie, and Willy Verstraete. **Antimicrobial mortar surfaces for the improvement of hygienic conditions**. *Journal of applied microbiology*, **108**(1):62–72, 2010. 31

[86] Jean Herisson. *Biodétérioration des matériaux cimentaires dans les ouvrages dassainissement–Etude comparative du ciment daluminate de calcium et du ciment Portland*. PhD thesis, Université Paris-Est, 2012. 32

[87] L Sutherland-Stacey, S Corrie, A Neethling, I Johnson, O Gutierrez, R Dexter, Z Yuan, J Keller, and G Hamilton. **In Situ Continuous Measurement of Dissolved Sulfide in Sewer Systems**. *Water Sci. Technol*, **57**(3):375–381, 2008. 41

[88] MJ Setzer. **Action of frost and deicing chemicals: basic phenomena and testing**. *Freezethaw durability of concrete*, pages 3–21, 1976. 44

[89] J Rouquerol, D Avnir, CW Fairbridge, DH Everett, JM Haynes, N Pernicone, JDF Ramsay, KSW Sing, and KK Unger. **Recommendations for the characterization of porous solids (Technical Report)**. *Pure and Applied Chemistry*, **66**(8):1739–1758, 1994. 44

[90] ASTM Standard. **C109/C109M**. *Standard Test Method for Compressive Strength of Hydraulic Cement Mortars (Using 2-in. or 50-mm Cube Specimens), ASTM International, West Conshohocken PA*, 2012. 45

[91] Anders Lindvall. **Duracrete–Probabilistic performance based durability design of concrete structures**. In *2nd International Symposium in Civil Engineering*, pages 1–10, 1998. 52

[92] Thomas De Larrard, Emilio Bastidas-Arteaga, Frédéric Duprat, and Franck Schoefs. **Effects of climate variations and global warming on the durability of RC structures subjected to carbonation**. *Civil Engineering and Environmental Systems*, **31**(2):153–164, 2014. 52

[93] Marlene C. Morris, Howard F. McMurdie, Boris Evans, Eloise H.and Paretzkin, Harry S. Parker, and Nicolas C. Panagiotopoulos. *Standard X-ray Diffraction powder Patterns*, **Section 18 Data for 58 substances**. Department of commerce/National bureau of standards., 1981. 67

[94] Janice L Bishop, Melissa D Lane, M Darby Dyar, Sara J King, Adrian J Brown, and Gregg A Swayze. **Spectral Properties of Ca-sulfates: Gypsum, Bassanite and Anhydrite**. *Submitted to American Mineralogist*, 2013. 67

[95] Lawrence A Hardie. **The gypsum-anhydrite equilibrium at one atmosphere pressure**. *The American Mineralogist*, **52**:171–200, 1967. 67

[96] Prinya Chindaprasirt and Sumrerng Rukzon. **Strength, porosity and corrosion resistance of ternary blend Portland cement, rice husk ash and fly ash mortar**. *Construction and Building Materials*, **22**(8):1601–1606, 2008. 134

[97] Haitao Zhao, Qi Xiao, Donghui Huang, and Shiping Zhang. **Influence of Pore Structure on Compressive Strength of Cement Mortar**. *Hindawi Publishing Corporation*, **2014**(247058):1–12, 2014. 134

[98] Bernhard Pichler, Christian Hellmich, Josef Eberhardsteiner, Jaromír Wasserbauer, Pipat Termkhajornkit, Rémi Barbarulo, and Gilles Chanvillard. **Strength evolution of hydrating cement pastes: the counteracting effects of capillary porosity and unhydrated clinker reinforcements**. *Poromechanics V ASCE*, pages 1837–1846, 2013. 134

[99] American Concrete Pipe Association. **Loads and supporting strengths**. In *Concrete Pipe Design Manual*, pages 27–82. 139

[100] Xia He, Francis L de los Reyes, Michael L Leming, Lisa O Dean, Simon E Lappi, and Joel J Ducoste. **Mechanisms of fat, oil and grease (FOG) deposit formation in sewer lines.** *Water research*, **47**(13):4451–9, sep 2013. 139

[101] Masoud Moradian, Mohammad Shekarchi, Farhad Pargar, Aboozar Bonakdar, and Mahdi Valipour. **Deterioration of Concrete Caused by Complex Attack in Sewage Treatment Plant Environment**. (February):124–134, 2012. 140

[102] E. Bastidas-Arteaga, a. Chateauneuf, M. Sánchez-Silva, Ph. Bressolette, and F. Schoefs. **A comprehensive probabilistic model of chloride ingress in unsaturated concrete**. *Engineering Structures*, **33**(3):720–730, mar 2011. 140

[103] Xiaoyan Sun, Guangming Jiang, Philip L Bond, Tony Wells, and Jurg Keller. **A rapid , non-destructive methodology to monitor activity of sulfide-induced corrosion of concrete based on H 2 S uptake rate**. *Water Research*, **59**:229–238, 2014. 140, 147, 148

[104] Ece Erdogmus, Brian N Skourup, and Maher Tadros. **Recommendations for Design of Reinforced Concrete Pipe**. *Journal of Pipeline Systems Engineering and Practice*, **1**(1):25–32, feb 2010. 140

[105] Camilo Garcia, Dulcy M Abraham, Sanjiv Gokhale, and Tom Iseley. **Rehabilitation Alternatives for Concrete and Brick Sewers**. *Practice Periodical on Structural Design and Construction*, **7**(4):164–173, nov 2002. 140

[106] Concrete Manufacturers Association. **Design Manual for Concrete Pipe Outfall Sewers**, 2009. 140, 141, 162

[107] Fazal Chughtai and Tarek Zayed. **Structural Condition Models for Sewer Pipeline**. In *Pipelines 2007: Advances and Experiences with Trenchless Pipeline Projects*, pages 1–11. ASCE, 2007. 140

[108] Naeem Ejaz, Jawad Hussain, Usman Ghani, Faisal Shabir, Usman Ali Naeem, Muhammad Ali Shahmim, and Muhammad Fiaz Tahir. **Performance of concrete under aggressive wastewater environment using differente binders**. *Life Science Journal*, **10**:141–150, 2013. 140

[109] Project Title and Submitting Principal Investigators. **Behavior and Design of Buried Concrete Pipes**. (June), 2006. 140, 142

[110] Hong Sima. **Selective inhibition of *acidophilic thiobacilli* for application of controlling microbially-induced corrosion in concrete sewers.** 1992. 140, 152, 153

[111] John C Matthews. **Large-Diameter Sewer Rehabilitation Using a Fiber-Reinforced Cured-in-Place Pipe**. *Practice Periodical on Structural Design and Construction*, **04014031**(5):1–5, mar 2014. 140

[112] Ji-dong Gu and Ralph Mitchell. **Biodeterioration**. In Eugene Rosenberg, Edward F. DeLong, Stephen Lory, Erko Stackebrandt, and Fabiano Thompson, editors, *The Prokaryotes - Applied Bacteriology and Biotecnhnology*, number Ford 1993, pages 309–341. Springer Berlin Heidelberg, Berlin, Heidelberg, 2013. 140

[113] Neil S Shifrin. **Pollution Management in the Twentieth Century**. **131**(5):676–691, 2005. 140

[114] E Hewayde, M Nehdi, E Allouche, and G Nakhla. **Effect of Mixture Design Parameters and Wetting-Drying Cycles on Resistance of Concrete to Sulfuric Acid Attack**. *Journal of Materials in Civil Engineering*, **19**(2):155–163, 2007. 141

[115] A K Parande. **Deterioration of reinforced concrete in sewer environments**. (March):11–20, 2006. 141

[116] Frank W Callaghan. **Pipe performance and experiences during seismic events in New Zealand over the last 25 years**. In *Pipelines 2012: Innovations in Design, Construction, Operations, and Maintenance*, pages 1136–1146. ASCE, 2012. 141

[117] Camille G Rubeiz. **Performance of pipes during earthquakes**. In *Pipelines 2009: Infrastructure's Hidden Assets*, pages 1205–1215. ASCE, 2009. 141

REFERENCES

[118] J M Doyle and S J Fang. **Design of buried pipes**. In W F Chen, editor, *Handbook Of Structural Engineering*, page Chapter 25. CRC Press, 1997. 141

[119] Fazal Chughtai and Tarek Zayed. **Infrastructure Condition Prediction Models for Sustainable Sewer Pipelines**. *Journal of Performance of Constructed Facilities*, **22**(October):333–341, 2008. 141, 152

[120] BN Chisala and DN Lerner. **Distribution of sewer exfiltration to urban groundwater**. In *Proceedings of the Institution of Civil Engineers-Water Management*, **161**, pages 333–341. Thomas Telford Ltd, 2008. 141

[121] J C McCormac and J K Nelson. *Design of reinforced concrete*. John Wiley & sons, New Jersey, 2009. 145

[122] Wolfgang Sand, Thierry Dumas, and Serge Marcdargent. **Accelerated biogenic sulfuric-acid corrosion test for evaluating the performance of calcium-aluminate based concrete in sewage applications**. In *Microbiologically Influenced Corrosion Testing*, pages 234–249. ASTM International, 1994. 147

[123] Ma. Guadalupe D. Gutiérrez-Padilla, Angela Bielefeldt, Serguei Ovtchinnikov, Mark Hernandez, and Joann Silverstein. **Biogenic sulfuric acid attack on different types of commercially produced concrete sewer pipes**. *Cement and Concrete Research*, **40**(2):293–301, feb 2010. 148, 152

[124] M Bohm and J S Devinny. **A Moving Boundary Diffusion Model for the Corrosion of Concrete Wastewater Systems: Simulation and Experimental Validation**. *Proceedings of the 1999 American Control Conference (Cat. No. 99CH36251) (1999)*, (June):1739–1743, 1999. 148

[125] Nele De Belie. **Microorganisms versus stony materials: a love–hate relationship**. *Materials and structures*, **43**(9):1191–1202, 2010. 148

[126] Haifeng Yuan. *Degradation modeling of concrete submitted to biogenic acid attack*. PhD thesis, Université Paris - Est, 2013. 148

[127] Emilie Hudon, Saeed Mirza, and Dominic Frigon. **Biodeterioration of concrete sewer pipes: State of the art and research needs**. *Journal of pipeline systems ...*, (May):42–52, 2011. 148, 155

[128] Keshab Raj Sharma, Zhiguo Yuan, David De Haas, Geoff Hamilton, Shaun Corrie, and Jurg Keller. **Dynamics and dynamic modelling of H_2S production in sewer systems**. *Water research*, **42**(10):2527–2538, 2008. 152, 162

[129] Infrastructural Products and Engineering Solutions Division. **Concrete pipe and portal culvert handbook**, 2009. 152

[130] Kyoohong Park, Hongsik Lee, Shaun Phelan, Susanthi Liyanaarachchi, Nyoman Marleni, Jegatheesan Veeriah Navaratna, Dimuth, and Li Shu. **Mitigation strategies of hydrogen sulphide emission in sewer networks - A review**. *International Biodeterioration and Biodegradation*, **95**:251–261, 2014. 153

[131] Computers & Structures Inc. *CSi Analysis Reference Manual*. 2013. 153

[132] Mary W Goodson and John E Anderson. **Soil-Structure Interaction A Case Study**. In *Structures Congress 2005*, pages 1–11. ASCE, 2005. 153

[133] H Díaz González and G Ángel Reyes. **Análisis comparativo de la teoría de Martson para tuberías enterradas y la modelación numérica con elementos finitos**, 1999. 153

[134] A.K. Agrawal, K. Ramalingam, S. Rozelman, F. Kulcsar, and N. Farooqui. **Asset Management and Nondestructive Evaluation of Force Mains in New York City**. In *Pipelines Congress 2008*, pages 1–11. ASCE, 2008. 153

[135] Sevket Ates. **Numerical modelling of continuous concrete box girder bridges considering construction stages**. *Applied Mathematical Modelling*, **35**:3809–3820, 2011. 153

[136] Rita Bento and M J Falcão-Silva. **ANALYTICAL MODEL FOR THE SEISMIC BEHAVIOR OF BURIED PIPELINE WHEN SUBJECTED TO GROUND LIQUEFACTION**. In *13th World Conference on Earthquake Engineering*, number 3155, Vancouver, B.C., Canada, 2004. 153

[137] NewYork State Department of Transportation. *Geotechnical desing manual. Chapter 21 Geotechnical aspects of pipe design and installation.* 2013. 153

[138] Thomas M Petry and Dallas N Little. **Review of stabilization of clays and expansive soils in pavements and lightly loaded structures-history, practice, and future**. *Journal of Materials in Civil Engineering*, **14**(6):447–460, 2002. 153

[139] T Wells and RE Melchers. **Modelling concrete deterioration in sewers using theory and field observations**. *Cement and Concrete Research*, **77**:82–96, 2015. xxvii, 155

[140] Elena Eijo-Río, Anna Petit-Boix, Gara Villalba, María Eugenia Suárez-Ojeda, Desirée Marin, Maria José Amores, Xavier Aldea, Joan Rieradevall, and Xavier Gabarrell. **Municipal sewer networks as sources of nitrous oxide, methane and hydrogen sulphide emissions: a review and case studies**. *Journal of Environmental Chemical Engineering*, **3**(3):2084–2094, 2015. 155

[141] American Society for Testing Materials. **ASTM C76M-14 Standard Specification for Reinforced Concrete Culvert , Storm Drain , and Sewer Pipe (Metric)**, 2014. 155, 158, 162

[142] Mauricio Sánchez-Silva and Georgia-Ann Klutke. *Reliability and Life-Cycle Analysis of Deteriorating Systems.* Springer, 2015. 156, 157

[143] Mauricio Sanchez-Silva. *Introducción a la confiabilidad y evaluación de riesgos. Teoría y aplicaciones en ingeniería.* Ediciones Uniandes, 2010. 156, 157, 158

[144] **A615/A615M Specification for Deformed and Plain Carbon-Steel Bars for Concrete Reinforcement ASTM International**. pages 1–6, 2013. 158

[145] American Society for Testing Materials. **ASTM C1417 M Standard Specification for Manufacture of Reinforced Concrete Sewer, Storm Drain, and Culvert Pipe for Direct Design [Metric]**, 2014. 158

[146] American Society for Testing Materials. **ASTM C1433 M Standard Specification for Precast Reinforced Concrete Monolithic Box Sections for Culverts, Storm Drains and Sewers**, 2014. 158

[147] American Concrete Pipe Association. **ASTM C655M-14 Standard Specification for Reinforced Concrete D-Load Culvert , Storm Drain , and Sewer Pipe (Metric)**, 2014. 158

[148] M Ahammed and RE Melchers. **Probabilistic analysis of underground pipelines subject to combined stresses and corrosion**. *Engineering structures*, **19**(12):988–994, 1997. 159

[149] Amir M Alani and Asaad Faramarzi. **Predicting the Probability of Failure of Cementitious Sewer Pipes Using Stochastic Finite Element Method**. *International journal of environmental research and public health*, **12**(6):6641–6656, 2015. 159, 161

[150] Drainage Section State of Florida Department of Transportation, Office of Design. *Drainage Handbook Optional Pipe Materials.* FDOT, 2014. 161

[151] Environmental Protection Agency (EPA). *Condition Assessment of Wastewater Collection Systems.* EPA, 2009. 161

[152] Svenung Saegrov. **Computer Aided Rehabilitation of Sewer and Storm Water Networks-CARE-S**. *Water Intelligence Online*, **5**:88, 2006. 161

...